



## ARCHIVIO ISTITUZIONALE DELLA RICERCA

### Alma Mater Studiorum Università di Bologna Archivio istituzionale della ricerca

TDP-43 Modulation by Tau-Tubulin Kinase 1 Inhibitors: A New Avenue for Future Amyotrophic Lateral Sclerosis Therapy

This is the final peer-reviewed author's accepted manuscript (postprint) of the following publication:

*Published Version:*

TDP-43 Modulation by Tau-Tubulin Kinase 1 Inhibitors: A New Avenue for Future Amyotrophic Lateral Sclerosis Therapy / Nozal, Vanesa; Martínez-González, Loreto; Gomez-Almeria, Marta; Gonzalo-Consuegra, Claudia; Santana, Paula; Chaikuad, Apirat; Pérez-Cuevas, Eva; Knapp, Stefan; Lietha, Daniel; Ramírez, David; Petralla, Sabrina; Monti, Barbara; Gil, Carmen; Martín-Requero, Angeles; Palomo, Valle; de Lago, Eva; Martinez, Ana. - In: JOURNAL OF MEDICINAL CHEMISTRY. - ISSN 0022-2623. - ELETTRONICO. - Online ahead of print.:(2022), pp. 1-23. [10.1021/acs.jmedchem.1c01942]

This version is available at: <https://hdl.handle.net/11585/844967> since: 2022-01-12

*Published:*

DOI: <http://doi.org/10.1021/acs.jmedchem.1c01942>

*Terms of use:*

Some rights reserved. The terms and conditions for the reuse of this version of the manuscript are specified in the publishing policy. For all terms of use and more information see the publisher's website.

(Article begins on next page)

This item was downloaded from IRIS Università di Bologna (<https://cris.unibo.it/>).  
When citing, please refer to the published version.

This is the final peer-reviewed accepted manuscript of:

[TDP-43 Modulation by Tau-Tubulin Kinase 1 Inhibitors: A New Avenue for Future Amyotrophic Lateral Sclerosis Therapy.](#)

Nozal V, Martínez-González L, Gomez-Almeria M, Gonzalo-Consuegra C, Santana P, Chaikuad A, Pérez-Cuevas E, Knapp S, Lietha D, Ramírez D, Petralla S, **Monti B**, Gil C, Martín-Requero A, Palomo V, de Lago E, Martinez A.

*J Med Chem.* 2022 Jan 27;65(2):1585-1607.

The final published version is available online at: [doi: 10.1021/acs.jmedchem.1c01942](https://doi.org/10.1021/acs.jmedchem.1c01942)

Rights / License:

The terms and conditions for the reuse of this version of the manuscript are specified in the publishing policy. For all terms of use and more information see the publisher's website.

*This item was downloaded from IRIS Università di Bologna (<https://cris.unibo.it/>)*

***When citing, please refer to the published version.***

This document is confidential and is proprietary to the American Chemical Society and its authors. Do not copy or disclose without written permission. If you have received this item in error, notify the sender and delete all copies.

### **TDP-43 modulation by tau tubuline kinase 1 inhibitors: a new avenue for future amyotrophic lateral sclerosis therapy**

Journal:	<i>Journal of Medicinal Chemistry</i>
Manuscript ID	jm-2021-01942r.R1
Manuscript Type:	Article
Date Submitted by the Author:	n/a
Complete List of Authors:	<p>Nozal, Vanesa; Consejo Superior de Investigaciones Cientificas, Centro de Investigaciones Biologicas; Instituto de Salud Carlos III</p> <p>Martinez-Gonzalez, Loreto; Consejo Superior de Investigaciones Cientificas, Centro de Investigaciones Biologicas; Instituto de Salud Carlos III</p> <p>Gomez-Almeria, Marta; Universidad Complutense de Madrid, Facultad de Medicina</p> <p>Gonzalo-Consuegra, Claudia; Universidad Complutense de Madrid, Facultad de Farmacia</p> <p>Santana, Paula; Universidad Autónoma de Chile - Campus El Llano Subercaseaux</p> <p>Chaikuad, Apirat; Goethe-Universitat Frankfurt am Main, Institut für Pharmazeutische Chemie</p> <p>Perez-Cuevas, Eva; Consejo Superior de Investigaciones Cientificas, Centro de Investigaciones Biologicas; Instituto de Salud Carlos III</p> <p>Knapp, Stefan; Goethe University Frankfurt, Institute of Pharmaceutical Chemistry</p> <p>Lietha, Daniel; Consejo Superior de Investigaciones Cientificas, Centro de Investigaciones Biologicas</p> <p>Ramirez, David; Universidad de Concepción Facultad de Ciencias Biológicas</p> <p>Petralla, Sabrina; Alma Mater Studiorum University of Bologna, Pharmacy and Biotechnology</p> <p>Monti, Barbara; University of Bologna, Department of Pharmacy and Biotechnology,</p> <p>Gil, Carmen; Consejo Superior de Investigaciones Cientificas, Centro de Investigaciones Biologicas</p> <p>Martin-Requero, Angeles; Consejo Superior de Investigaciones Cientificas, Centro de Investigaciones Biologicas; Instituto de Salud Carlos III</p> <p>Palomo, Valle; Consejo Superior de Investigaciones Cientificas, Centro de Investigaciones Biologicas; Instituto de Salud Carlos III</p> <p>de Lago, Eva; Universidad Complutense de Madrid, Facultad de Medicina; Instituto de Salud Carlos III</p> <p>Martínez, Ana; Consejo Superior de Investigaciones Cientificas, Centro de Investigaciones Biologicas; Instituto de Salud Carlos III</p>

SCHOLARONE™  
Manuscripts

1  
2  
3  
4  
5  
6  
7  
8  
9  
10  
11  
12  
13  
14  
15  
16  
17  
18  
19  
20  
21  
22  
23  
24  
25  
26  
27  
28  
29  
30  
31  
32  
33  
34  
35  
36  
37  
38  
39  
40  
41  
42  
43  
44  
45  
46  
47  
48  
49  
50  
51  
52  
53  
54  
55  
56  
57  
58  
59  
60



REVISED 1 14.12.2021

**TDP-43 modulation by tau tubulin kinase 1 inhibitors: A new avenue for future amyotrophic lateral sclerosis therapy**

Vanesa Nozal,<sup>1,2</sup> Loreto Martínez-González,<sup>1,2</sup> Marta Gomez-Almeria,<sup>3</sup> Claudia Gonzalo-Consuegra,<sup>3</sup> Paula Santana,<sup>4</sup> Apirat Chaikwad,<sup>5,6</sup> Eva Pérez-Cuevas,<sup>1,2</sup> Stefan Knapp,<sup>5,6</sup> Daniel Lietha,<sup>1</sup> David Ramírez,<sup>7</sup> Sabrina Petralla,<sup>8</sup> Barbara Monti,<sup>8</sup> Carmen Gil,<sup>1</sup> Angeles Martín-Requero,<sup>1,2</sup> Valle Palomo,<sup>1,2</sup> Eva de Lago,<sup>2,3</sup> Ana Martinez<sup>1,2</sup> \*

<sup>1</sup>Centro de Investigaciones Biológicas Margarita Salas-CSIC, Ramiro de Maeztu 9, 28040 Madrid (Spain)

<sup>2</sup>Centro de Investigación Biomédica en Red de Enfermedades Neurodegenerativas (CIBERNED), Instituto de Salud Carlos III, 28031 Madrid (Spain)

<sup>3</sup>Instituto de Investigación en Neuroquímica, Dpto de Bioquímica y Biología Molecular, Facultad de Medicina, Universidad Complutense de Madrid, 28040 Madrid (Spain)

<sup>4</sup>Facultad de Ingeniería, Instituto de Ciencias Químicas Aplicadas, Universidad Autónoma de Chile, el Llano Subercaseaux 2801, San Miguel, Santiago (Chile)

<sup>5</sup>Institute for Pharmaceutical Chemistry, Goethe University Frankfurt, Max von Lauestrasse 9, 60438 Frankfurt (Germany)

<sup>6</sup>Structural Genomics Consortium, Buchmann Institute for Life Sciences, Goethe University Frankfurt, Max von Lauestrasse 15, 60438 Frankfurt (Germany)

<sup>7</sup>Departamento de Farmacología, Facultad de Ciencias Biológicas, Universidad de Concepción. Víctor Lamas 1290, PO Box 160-C, Concepción (Chile)

<sup>8</sup>Department of Pharmacy and Biotechnology, University of Bologna, Via Selmi 3, 40126 Bologna (Italy)

Corresponding author:

Prof. Ana Martinez

e-mail: ana.martinez@csic.es

**Abstract.**

Amyotrophic Lateral sclerosis (ALS) is a fatal neurodegenerative disease without any effective treatment. Protein TDP-43 is a pathological hallmark of ALS, both in sporadic and familiar patients. Post-translational modifications of TDP-43 promote its aggregation in the cytoplasm. Tau tubulin kinase (TTBK1) phosphorylates TDP-43 in cellular and animal models, thus TTBK1 inhibitors emerge as a promising therapeutic strategy for ALS. The design, synthesis, biological evaluation, kinase-ligand complex structure determination and molecular modeling studies confirmed novel pyrrolopyrimidine derivatives as valuable inhibitors for further development. Moreover, compound **29** revealed good brain penetration *in vivo*, and was able to reduce TDP-43 phosphorylation not only in cell cultures but also in spinal cord of transgenic TDP-43 mice. A shift to M2 anti-inflammatory microglia was also demonstrated *in vivo*. Both of these activities led to motor neuron preservation in mice, proposing pyrrolopyrimidine **29** as a valuable lead compound for future ALS therapy.

**Keywords:** TTBK1 inhibitors, ALS, TDP-43 phosphorylation, drug design, kinase

## 1. Introduction

Amyotrophic lateral sclerosis (ALS) is a fatal and rare neurodegenerative disease that affects motoneurons causing the death of the patients within three to five years after disease onset due to cardiorespiratory failure. Despite this fatal outcome, disease-modifying agents have not been discovered and current therapeutic options only expand lifespan of the patients up to several months. Multiple pathological mechanisms have been described to occur in the affected motor neurons and among them, deposits of TAR DNA binding protein of 43 kDa (TDP-43), which are present in the 97% of the patients independently from their etiological origin, sporadic or familial.<sup>1</sup> TDP-43 is a highly conserved nuclear protein that plays many different roles in RNA metabolism such as transcription, splicing, transport, stability through recruitment into stress granules and microRNA biosynthesis.<sup>2</sup> In ALS and other TDP-43-pathies such as the rare Alexander's disease, the frontotemporal dementia (FTD-TDP) or the prevalent limbic-predominant age-related TDP-43 encephalopathy (LATE), nuclear localization of TDP-43 is lost.<sup>3</sup> Elevated levels of this protein are present in the cytoplasm of ALS patients which are affected by different post-translational modifications thought to impede the return of the protein to the nucleus.<sup>4</sup> Among them, aberrant hyperphosphorylation is the most relevant one in TDP-43 inclusions.<sup>5</sup> Therefore, the recovery of TDP-43 homeostasis is an emergent therapeutic approach for the discovery of new drugs for ALS and other severe diseases.<sup>6</sup>

Only few kinases have been described to participate directly or indirectly in TDP-43 phosphorylation including glycogen synthase kinase 3 $\beta$  (GSK3 $\beta$ ),<sup>7</sup> casein kinase 1 (CK1),<sup>8</sup> cell division cycle kinase 7 (CDC7),<sup>9</sup> mitogen-activated protein kinases (MAPK/ERK)<sup>10</sup> and tau tubulin kinases (TTBK1/2).<sup>11</sup> Consequently, inhibitors of these proteins have thus been considered as an emerging therapeutic option.<sup>12</sup> Several inhibitors of GSK3 $\beta$ , CK1 and CDC7 have been described and tested in ALS models.<sup>13,14,15</sup> In addition, despite the fact that inhibitors for TTBK1/2 have been recently disclosed,<sup>16</sup> their role in TDP-43 pathologies has not been explored so far.

1  
2  
3 TTBKs belong to the superfamily of CK1 which contains two isoforms in human: TTBK1  
4 and TTBK2 with different expression patterns throughout the body and different  
5 physiological roles. TTBK2 expression is ubiquitous and mutations in *TTBK2* gene trigger  
6 spinocerebellar ataxia 11 (SCA11) since the protein is involved in ciliogenesis.  
7 Furthermore, mice that presented truncated TTBK2 show embryonic lethality with strong  
8 neural tube and sonic hedgehog signalling defects. These data emphasize the relevance  
9 of this kinase in modulating physiological pathways and the challenge to be targeted by  
10 small molecules without toxic events.<sup>17-18</sup> On the other hand, TTBK1 is specifically  
11 expressed in the central nervous system (CNS) and it is linked to neuronal pathological  
12 roles.<sup>19</sup> TTBK1 has been described for the first time in 2006 as a kinase responsible for  
13 the phosphorylation and aggregation of tau.<sup>20</sup> Since then, multiple studies have  
14 demonstrated the role of TTBK1 in the modulation of tau linked with Alzheimer's disease  
15 (AD), as it is the main kinase responsible for the phosphorylation of Ser422, a key epitope  
16 in the early formation of fibrils prior to neurofibrillary tangles (NFT).<sup>21-22</sup> Regarding TDP-  
17 43 pathologies, Liachko *et al.* established a relevant role of TTBK1 in TDP-43  
18 phosphorylation, demonstrating the ability of the kinase to phosphorylate TDP-43 Ser409  
19 and Ser410 both *in vitro* and *in vivo*. siRNA treatment in a *C. elegans* model resulted in  
20 different outcomes for the two isoforms where, only depletion of TTBK1 by siRNA  
21 resulted in significant reduced phosphorylation of TDP-43.<sup>11</sup> Thus, TTBK1 has emerged  
22 as a potential drug target for neurodegenerative diseases where the pathology of TDP-  
23 43 plays a key role and its inhibitors may play a crucial role in several unmet diseases  
24 such as ALS, LATE and FTD.<sup>23</sup>

25  
26  
27  
28  
29  
30  
31  
32  
33  
34  
35  
36  
37  
38  
39  
40  
41  
42  
43  
44  
45  
46  
47  
48  
49  
50 Only few small-molecules have been reported inhibiting TTBK1 (Figure 1). Two chemical  
51 diverse compounds, 3-[(6,7-dimethoxyquinazolin-4-yl)amino]phenol (**AZ-1**) and methyl  
52 2-bromo-5-(7*H*-pyrrolo[2,3-*d*]pyrimidin-4-ylamino)benzoate (**AZ-2**), have been identified  
53 as binders of TTBK1 using surface plasmon resonance.<sup>24</sup> Furthermore, the crystal  
54 structure of both compounds in complex with the kinase domain of TTBK1 has been  
55  
56  
57  
58  
59  
60

determined, but neither the  $IC_{50}$  values for TTBK1 and TTBK2 nor their selectivity against other kinases has been described but their  $K_D$ . The heterocyclic compound 3-{5-[(4-amino-4-methylpiperidin-1-yl)methyl]pyrrolo[2,1-f][1,2,4]triazin-4-yl}amino)-5-bromophenol (**2KC**) with equipotent  $IC_{50}$  values for TTBK1 and TTBK2 (120 nM and 170 nM, respectively) has been also described in crystallographic complex with the kinase domain of TTBK1.<sup>25</sup> However, neither the kinase selectivity profile of these three compounds nor their behavior in cellular models have been reported. During the preparation of this manuscript, the first brain-penetrant TTBK1 inhibitors have been reported, including the azaindazole **TTBK1-IN-1**, and despite their lack of selectivity for TTBK2, target engagement and decrease of tau phosphorylation *in vivo* have been shown.<sup>16, 26</sup> These data corroborate the therapeutic relevance of TTBK1 inhibitors for tauopathies and especially for Alzheimer's disease.

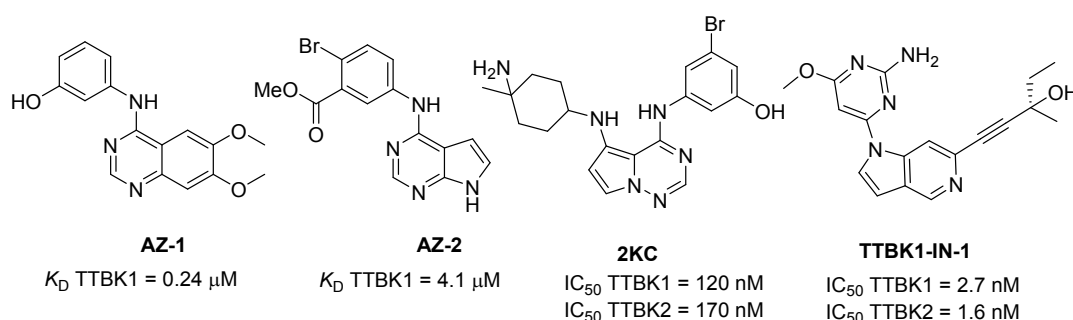


**Figure 1.** Chemical structure of the few described TTBK1 inhibitors and their reported  $K_D$  or  $IC_{50}$  values.

In this work we describe the design, synthesis and optimization of new TTBK1 isoform-selective inhibitors for the treatment of TDP-43 proteinopathies. A family of more than sixty heterocyclic compounds was synthesized and their inhibition of TTBK1 and TTBK2 was tested *in vitro*. Their selectivity for TTBK1 isoform, permeability through the blood-brain barrier, crystal structures of the kinase-inhibitor complexes with TTBK1 and TTBK2, molecular dynamics and cellular activity in ALS disease models are presented. Finally, one of the most promising candidates was studied in a TDP-43<sup>A315T</sup>-transgenic mouse model. Our results confirmed the therapeutic potential of TTBK1 for ALS and other TDP-

43-pathies and the compounds reported represent promising lead structures for the treatment of these diseases.

## 2. Results and discussion

### 2.1 Design, synthesis and enzymatic evaluation of TTBK inhibitors

When this medicinal chemistry program began few years ago, the kinase domain of TTBK1 with ATP (PDB id. 4BTJ) together with three small molecules that bind to the adenine binding pocket (PDB id. 4BTM, 4BTK and 4NFN) have been available in the Protein Data Bank.<sup>24-25</sup> Until very recently, the crystal structure of the catalytic domain of TTBK2 has not been determined.<sup>22, 27</sup> This body of structural information was considered a starting point for our drug design program. As such, the design of new compounds aimed to study the importance of two hydrogen bonds with Gln108 and Gln110 located in the hinge region and explore the druggability of the hydrophobic pocket around Asp176 and the catalytic Lys63 (Figure 2).

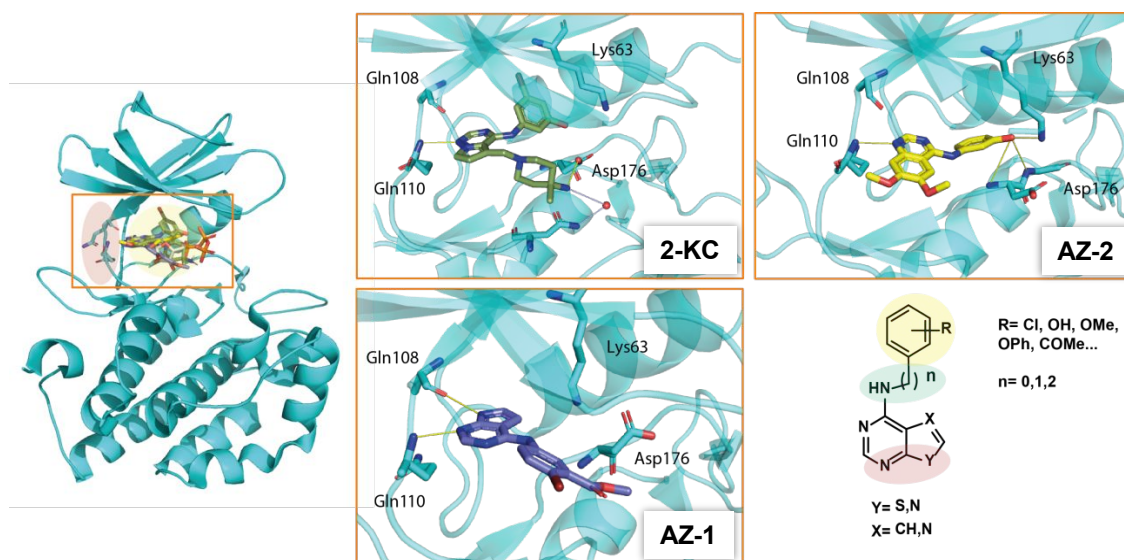
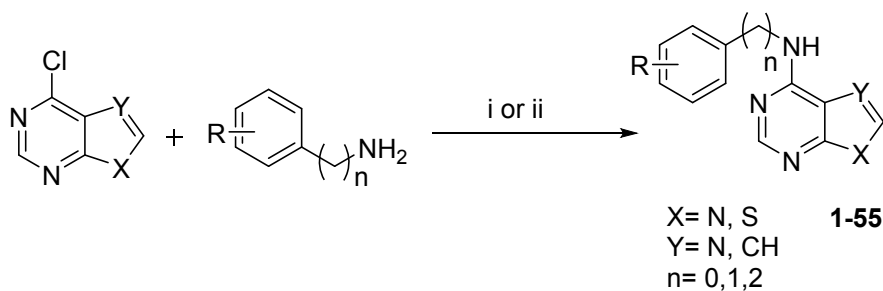


**Figure 2.** Crystal structure of kinase domain of TTBK1 with compounds AZ-1, AZ-2 and 2KC (PDB id. 4BTM, 4BTK and 4NFN) that lead to the design of the new TTBK1 inhibitors.

Hence, we chose a [6+5] heterocycle as a central core, which is considered as privileged scaffold for protein kinase inhibitors,<sup>28</sup> varying the nature of the five-membered ring to

1  
2  
3 explore the importance of a hydrogen-donor atom for the interaction with Gln110 and  
4 Gln108. Furthermore, we linked directly to this heterocycle, a phenyl ring with different  
5 substituents: halogens, hydrogen bond donors and acceptors, in different positions. The  
6 introduced phenyl ring would presumably establish interactions in the hydrophobic  
7 pocket (yellow area in Figure 2). The nature and length of the linker were also varied to  
8 explore this hydrophobic region (green area in Figure 2).

9  
10  
11  
12  
13  
14  
15  
16  
17  
18  
19  
20  
21  
22  
23  
24  
25  
26  
27  
28  
29  
30  
31  
32  
33  
34  
35  
36  
37  
38  
39  
40  
41  
42  
43  
44  
45  
46  
47  
48  
49  
50  
51  
52  
53  
54  
55  
56  
57  
58  
59  
60  
Synthesis of the compounds was easily realized implementing a one-step reaction with indium trichloride as a Lewis acid to facilitate the aromatic nucleophilic substitution of pi-deficient heterocycles (Scheme 1).<sup>29</sup> In cases where a halogen atom was a substituent in the phenyl ring, we discarded the use of  $\text{InCl}_3$  to avoid the polymerisation of the building blocks. Synthesis of these compounds has been achieved using THF as reagents solvent and under microwave irradiation. A first family of 27 compounds (**1-27**) was synthesized following this methodology with moderate to very good yields (Scheme 1 and Table 1). Their chemical structure was confirmed by NMR ( $^1\text{H}$  and  $^{13}\text{C}$  NMR) and other analytical methods as detailed in the experimental section.

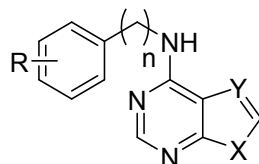


**Scheme 1.** i)  $\text{InCl}_3$  (0.1 eq), MW, MeCN, 100 °C; ii) MW, THF, 100 °C (See Table 1 and 2 for R description)

The inhibitory activities of the new prepared compounds against TTBK isoforms 1 and 2 were evaluated in the Medical Research Council (MRC) Phosphorylation Unit (University of Dundee). Data are shown in Table 1. Initially the compounds were tested at a fixed concentration of 10  $\mu\text{M}$ , and when the inhibition was larger than 50%, a dose-response was conducted to determine  $\text{IC}_{50}$  values. Overall, the tested compounds showed TTBK1 inhibition in the low micromolar range and were either equipotent inhibiting TTBK2 or

showed approximately up to one order of magnitude lower activity. These results and the calculation of the “TTBK1-selectivity index” defined as  $IC_{50}(\text{TTBK1})/IC_{50}(\text{TTBK2})$ , allowed us to establish a limited structure-activity relationships for improving TTBK1 activity.

**Table 1.** Chemical structure, yield and enzymatic inhibition of the synthesized compounds **1-27** against TTBK1 and TTBK2.



Comp.	Y	X	n	R	Yield (%)	A. TTBK1 $IC_{50}$ ( $\mu\text{M}$ ) or %inh@10 $\mu\text{M}$	B. TTBK2 $IC_{50}$ ( $\mu\text{M}$ ) or %inh@10 $\mu\text{M}$	Selectivity index A/B
1	N	NH	0	3-OH	29	9.15 $\mu\text{M}$	13%@10 $\mu\text{M}$	0.22
2	N	NH	0	4-OH	20	3%@10 $\mu\text{M}$	1%@10 $\mu\text{M}$	-
3	N	NH	0	4-morpholine	70	25%@10 $\mu\text{M}$	12%@10 $\mu\text{M}$	-
4	N	NH	0	4-Cl	75	8%@10 $\mu\text{M}$	1%@10 $\mu\text{M}$	-
5	CH	S	0	4-Cl	50	20%@10 $\mu\text{M}$	-	-
6	CH	S	0	H	70	17%@10 $\mu\text{M}$	-	-
7	CH	NH	0	3-OH	87	6.10 $\mu\text{M}$	6.70 $\mu\text{M}$	0.90
8	CH	NH	0	4-OH	38	3.00 $\mu\text{M}$	7.40 $\mu\text{M}$	0.45
9	CH	NH	0	4-morpholine	24	4.90 $\mu\text{M}$	15.70 $\mu\text{M}$	0.30
10	CH	NH	0	4-Cl	92	3.20 $\mu\text{M}$	20.30 $\mu\text{M}$	0.15
11	CH	NH	1	4-Cl	55	32%@10 $\mu\text{M}$	10%@10 $\mu\text{M}$	-
12	CH	NH	2	4-Cl	25	18.20 $\mu\text{M}$	86.00 $\mu\text{M}$	
13	CH	NH	1	4-OH	14	23%@10 $\mu\text{M}$	10%@10 $\mu\text{M}$	-
14	CH	NH	2	4-OH	23	12.80 $\mu\text{M}$	37.70 $\mu\text{M}$	0.33
15	CH	NH	0	3-Cl	49	15.20 $\mu\text{M}$	13.90 $\mu\text{M}$	1.09
16	CH	NH	0	2-Cl	69	21.80 $\mu\text{M}$	42.10 $\mu\text{M}$	0.51
17	CH	NH	0	2-OH	20	14%@10 $\mu\text{M}$	1%@10 $\mu\text{M}$	-
18	CH	NH	0	[b]cyclohexyl	23	23%@10 $\mu\text{M}$	10%@10 $\mu\text{M}$	-
19	CH	NH	0	[b]1,3dioxole	15	1.58 $\mu\text{M}$	7.58 $\mu\text{M}$	0.21
20	CH	NH	0	4-COMe	25	4.30 $\mu\text{M}$	9.30 $\mu\text{M}$	0.46
21	CH	NH	0	3-morpholine	58	4.70 $\mu\text{M}$	5.70 $\mu\text{M}$	0.82
22	CH	NH	0	H	64	0.79 $\mu\text{M}$	1.68 $\mu\text{M}$	0.47
23	CH	NH	0	4-OMe	74	0.52 $\mu\text{M}$	1.32 $\mu\text{M}$	0.39
24	CH	NH	0	4-OCF <sub>3</sub>	92	1.00 $\mu\text{M}$	8.80 $\mu\text{M}$	0.11
25	CH	NH	0	4-OiPr	66	1.50 $\mu\text{M}$	8.40 $\mu\text{M}$	0.17



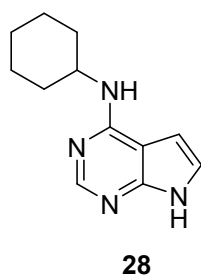
<b>26</b>	CH	NH	0	4-OEt	20	2.30 $\mu$ M	13.70 $\mu$ M	0.16
<b>27</b>	CH	NH	0	4-OPh	53	0.39 $\mu$ M	0.85 $\mu$ M	0.45

Considering the main heterocycle, pyrrolopyrimidine-derived compounds were more active than their purine derivative analogues (see compounds **1-4** vs **7-10**) that lacked kinase inhibitory activity. The thienopyrimidine-derived compounds **5** and **6** resulted also in inactive compounds. Altogether, these results highlighted the importance of the presence of a hydrogen-donor atom at position 7 in the five membered-ring and motivated us to choose the pyrrolopyrimidine moiety as the main scaffolding heterocycle.

The length of the connector of the phenyl moiety attached at the exocyclic amino group was also crucial for TTBK1 inhibition. Thus, the presence of only one methylene group in the linker affected negatively activity and resulted in inactive compounds (**11** and **13**). Also the introduction of two methylene groups resulted in less potent compounds than those with the phenyl ring directly attached to the amine (derivatives **8** vs **14**, and **10** vs **12**).

Moreover, the position of substituents in the phenyl ring affects the potency of the inhibitors, highlighting *para*- substitution as the more favourable modification to increase TTBK1 inhibition (i.e. **10**>**15**>**16** or **8**>**7**>**17**). Interestingly, the best IC<sub>50</sub> value (in the low micromolar range) was obtained with a compound bearing a second aromatic ring in the *para*- position of the aniline ring (compound **27**).

Finally, we synthesized compound **28** (Figure 3) where the phenyl ring was replaced by the saturated cyclohexyl moiety. The lack of TTBK1 inhibition highlighted the importance of this aromatic ring for compound activity.

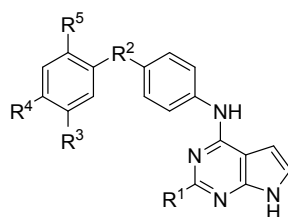


Yield (%)	TTBK1 %inh@10 μM	TTBK2 %inh@10 μM
26%	3 %	15%

**Figure 3.** Chemical structure, yield and inhibition of TTBK1/2 of compound **28**.

The discovery of **27** motivated us to further exploit this family of compounds, consequently we designed a second subfamily of ligands harbouring two aromatic rings with different substituents and linkers connected to a pyrrolopyrimidine heterocycle. These compounds (**29-54**) were prepared following the reaction conditions of Scheme 1 and were enzymatically evaluated against TTBK1 and TTBK2 as outlined before. Data are summarized in Table 2, revealing more potent TTBK1 inhibitors in this second set of compounds with  $IC_{50}$  values in submicromolar range. Furthermore, and although selectivity in these two isoenzymes is a great challenge, compounds **29** and **39** may be considered as TTBK1 selective inhibitors as a factor of 10 is present in their  $IC_{50}$  values.

**Table 2.** Chemical structure, yield and biological inhibition of the synthesized compounds **29-55** against TTBK1 and TTBK2.



Comp.	R <sup>1</sup>	R <sup>2</sup>	R <sup>3</sup>	R <sup>4</sup>	R <sup>5</sup>	Yield (%)	A. TTBK1 $IC_{50}$ (μM) or %inh@10 μM	B. TTBK2 $IC_{50}$ (μM) or %inh@10 μM	Selectivity index A/B
<b>29</b>	H	-O-	H	Cl	H	62	0.24 μM	4.22 μM	0.05
<b>30</b>	H	-O-	H	F	H	40	0.77 μM	3.02 μM	0.25
<b>31</b>	H	-O-	H	CN	H	6	0.44 μM	2.14 μM	0.20
<b>32</b>	H	-O-	H	OMe	H	63	0.54 μM	0.97 μM	0.55
<b>33</b>	H	-O-	H	CF <sub>3</sub>	H	74	5.03 μM	5%@10 μM	0.06

<b>34</b>	H	-O-	H	Br	H	83	0.75 $\mu$ M	1.21 $\mu$ M	0.61
<b>35</b>	H	-O-	H	NO <sub>2</sub>	H	83	0.42 $\mu$ M	1.24 $\mu$ M	0.33
<b>36</b>	H	-O-	H	NH <sub>2</sub>	H	9	0.52 $\mu$ M	4.90 $\mu$ M	0.10
<b>37</b>	H	-O-	H	Me	H	57	1.02 $\mu$ M	8.79 $\mu$ M	0.11
<b>38</b>	H	-O-	Me	H	H	80	2.20 $\mu$ M	6.40 $\mu$ M	0.34
<b>39</b>	H	-O-	Cl	H	H	62	1.55 $\mu$ M	1%@10 $\mu$ M	0.02
<b>40</b>	H	-O-	CF <sub>3</sub>	H	H	78	5.61 $\mu$ M	1%@10 $\mu$ M	0.06
<b>41</b>	H	-O-	OMe	H	H	33	0.84 $\mu$ M	6.79 $\mu$ M	0.12
<b>42</b>	H	-O-	H	H	Cl	79	0.53 $\mu$ M	0.49 $\mu$ M	1.08
<b>43</b>	H	-O-	H	H	OMe	64	3.56 $\mu$ M	9.54 $\mu$ M	0.37
<b>44</b>	H	-O-	H	Cl	Cl	63	2.30 $\mu$ M	5.72 $\mu$ M	0.40
<b>45</b>	NH <sub>2</sub>	-O-	H	Cl	H	70	0.45 $\mu$ M	2.70 $\mu$ M	0.16
<b>46</b>	NH <sub>2</sub>	-O-	H	CF <sub>3</sub>	H	77	0.58 $\mu$ M	4.49 $\mu$ M	0.13
<b>47</b>	NH <sub>2</sub>	-O-	Cl	H	H	16	0.37 $\mu$ M	3.05 $\mu$ M	0.12
<b>48</b>	NH <sub>2</sub>	-O-	CF <sub>3</sub>	H	H	45	1.32 $\mu$ M	3.90 $\mu$ M	0.33
<b>49</b>	H	-S-	H	NO <sub>2</sub>	H	42	2.72 $\mu$ M	22.72 $\mu$ M	0.11
<b>50</b>	H	-S-	H	NH <sub>2</sub>	H	69	0.65 $\mu$ M	4.94 $\mu$ M	0.13
<b>51</b>	H	-OCH <sub>2</sub> -	H	H	H	28	0.75 $\mu$ M	1.21 $\mu$ M	0.61
<b>52</b>	H	-CO-	H	H	H	97	1.71 $\mu$ M	11.92 $\mu$ M	0.14
<b>53</b>	H	-CO-	H	F	H	19	1.50 $\mu$ M	5.4 $\mu$ M	0.27
<b>54</b>	H	-CO-	Cl	Cl	H	35	9%@10 $\mu$ M	-	-

In the light of these biological activities, some conclusions may be drawn: the preferred connector between the two phenyl rings is the ether one (-O-), followed by the thioether (-S-) and the carbonyl moiety (-CO-). In that sense, compounds **52** and **53**, with a carbonyl group linking the phenyl groups, resulted in less potency than their counterparts **27** and **30**, respectively, which have an ether group as linker. At the same time derivatives **35** and **36** were slightly more or equipotent than their thio- analogs **49** and **50**, respectively.

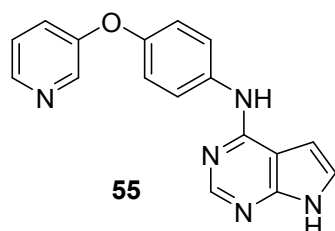
Introduction of an amino group in position 2 of the pyrrolopyrimidine core lead to potent compounds against TTBK1 but less selective (**29**, **33**, **39**, **40** vs **45-48** respectively).

Regarding the substitution in the second phenyl ring, a combination of steric and electrostatic factors may influence the inhibition of the two isoforms. Thus, the most selective TTBK1 inhibitors were derivatives **29**, **33**, **39** and, **40** with chlorine or

1  
2  
3 trifluoromethyl- substituents in positions *meta*- and *para*-, with compound **29** being  
4  
5 identified as the most potent and selective TTBK1 inhibitor.

6  
7 Finally, introduction of the pi-deficient pyridine heterocycle (compound **55**, Figure 4)  
8  
9 trends to increase selectivity in comparison to its analog **27**.

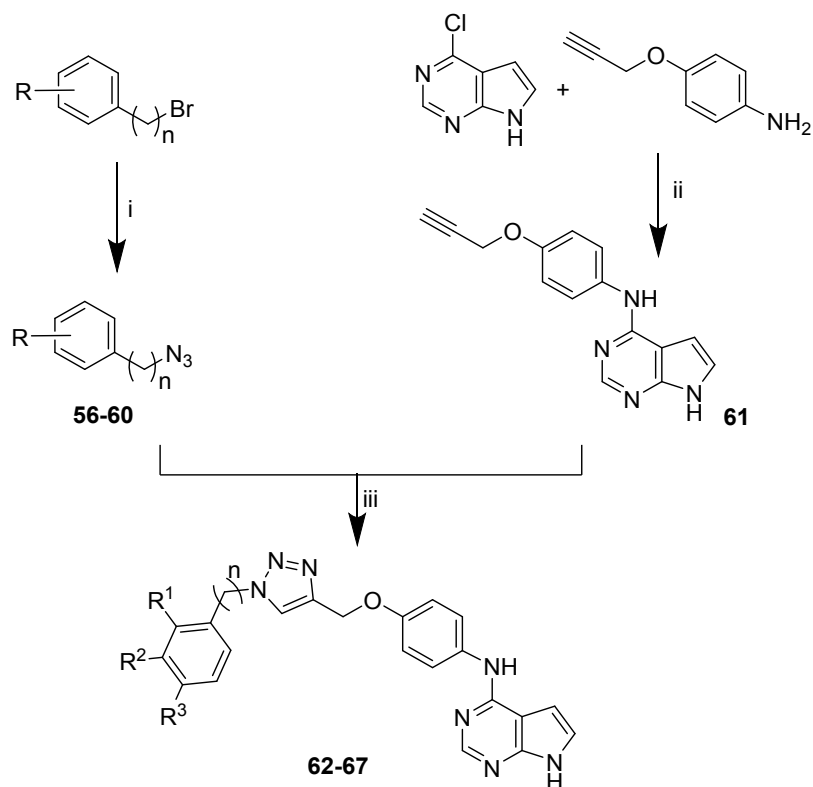
10  
11  
12  
13  
14  
15  
16  
17  
18  
19  
20  
21



Yield (%)	TTBK1 IC <sub>50</sub> (μM)	TTBK2 IC <sub>50</sub> (μM)	Selectivity index
35	0.75	6.05	0.12

22 **Figure 4.** Chemical structure, yield and inhibition of TTBK1/2 of compound **55**.

23  
24  
25  
26 A third subfamily of compounds were synthesized exploring modifications in the second  
27 aromatic group. In this series, we prepared a set of different organic azides (**56-60**) and  
28 the alkyne **61** and, using the copper(I)-catalyzed alkyne-azide cycloaddition (CuAAC)  
29 methodology,<sup>30</sup> new ligands bearing a triazole ring (**62-67**) were synthesized with good  
30 yields (Scheme 2, Table 3).  
31  
32  
33  
34  
35  
36  
37  
38  
39  
40  
41  
42  
43  
44  
45  
46  
47  
48  
49  
50  
51  
52  
53  
54  
55  
56  
57  
58  
59  
60



**Scheme 2.** i) NaN<sub>3</sub> (1.5 eq.), DMF, r.t.; ii) InCl<sub>3</sub> (0.1 eq.), MW, MeCN, 100 °C; iii) CuSO<sub>4</sub> (0.1 eq.), tris(benzyltriazolylmethyl)amine (0.1 eq.), sodium ascorbate (0.2 eq.), DMF, r.t.

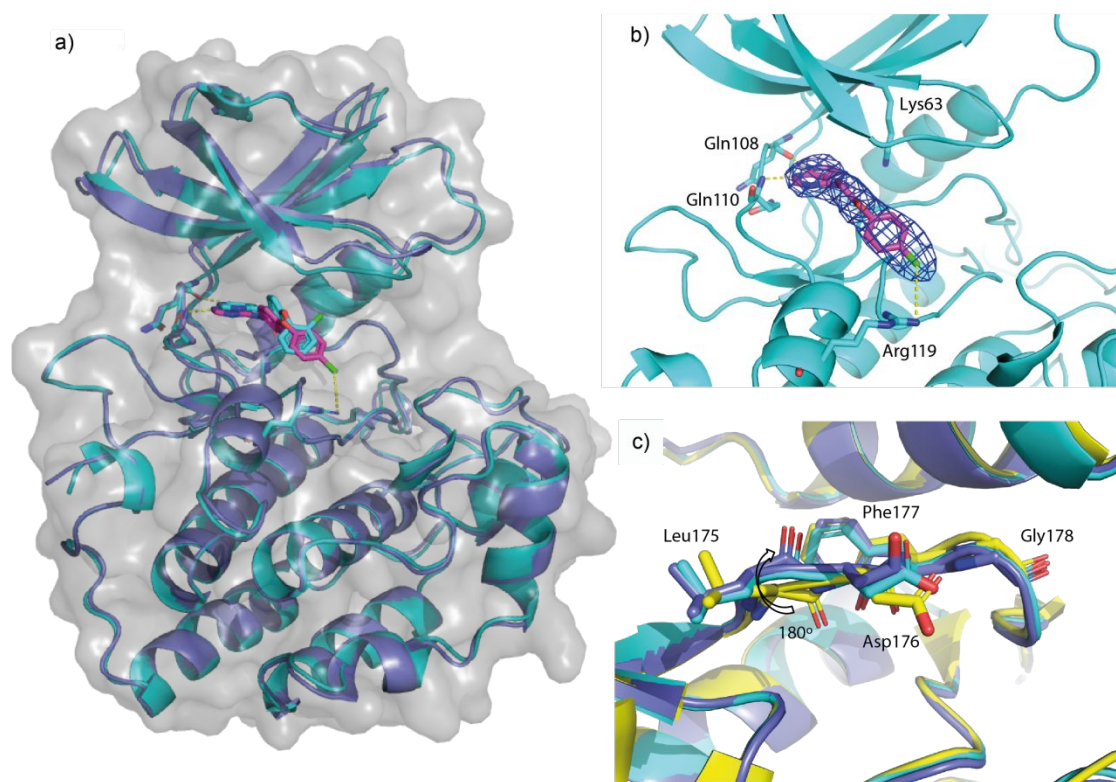
Data on this series are summarized in Table 3. In general, compounds containing a triazole ring resulted in moderate selective TTBK1 inhibitors.

**Table 3.** Chemical structure, yield and biological inhibition of the synthesized compounds **62-67** against TTBK1 and TTBK2.

Comp.	n	R <sup>1</sup>	R <sup>2</sup>	R <sup>3</sup>	Yield (%)	A. TTBK1 IC <sub>50</sub> (μM) or %inh@10 μM	B. TTBK2 IC <sub>50</sub> (μM) or %inh@10 μM	Selectivity index A/B
<b>62</b>	0	H	H	H	34	29%@10 μM	1%@10 μM	-
<b>63</b>	1	H	H	Cl	64	0.61 μM	2.87 μM	0.21
<b>64</b>	1	Cl	H	H	31	0.36 μM	2.75 μM	0.13
<b>65</b>	1	H	Cl	H	33	0.48 μM	2.03 μM	0.24
<b>66</b>	2	H	H	H	64	0.39 μM	2.61 μM	0.15
<b>67</b>	1	H	H	CH <sub>3</sub>	73	0.99 μM	1.75 μM	0.57

## 2.2. Elucidation of ligand-kinase binding modes

Since the homology of kinase domains of the two isoforms is high with 88% identity and 96% similarity, we aimed to crystallize different protein-ligand complexes and computationally study the binding mode of the compounds with the different kinases in order to explain the experimentally-observed selectivity of the synthesized inhibitors. For this purpose, we crystallized the kinase domain of TTBK1 (13-313) and TTBK2 (6-299) (see experimental section for detailed information) with different compounds, including **23**, **27**, **29**, **32** and **42** (Figure S1, Figure 5, Table S1). Among these the derivatives **29** and **42** (Figure 5) were of particular interest as they had different affinities for TTBK1 and TTBK2.



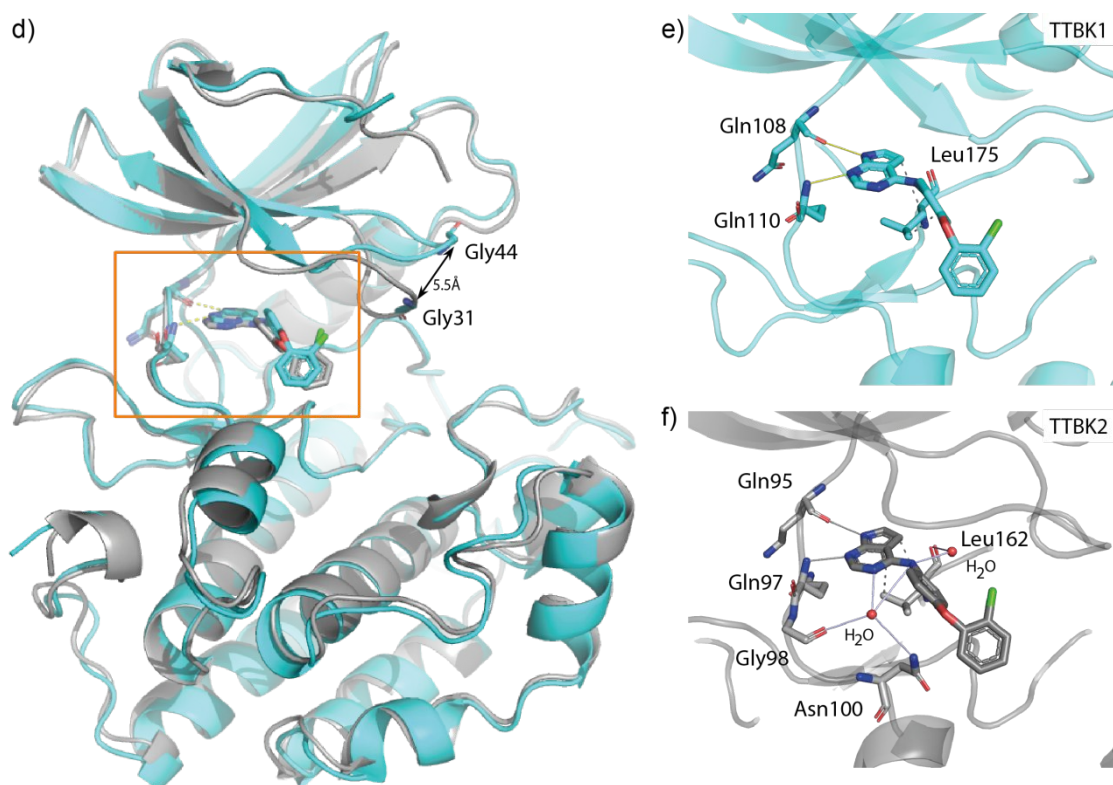


**Figure 5.** Crystal structures determined by X-ray diffraction of the synthesized compounds with the kinase domain of TTBK: a) Structure of TTBK1 in complex with **29** (in cyan) and **42** (in purple); b) Density map and binding mode of **29** with TTBK1 showing interaction with Arg119; c) TTBK1 bound to pyrrolopyrimidines displays a flipped conformation of the backbone carbonyl in Leu175 previous to the DFG (Asp176 – Phe177 – Gly178) motif, compared to ATP bound TTBK1 (yellow PDB id. 4BTJ); d) Superposition of the structures of TTBK1 (cyan) and TTBK2 (grey) bound to compound **42**; e) f) detail of the interactions of compound **42** with TTBK1 and TTBK2 (respectively).

The structures confirmed that all compounds bound to the ATP pocket forming canonical hydrogen bonds with the hinge region residues Gln108 and Gln110 of TTBK1 and residues Gln95 and Gln97 of TTBK2. Only in TTBK2 a water-mediated hydrogen bond was formed between the nitrogen in the position 1 of the pyrrolopyrimidine ring, Gly98 and Asn100. Crystal structures of TTBK1 with derivatives **29** and **42** were highly similar (Figure 5a, 5c). However, despite the initial hypothesis of interaction with the catalytic lysine located in the hydrophobic pocket, all the compounds displayed their aromatic substituents towards the front pocket. In this binding mode, the interaction between compound **29** and Arg119 in TTBK1, that was not observed in the complex with **42**, seemed to be important for the potency of the compound for TTBK1.

1  
2  
3 Comparison of the structures of compound **42** bound to both TTBK isoenzymes revealed  
4 some interesting points. first, the glycine-rich loop was displaced up to 5.5 Å between  
5 the two isoforms which may also be attributed to crystal packing (Figure 5d). In addition,  
6 this inhibitor formed two water-mediated hydrogen bonds with TTBK2 that were absent  
7 for TTBK1 (Figure 5e, 5f).  
8  
9  
10  
11  
12

13  
14 A conformational change N-terminal to the DFG motif appeared to be induced by these  
15 pyrrolopyrimidines, resulting in flipping of the backbone carbonyl of Leu175 compared to  
16 the canonical TTBK1 conformation (Figure 5c). This flip is also observed for TTBK2  
17 allowing the establishment of a water-mediated-hydrogen bond between Leu162 and the  
18 exocyclic amine group (Figure 5f). The DFG region has been previously demonstrated  
19 to exhibit high plasticity allowing alternative DFG conformations in various kinases.<sup>31</sup> In  
20 addition, such conformational flip allowed Leu175 N-terminal to the DFG motif to form  
21 hydrophobic stacking with the pyrrolopyrimidine moiety, a binding mode unique to a  
22 subset of kinases that enables an accommodation of kinase inhibitors in the back pocket  
23 and may increase inhibitor potency and selectivity.<sup>32</sup>  
24  
25  
26  
27  
28  
29  
30  
31  
32  
33  
34  
35

36 Since all the residues within (5 Å radius to the ligand are 100% conserved in both  
37 isoforms, the observed compound selectivity likely resulted from different dynamic  
38 behavior. We therefore performed a molecular mechanic experiment to explain the SAR  
39 studies and the selectivity of the compounds towards both isoforms. We use the crystal  
40 structures that we obtained as a starting point of these studies. Docking using Glide  
41 software and subsequent MM-GBSA calculations were performed to obtain a correlation  
42 between calculated free binding energies ( $\Delta G_{\text{bind}}$ ) and the observed  $IC_{50}$  values of the  
43 active compounds (**1-55**) against TTBK1. A good correlation coefficient was obtained  
44 ( $R^2= 0.7733$ ), which allowed us to validate these calculations and study the relationship  
45 between the predicted free energy values and the experimentally biological activity data  
46 (Figure S2).  
47  
48  
49  
50  
51  
52  
53  
54  
55  
56  
57  
58  
59  
60



1  
2  
3 Taking into an account the particular contribution of the energetic terms to the total  
4  $\Delta G_{\text{bind}}$ , we observed that Coulomb interactions are important to the increased potency of  
5 the compounds and penalize those with lower  $IC_{50}$  values together with van der Waals  
6 energies which were also rather low for those compounds with  $pIC_{50}$ s below 5.5 (Table  
7 S2). These energetic contributions are also important when comparing the free binding  
8 energies for selective and non-selective inhibitors, were differences up to 11 Kcal/mol  
9 are found in the solvation contribution term (Table S3).  
10  
11

12  
13  
14 In order to study the dynamics of the binding with the different isoforms, we next  
15 performed molecular dynamic (MD) studies with selected compounds. Thus, we studied  
16 complexes of both isoforms with inhibitors **29**, **39** and **42** which present different patterns  
17 of substitution in the second aromatic ring and different selectivity profiles. Crystal  
18 structures were used as starting point for complex **29**-TTBK1, **42**-TTBK1 and **42**-TTBK2.  
19 For those cases where the experimental structure was not available, the binding pose  
20 obtained by docking studies was the initial point for the MDs.  
21  
22

23  
24 It was noticed that all the compounds are stable in the catalytic cavity except for  
25 compound **39** (Figure 6a). The root-mean-square deviation of atomic positions (RMSD)  
26 value for this compound along the MD study doubles the rest of the compounds which  
27 might be directly related to its low potency for TTBK2 inhibition. It was observed that the  
28 stability of the modification in compounds within both isoforms was very similar, mainly  
29 of pyrrolopyrimidine and phenyl-ether moieties as it can be deduced from the root-mean-  
30 square fluctuations of the atoms (RMSF) calculations (Figure 6b). The main difference  
31 was the second ring (chloro-phenyl moiety), which was much more mobile in compound  
32 **39** (RMSF up to 4.5 Å) reinforcing the hypothesis of weak interaction for this molecule.  
33  
34 This compound was only able to establish short hydrophobic interactions; hence the  
35 second aromatic ring was not fixed within the front pocket (Figure S3). The potent  
36 compounds **29** and **42** remained tightly positioned towards the Arg119, although only  
37 compound **29** was able to establish halogen bonds with this residue.  
38  
39  
40  
41  
42  
43  
44  
45  
46  
47  
48  
49  
50  
51  
52  
53  
54  
55  
56  
57  
58  
59  
60

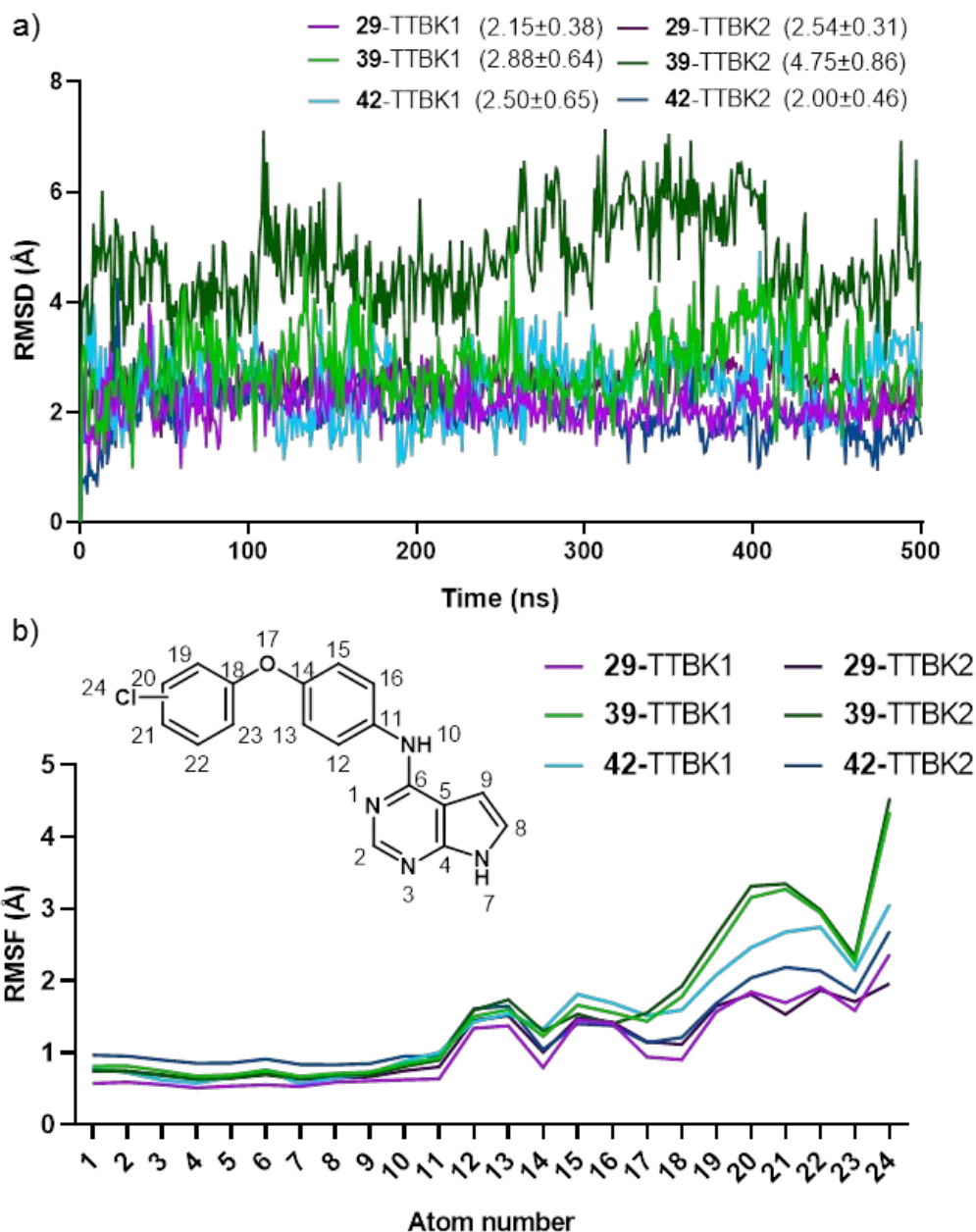


**Figure 6.** a) RMSD of the MD trajectories for compounds **29**, **39** and **42** in TTBK1 and TTBK2. b) RMSF of the atoms within compound **29**, **39** and **42** during the molecular dynamic studies.

To study carefully how the conformation of the compounds changed during the MD, we clustered every trajectory based on the position of the ligand atoms in each simulation. This allowed us to confirm how stable both compounds **29** and **42** are when interacting with TTBK1 and/or TTBK2. On the contrary, compound **39** presented different conformations where the chlorophenyl moiety flipped, placing the second aromatic ring in different dispositions within the hydrophobic pocket impeding a stable conformation of

the ring and reinforcing the idea of weak interactions related to low potency of the compound (Figure 7).

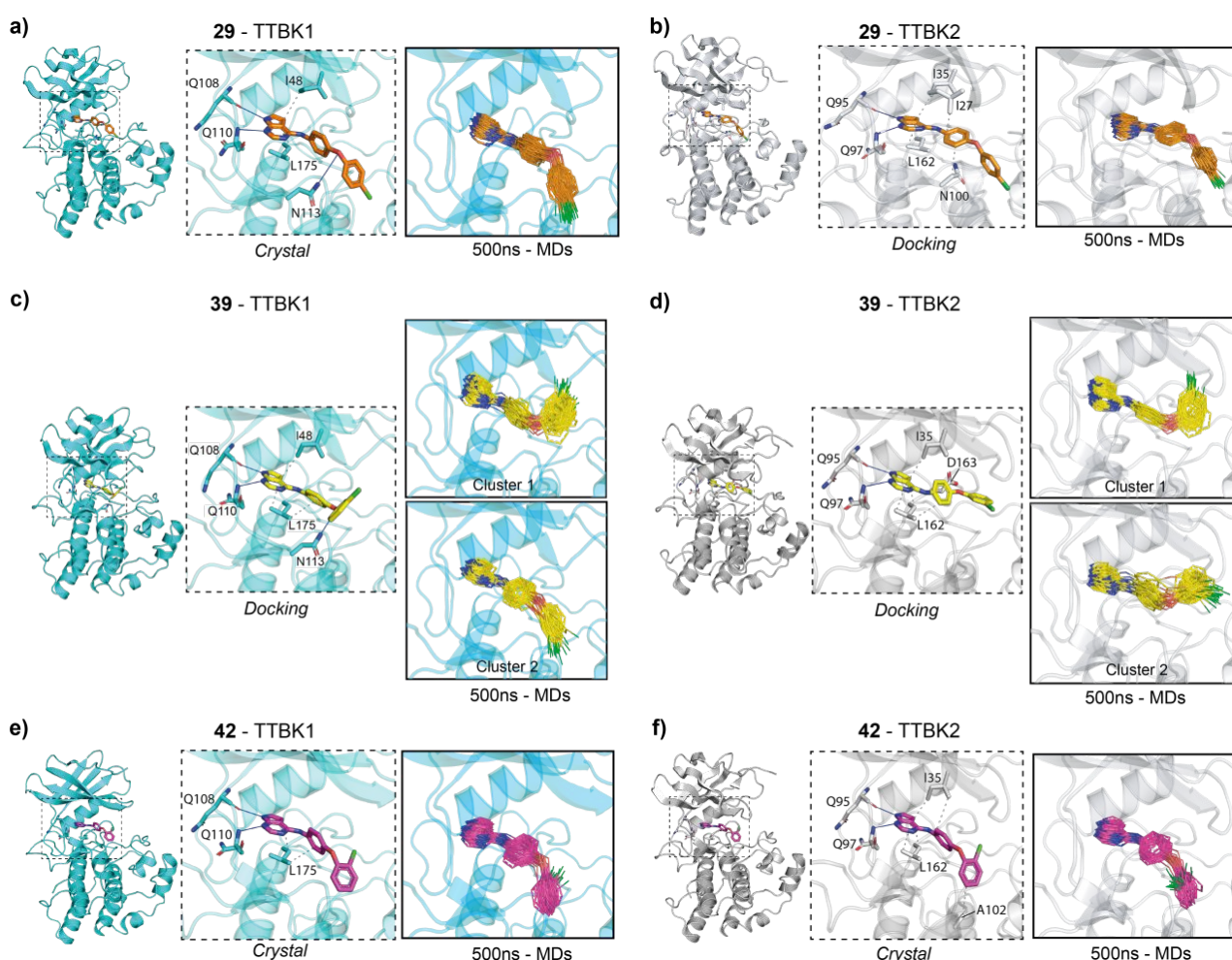


**Figure 7.** MD simulations of the compounds **29** (a-b), **39** (c-d) and **42** (e-f) with the kinase domain of TTBK1 (a, c, e) and TTBK2 (b, d, f). Middle panel shows a zoom with the interactions identified for each compound. Hydrogen bonds and hydrophobic interactions are shown as blue and gray lines. Right panel shows most populated clusters obtained from the analysis of the 500 ns MD simulation.

Finally, since these TTBK1 inhibitors were ATP-competitive, we performed a kinase profiling for a set of selected kinases from different families of the human kinome. We screened the TTBK1 inhibitor **29** at a fixed concentration of 10  $\mu$ M against more than twenty different kinases calculating the selectivity score (Figure 8). In this case, the  $S_{35}$  value, which determines the fraction of kinases that are targeted by the compound **29** beyond 35% of residual activity,<sup>33</sup> was 0.04, showing selectivity over similar kinases.

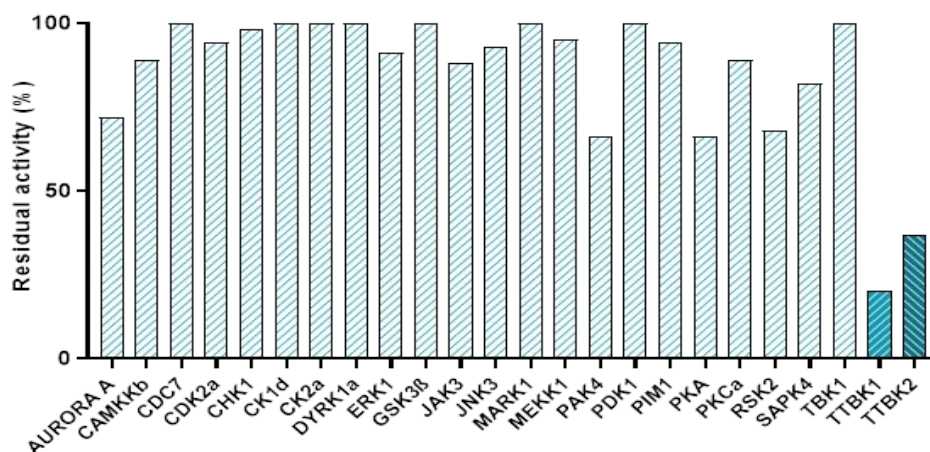
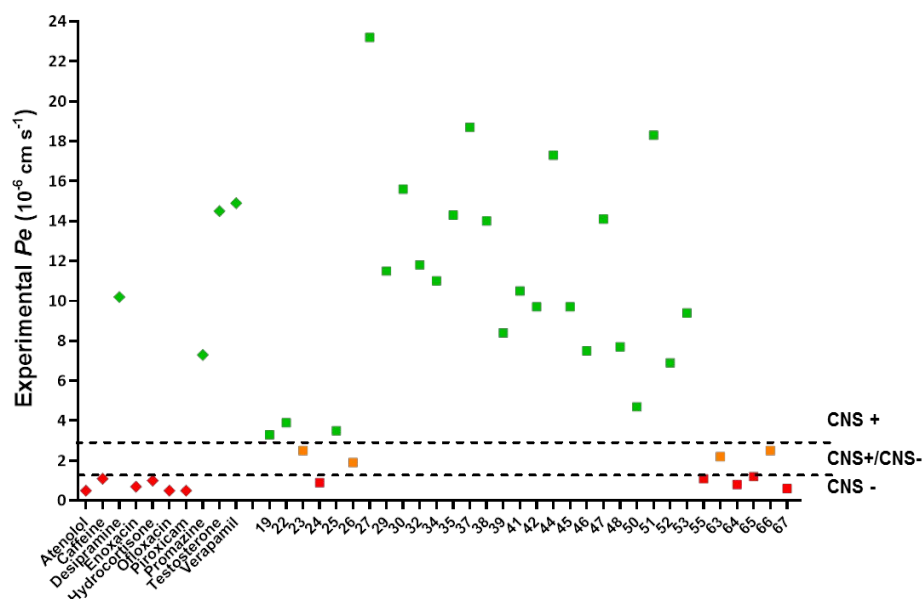


Figure 8. Kinase profiling of TTBK1 inhibitor derivative 29.

### 2.3 Blood-Brain Barrier permeability studies

An important property for a drug candidate or chemical probe that is intended to be used for exploring a central nervous system disease, such as ALS, is penetration through the blood-brain barrier (BBB). Using a parallel artificial membrane permeability assay (PAMPA), we determined the predicted brain permeability for all the compounds with adequate potency (TTBK1  $IC_{50}$  below 2.5  $\mu M$ ). Methodology and individual data are found in the experimental section and supplementary material (Table S4, Figure S4), while Figure 9 depicted the results of this assay. Compounds **31** and **36** were not soluble under the experimental conditions and could not be tested. In general, all the compounds are predicted as permeable over the BBB, with the exception of four compounds (**23**, **24**, **26** and **55**) and those ones containing the triazole ring (**63-67**). All these compounds were discarded from subsequent cellular assays.



**Figure 9.** Permeability across the blood-brain barrier of control drugs (diamonds) and TTBK1 inhibitors (squares) evaluated using PAMPA methodology (CNS+, permeable, green; CNS- not permeable, red; CNS+/- are in the shadow area and could or could not cross the barrier by passive permeation, orange).

#### 2.4 TDP-43 modulation by TTBK1 inhibitors in cellular cultures

The potential decrease of TDP-43 phosphorylation in cellular models was studied only for those brain-permeable TTBK1 inhibitors with a selectivity index regarding this isoform (below 0.25). These criteria resulted in 14 compounds that were tested initially in a human neuroblastoma cell-based model of induced TDP-43 phosphorylation. The SH-SY5Y cell line was exposed to the toxic insult of ethacrynic acid (EA) for 24 h which increased phosphorylated TDP-43 levels by glutathione depletion causing cell death.<sup>34</sup> In that model, the neuroprotective activity against EA was determined pre-treating the cells with the TTBK1 inhibitors 1 h prior the addition of EA (40  $\mu$ M). An initial cell viability study at different compound concentrations (5 and 10  $\mu$ M, Figure S5) ruled out derivative **30** and **31** from the assay and fixed the study dose at 5  $\mu$ M. As controls, we used a previously reported TTBK1 inhibitor, methyl 2-bromo-5-(7*H*-pyrrolo[2,3-*d*]pyrimidin-4-ylamino) benzoate (**AZ2**) re-synthesized in our laboratory, and the known GSK3 inhibitor, tideglusib, that showed good results in this cell-based ALS model.<sup>13</sup> As observed in Figure 10, three compounds (**29**, **37** and **39**) were neuroprotective in this model as they



rescued the cells from the death induced by EA (Figure 10a). The next step was to evaluate if this neuroprotective activity was due to direct modulation of TDP-43. Using Western-blot analysis, we showed that the new synthesized compounds were able to reduce TDP-43 hyperphosphorylation to control levels at the important epitopes Ser409 and Ser410, however the reported TTBK1 inhibitor **AZ2** did not produce such an effect significantly (Figure 10b). We then determined the IC<sub>50</sub> of **AZ2**, following the same procedure previously described for the pyrrolopyrimidine compounds, determining values much higher and less selective (TTBK1 IC<sub>50</sub> 2.2 μM; TTBK2 IC<sub>50</sub> 4.2 μM) than those measured on our derivatives, which may explain the lack of reduction in TDP-43 phosphorylation.

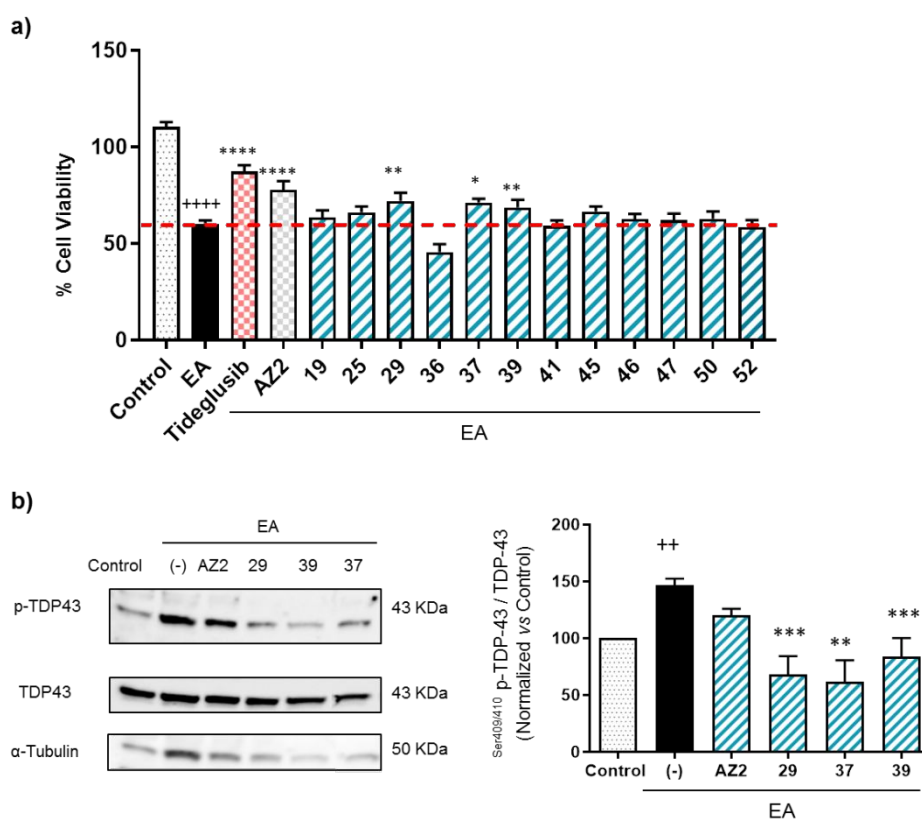


**Figure 10.** Neuroprotective effect of TTBK1 inhibitors in ethacrynic acid treated SH-SY5Y neuroblastoma cells. a) Cell viability measured by MTT assay after being exposed to EA for 24 h in the presence or absence of drugs treatment (5 μM). b) Representative immunoblot showing TDP-43 phosphorylation levels of SH-SY5Y cells treated with compounds **AZ2**, **29**, **37** and **39** (5 μM). Each data point represents the mean ± SEM of three replications in four different experiments (\*p < 0.05; \*\*p < 0.01, \*\*\*p < 0.001, \*\*\*\*p < 0.0001 significantly different from EA-treated cells; ++p < 0.01, +++p < 0.0001 significantly different from control cells).

We have previously shown that decreased TDP-43 phosphorylation by other kinase inhibitors such as CDC7, CK1 or GSK3 inhibitors restore the physiological nuclear localization of TDP-43.<sup>13-15</sup> To test if the decrease of TDP-43 phosphorylation using TTBK1 inhibitors also reestablishes the homeostasis of TDP-43 raising its nuclear localization, we carried out immunofluorescence analyses in EA-treated SH-SY5Y cells. Our findings demonstrated that compound **29** reduced the cytosolic accumulation of TDP-43 in EA-treated cells, restoring its nuclear localization and therefore the homeostasis of the main pathological hallmark of ALS (Figure 11).

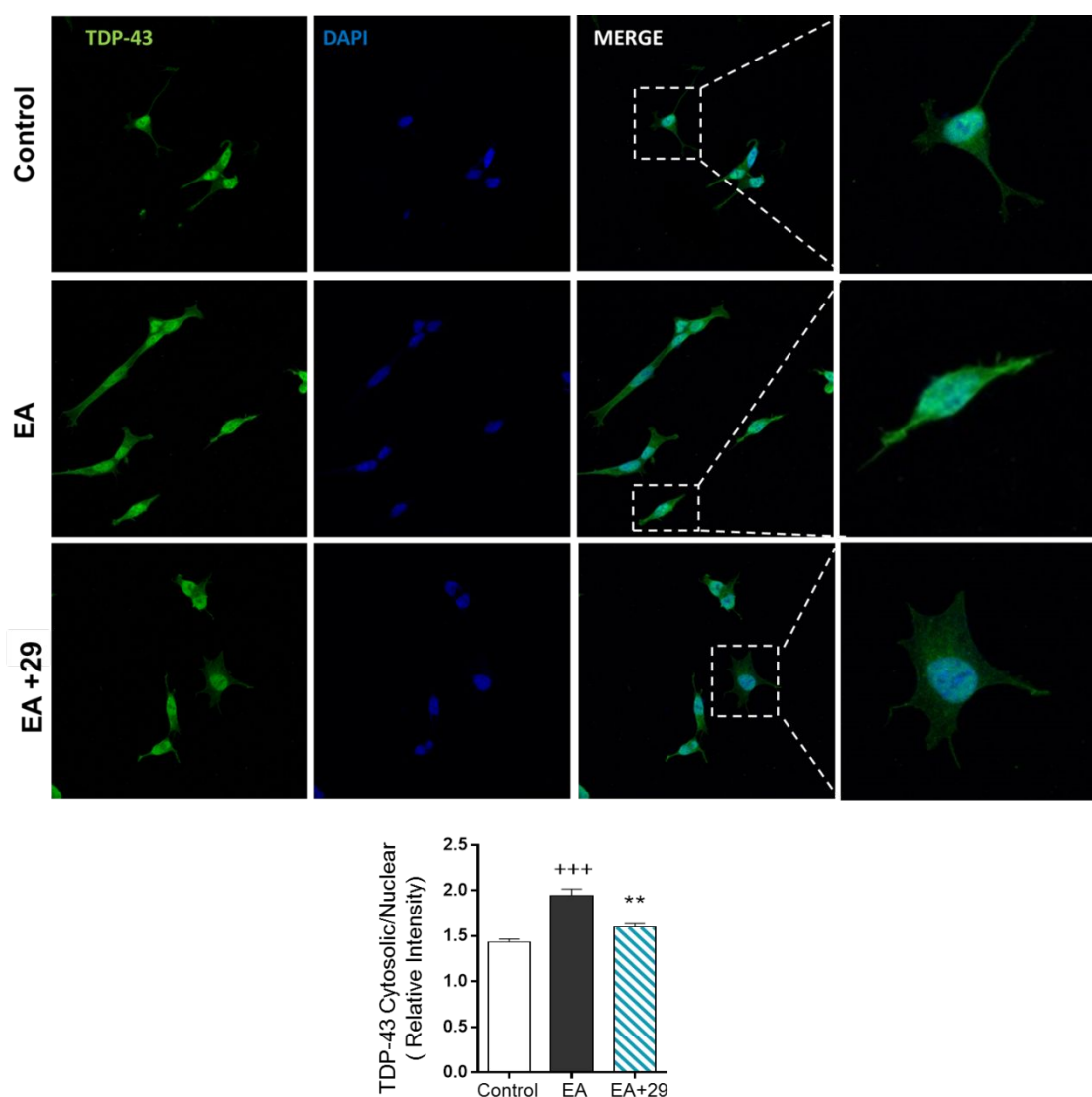


**Figure 11.** Immunofluorescence analysis of the subcellular localization of TDP-43 in SH-SY5Y cells. Cells were pre-treated with compound **29** (5  $\mu$ M) and exposed to EA (40  $\mu$ M) for 24 hours. TDP-43 localization was assessed by Confocal Laser Scanning Microscopy. Scale bar: 10  $\mu$ m and 20  $\mu$ m. Quantification of cytosolic TDP-43 was analysed in at least 50 different cells from 3 separate wells (n=3). Data represent the

1  
2  
3 mean  $\pm$  SEM (magnification 63x). (\*\* $p < 0.005$  significantly different from SH-SY5Y EA-treated cells,  
4 +++ $p < 0.001$  significantly different from control).  
5  
6  
7  
8

9 TTBK1 is an enzyme that has been linked to Alzheimer's disease and  
10 hyperphosphorylation of tau, especially at epitope Ser422, important for the pretangle  
11 formation. Recently, some non-specific TTBK1/2 inhibitors have shown the ability to  
12 reduce tau phosphorylation both in cellular models and *in vivo*.<sup>16</sup> For this reason, the new  
13 synthesized TTBK1 ligands were evaluated in a model of tau hyperphosphorylation  
14 induced by okadaic acid (OA).<sup>35</sup> In that assay, the compounds were able to rescue the  
15 SH-SY5Y cells from death induced by OA at two different compound concentrations of  
16 1 and 5  $\mu\text{M}$  (Figure S6), confirming that our TTBK1 inhibitors in addition to TDP-43, also  
17 reduce the toxicity exerted by tau phosphorylation expanding their therapeutic potential  
18 for different tauopathies.  
19  
20  
21  
22  
23  
24  
25  
26  
27  
28  
29  
30

### 31 **2.5 Immunomodulatory effect of TTBK1 inhibition**

32  
33 Chronic inflammation is another common feature observed in ALS, indicating an  
34 essential role of microglia in disease development and progression.<sup>36</sup> Thus, we decided  
35 to study the potential role of TTBK1 inhibition in microglia and its immunomodulatory  
36 effects. Therefore, we evaluated the effect of compound **29** on the expression of  
37 inducible nitric oxide synthase (iNOS) and of the triggering receptor expressed on  
38 myeloid cells 2 (TREM2) in primary cultures of rat microglia after 24 h exposure to the  
39 widely used pro-inflammatory stimulus lipopolysaccharide (LPS, 100 ng/mL). iNOS is  
40 widely considered a marker of M1 neurotoxic microglia, while TREM2 a marker of M2  
41 neuroprotective microglia. When cells were stimulated with LPS, we observed the  
42 expected iNOS induction, which was reduced by the treatment with compound **29**, along  
43 with an increase in TREM2 expression (Figure 12) suggesting an immunomodulatory  
44 effect of the TTBK1 inhibitor **29**. Compounds that induce microglia switch from  
45  
46  
47  
48  
49  
50  
51  
52  
53  
54  
55  
56  
57  
58  
59  
60



inflammatory M1-type to anti-inflammatory M2-type have been proposed to attenuate neuro-inflammation and bolster neuronal protection and recovery.<sup>37</sup>

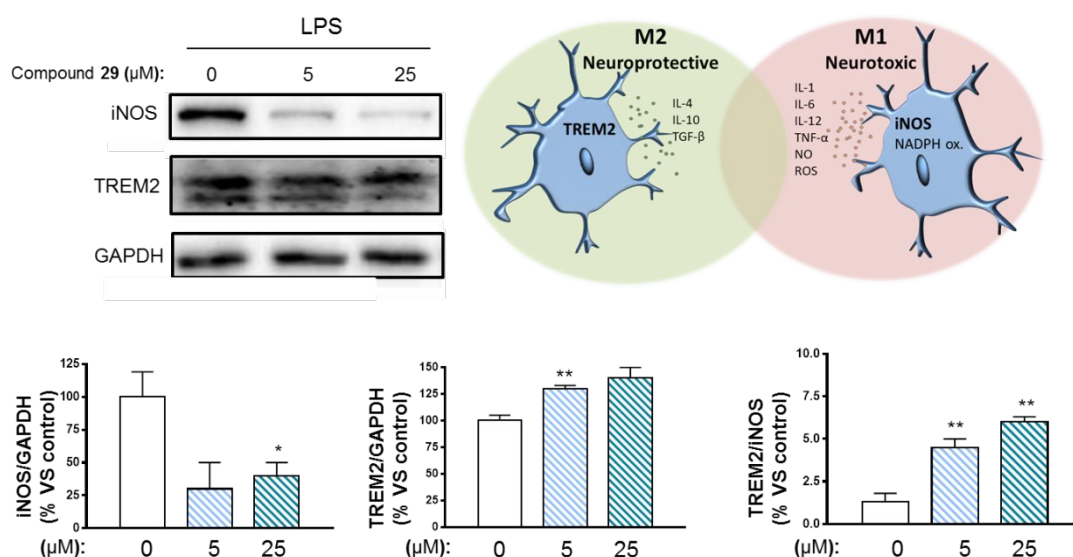


**Figure 12.** Immunomodulatory effect of compound **29** in primary rat microglial cells. Representative immunoblot showing iNOS and TREM2 protein expression in LPS-treated (100 ng/mL) microglia cells in the presence or absence of compound **29** at increasing concentrations (5 and 25 μM). GAPDH was used for endogenous normalization. Densitometric data represent the mean ± SEM of 3 independent experiments. (\*p < 0.05; \*\*p < 0.01 significantly different from LPS-treated control cells).

## 2.6 *In vivo* TDP-43 modulation by a TTBK1 inhibitor

Based in the promising results showed by the new TTBK1 inhibitors in cellular models, we explore the effects of compound **29** in the TDP-43 (A315T) transgenic mouse model, one of the first experimental models of ALS based on mutations in TDP-43 protein.<sup>38</sup>

Firstly, we investigated the plasma pharmacokinetics and brain distribution of compound **29** in BALB/c wild type mice following a single intraperitoneal dose administration at 5 mg/kg or oral administration at 10 mg/kg. Results are collected in Table 4 and show that compound **29** exhibits the greatest plasma concentration between 1 to 2 h, suggesting prolonged absorption and a high brain penetration in mice by the two routes of administration. Based on these results, we decided to use the intraperitoneal dose of 5 mg/kg in the efficacy study.

**Table 4.** Pharmacokinetic parameters of compound **29** in plasma and brain following a single intraperitoneal (Dose: 5 mg/kg) and oral (Dose: 10 mg/kg) administration in male BALB/c mice.

Route	Dose	Matrix	T <sub>max</sub> (h)	C <sub>max</sub> (ng.mL <sup>-1</sup> )	AUC <sub>last</sub> (h.ng.mL <sup>-1</sup> )	T <sub>1/2</sub> (h)	Brain-Kp (AUClast)
i.p	5 mg/kg	Plasma	1.00	1429.08	5958.82	3.75	2.63
		Brain <sup>a</sup>	1.00	4174.12	15652.49	3.46	
p.o	10 mg/kg	Plasma	2.00	2265.04	18406.33	3.30	2.67
		Brain <sup>a</sup>	2.00	4923.89	49172.57	3.40	

<sup>a</sup>Brain concentration and AUC. expressed as ng.g<sup>-1</sup> and h.ng.g<sup>-1</sup> respectively.

To this end, TDP-43 (A315T) transgenic mice and wild-type animals were daily treated with the TTBK1 inhibitor **29** or vehicle from the age of 65 days up to 95 days. The main goal of our study was to confirm the previously observed TDP-43 phosphorylation decrease and immunomodulatory effect of **29** together with the potential effect of these two relevant biological events in motor neuron preservation in the spinal cord.

We first analysed whether chronic treatment with our TTBK1 inhibitor could prevent enhanced TDP-43 phosphorylation *in vivo*. Immunoblot analyses shown in Figure 13 revealed an increase in TDP-43 phosphorylation levels at the lumbar region in the spinal cord of transgenic mice compared to wild-type animals, which was statistically significantly reduced with compound **29** treatment (Figure 13a). No apparent effect on total levels of TDP-43 was appreciated between transgenic groups (Figure 13b).

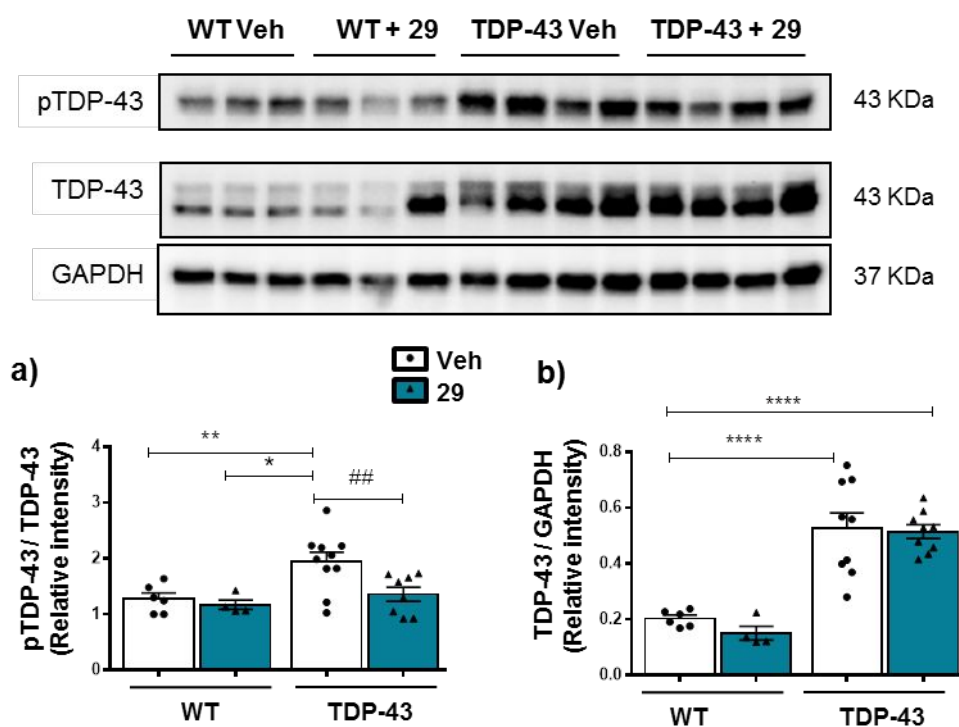


**Figure 13.** TDP-43 phosphorylated (a) and total TDP-43 (b) levels in the spinal cord of transgenic TDP-43 and wild-type mice treated with compound **29** or vehicle. Representative immunoblots are shown. Data represent the mean  $\pm$  SEM of different observations. Data were assessed by one-way ANOVA followed by the Bonferroni test ( $*p < 0.05$ ,  $**p < 0.01$ ,  $****p < 0.00001$  vs. WT group;  $##p < 0.01$  vs. TDP-43-Veh group).

We have already mentioned the pathogenic role of glial reactivity and related inflammatory processes in ALS neurodegeneration. In order to confirm the immunomodulatory effect of compound **29** *in vivo*, we examined iNOS and TREM2 protein expression in the spinal cord of TDP-43 (A315T) transgenic mice treated with **29** by Western Blot analysis. TDP-43 transgenic mice showed an increased in iNOS expression compared to wild type animals, which was significantly reduced in **29**-treated animals (Figure 14a). This effect was accompanied by an increase in the anti-inflammatory microglial marker TREM2 (Figure 14b), confirming the microglia switch from pro-inflammatory M1-type to anti-inflammatory M2-type (Figure 14c) observed in the *in vitro* studies. Similar results were obtained by immunofluorescence analysis, where treatment with TTBK1 inhibitor **29** decreased both microglial (Iba-1) and astrocytes (GFAP) reactivity compared to the controls (Figure S7).

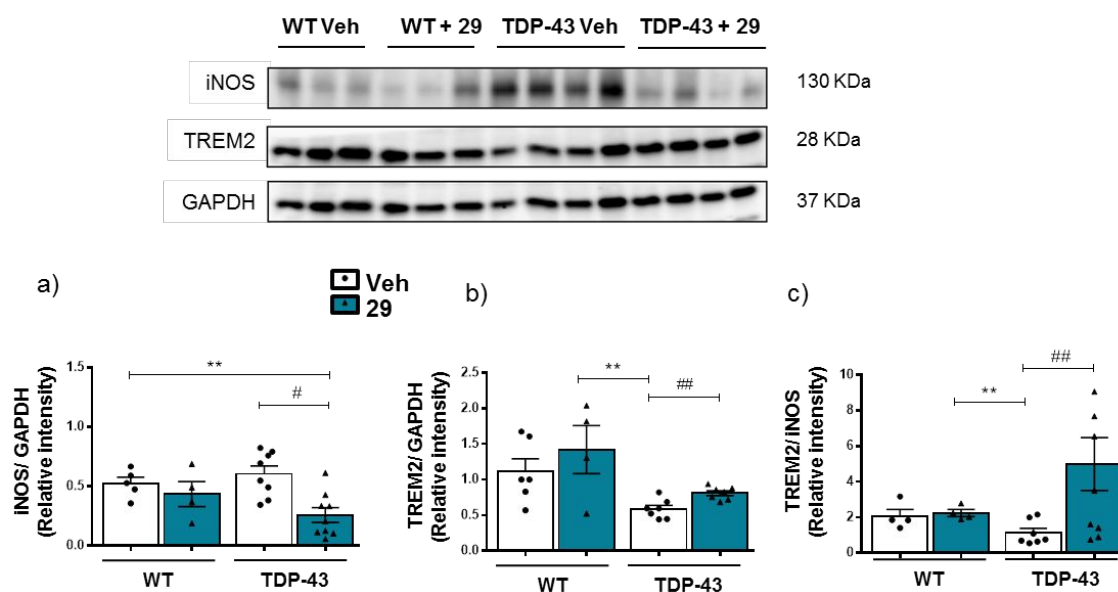


**Figure 14.** Immunomodulatory effect of compound **29** in the lumbar region of the spinal cord of wild-type and TDP-43 transgenic mice. Protein expression and densitometric data of (a) iNOS (b) TREM2 and (c) the ratio TREM2/iNOS showing microglia switch from inflammatory M1-type to anti-inflammatory M2-type. GAPDH was used for endogenous normalization. Representative immunoblot are shown. Densitometric data represent the mean  $\pm$  SEM of different observations. Data were assessed by one-way ANOVA followed by the Bonferroni test (\*\* $p < 0.01$  vs. WT group; # $p < 0.05$ , ## $p < 0.01$  vs. TDP-43-Veh group).

Finally, we investigate if the reduction of TDP-43 phosphorylation combined with the anti-inflammatory effect observed in the spinal cord of the transgenic mice treated with compound **29**, contributes to avoid the motor neuron degeneration typical of this TDP-43 transgenic mice at advanced stages of disease progression. The reduction in the number of motor neurons observed in the ventral horn in transgenic animals, measured by two different markers: Nissl staining and choline acetyl transferase (ChAT) immunohistochemistry, was significantly prevented in those animals that received compound **29** as treatment (Figure 15).

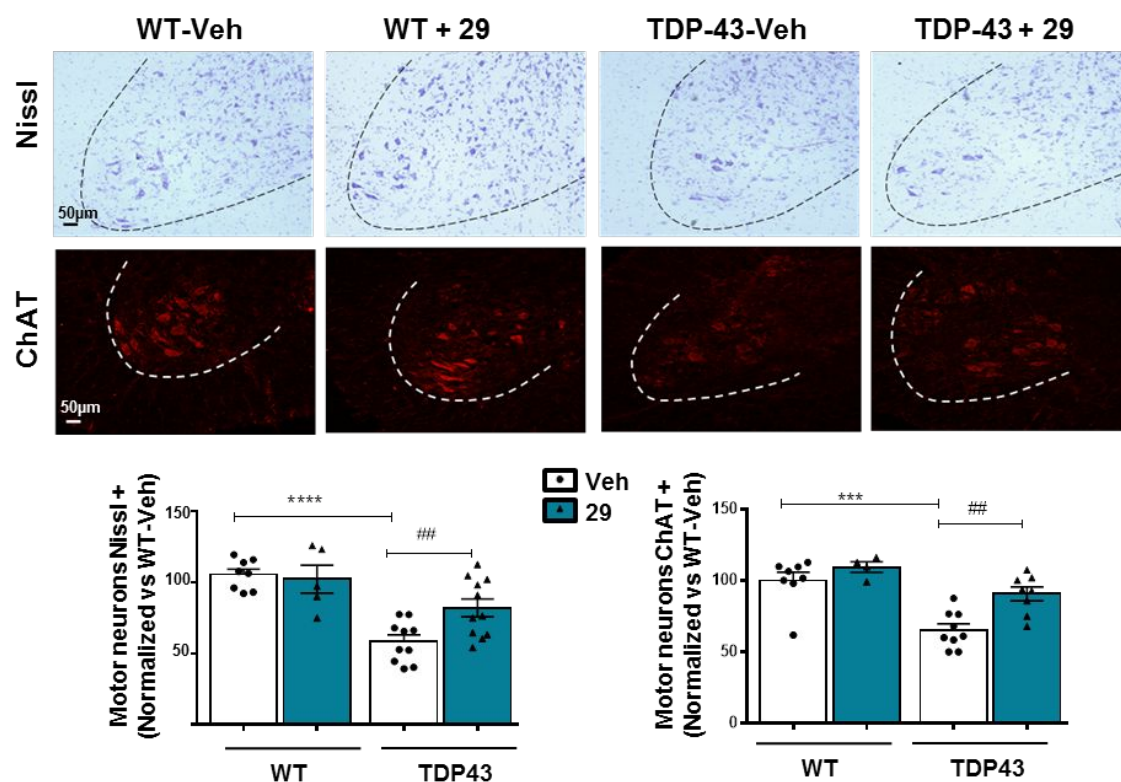


**Figure 15.** Representative images of Nissl-stained motor neurons and ChAT immunostained sections in the anterior horn of the spinal cord of TDP-43 mice and wild-type treated with compound **29** or vehicle. Quantification of the number of motor neurons Nissl+ and ChAT+ normalized vs WT-Veh is shown. Data were assessed by one-way ANOVA followed by the Bonferroni test (\*\*p < 0.001, \*\*\*\*p < 0.0001 vs. WT-Veh group; ##p < 0.01 vs. TDP-43-Veh).

Taken together, these results demonstrate that TTBK1 inhibition is a potential, effective and viable strategy to protect motor neuron degeneration in ALS and TDP-43 proteinopathies in murine models, and the pyrrolopyrimidine **29** may be a good drug candidate for further development.

## 2.7 TTBK1 inhibitor modulates TDP-43 pathology in a patient cell-based ALS model

Finally, with the aim to help in the translation of these promising results to the clinical setting, the modulatory effect of compounds **29** and **39** on the TDP-43 homeostasis was tested in a remarkable human cell-based model of the disease recently developed in our group. Cultures of immortalized lymphocytes from ALS patients recapitulate very well TDP-43 pathological features and represent a novel and effective platform to evaluate

1  
2  
3 new drugs.<sup>39</sup> Lymphocytes were obtained from blood samples of patients or healthy  
4  
5 individuals (Table 5) after written informed consent.  
6  
7

8 **Table 5.** Demographic and clinical characteristics of subjects included in this study  
9

	Control (n=5)	ALS (n=5)
<b>Gender (M/F)</b>	(2/3)	(2/3)
<b>Age (<math>\pm</math> SD)</b>	62 $\pm$ 7	65 $\pm$ 1
<b>Type of onset</b>		
Bulbar	NA	4
Limb	NA	1

10  
11  
12  
13  
14  
15  
16  
17 Control: Individuals without sing of neurological degeneration; NA: not applicable.  
18 All patients were negative for *SOD1*, *TARDBP* and *C9orf72* mutations.  
19  
20

21 Thus, to confirm the privileged therapeutic profile of TTBK1 inhibitors in the modulation  
22 of TDP-43 proteinopathy, sporadic ALS-patient lymphoblasts were treated with both  
23 compounds for 24 h resulting in reduced phosphorylation and cytosolic levels of TDP-  
24 43, with simultaneous recovery of nuclear TDP-43 localization (Figure 16). These results  
25 highlight and demonstrate the importance of TTBK1 in the modulation of TDP-43  
26 proteinopathy in a human cell-based model of sporadic ALS and reinforce the novelty of  
27 TTBK1 inhibition as an interesting approach for the pharmacological treatment of this  
28 devastating disease.  
29  
30  
31  
32  
33  
34  
35  
36  
37  
38  
39  
40  
41  
42  
43  
44  
45  
46  
47  
48  
49  
50  
51  
52  
53  
54  
55  
56  
57  
58  
59  
60

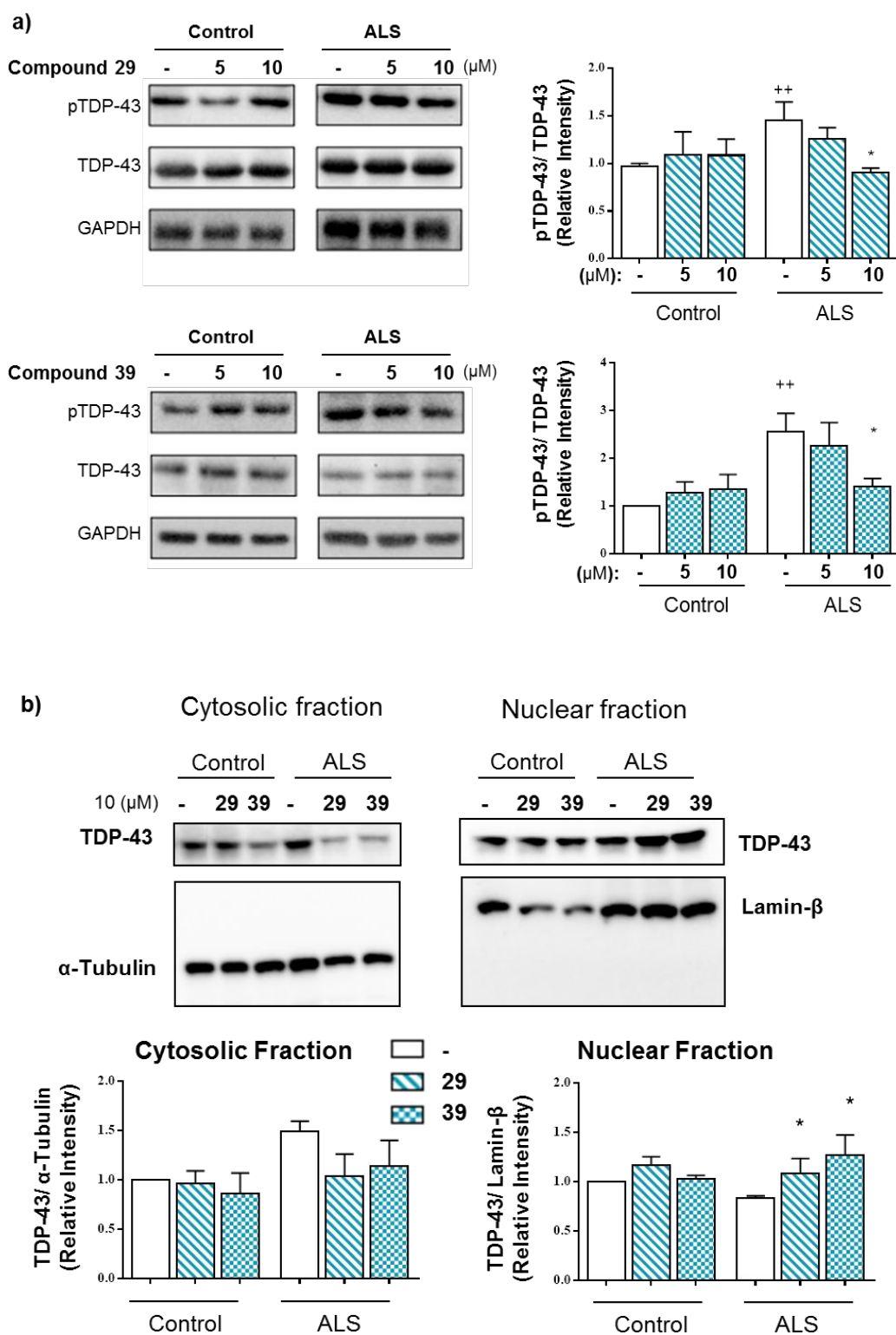


**Figure 16.** Effects of TTBK1 inhibitors on phosphorylation and subcellular localization of TDP-43 in ALS and control lymphoblasts. 24 h after compounds **29** and **39** addition, cells were harvested and processed for Western blotting analysis. a) Representative immunoblots showing the effect of TTBK1 inhibitors decreasing TDP-43 phosphorylation. b) Cytosolic and nuclear fractions analyzed by Western blotting.  $\alpha$ -tubulin and Lamin B1 antibodies were used as loading and purity control of the cytosolic and nuclear fractions,

1  
2  
3 respectively. Densitometric analyses represent the mean  $\pm$  SEM of different observations carried out in  
4 independent cell lines ( $n = 5$ ) from each group ( $*p < 0.05$  significantly different from ALS untreated cells).  
5

## 6 7 **Conclusions**

8  
9 Overall, we have achieved the design, synthesis and optimization of a new family of  
10 small molecules resulting in rather potent and selective TTBK1 inhibitors based on a  
11 pyrrolopyrimidine scaffold. These compounds showed ability to decrease TDP-43  
12 phosphorylation both in *in vitro* and in a TDP-43-transgenic mice model, demonstrating  
13 their relevance as lead structures for different TDP-43-pathies such as ALS. Moreover,  
14 in two different cellular models, including a ALS patient cell-based model, the developed  
15 TTBK1 inhibitors were able to recover the nuclear/cytosolic balance of TDP-43 which  
16 emphasizes the therapeutic potential of these compounds. Interestingly, experimentally  
17 calculated brain permeability predicted a good brain penetration for several compounds  
18 that was confirmed experimentally *in vivo* for compound **29** showing a ratio brain-to-  
19 plasma of 3:1. In addition, crystal structures of ligand complexes for TTBK1 and TTBK2  
20 can throw some new clues for specific TTBK1 modulation.  
21  
22  
23  
24  
25  
26  
27  
28  
29  
30  
31  
32  
33  
34

35 Altogether, we reported a new family of TTBK1 inhibitors that for the first time modulate  
36 TDP-43 pathology in different models and can be considered new disease modifying  
37 drugs for ALS and others TDP-43-pathies such as FTD, LATE or Alexander's syndrome.  
38  
39 Only future clinical trials will have the final confirmation of their therapeutic relevance.  
40  
41  
42  
43  
44  
45  
46  
47

## 48 **Experimental Section**

### 49 **Chemistry**

50 Reagents were obtained from the commercial sources and used without further  
51 purification. Purifications of crudes were performed with the indicated solvent as eluent  
52 by flash column chromatography carried out at medium pressure using silica gel (E.  
53 Merck, Grade 60, particle size 0.040–0.063 mm, 230–240 mesh ASTM) or IsoleraOne  
54  
55  
56  
57  
58  
59  
60



1  
2  
3 flash purification system from Biotage.  $^1\text{H-NMR}$  and  $^{13}\text{C-NMR}$  data were obtained from  
4 a Bruker AV300 or AV500 MHz spectrometer. Chemical shifts,  $\delta$ , are expressed in ppm  
5 and calculated taking the reference of the appropriated deuterated solvents. Signal  
6  
7 multiplicities (bs: broad signal, s: singlet, d: doublet, dd: doublet of doublets, ddd: doublet  
8  
9 of doublet of doublets, t: triplet, td: triplet of doublets, q: quartet, m: multiplet) and coupling  
10  
11 constants ( $J = \text{Hz}$ ) are indicated for each molecule. Acquired spectroscopic data was  
12  
13 analysed with MestreNova 10.2 software. The microwave assisted synthesis was carried  
14  
15 out using a Biotage Initiator eight single-mode cavity instrument from Biotage.  
16  
17 Experiments were performed with temperature control mode in sealed microwave  
18  
19 process vials. The temperature was measured with an IR sensor on the outside of the  
20  
21 reaction vessel. Stirring was provided by an in situ magnetic stirrer. High Performance  
22  
23 Liquid Chromatography (HPLC) analyses were performed in a Thermo Finnigan  
24  
25 Surveyor UV-Vis Plus Detector coupled with Finnigan<sup>TM</sup> LXQ <sup>TM</sup>. The column used for  
26  
27 the analysis was a SunFire<sup>®</sup> C18, 3.5 $\mu\text{m}$ , 4.6x50mm and UV-Vis spectra of the samples  
28  
29 were acquired. Melting points were determined in a Büchi Melting Point M-560. High  
30  
31 resolution mass spectrometry (HRMS) was done in a spectrometer Agilent 6500 using  
32  
33 positive electro spray techniques (ESI). Values are expressed in mass units ( $m/z$ ).  
34  
35 Elemental analyses were performed by the analytical department at CAI-UCM, and the  
36  
37 results obtained were within  $\pm 0.4\%$  of the theoretical values using the analyzer LECO  
38  
39 CHNS-932. All the final compounds have a purity  $\geq 95\%$  tested by HPLC.  
40  
41  
42  
43  
44  
45

46 General procedure for the synthesis of derivatives 1-55: (a) 1 eq of 6-chloro-7-  
47  
48 deazapurine, 6-chloropurine or 6-chlorothienopyrimidine, 1 eq of the corresponding  
49  
50 aniline and 0.1 eq of indium trichloride were dissolved in 2 mL of acetonitrile. The crude  
51  
52 is stirred under microwave irradiation at 100 °C until the completeness of the reaction.  
53  
54 (b) 1 eq of 6-chloro-7-deazapurine, 6-chloropurine or 6-chlorothienopyrimidine and 1 eq  
55  
56 of the corresponding aniline were dissolved in 2 mL of tetrahydrofuran. The crude is  
57  
58 stirred under microwave irradiation at 100 °C until the completeness of the reaction.  
59  
60

1  
2  
3 The corresponding crude is extracted using 20 mL of EtOAc and washed with NaHCO<sub>3</sub>  
4 and brine, the organic layer is dried over MgSO<sub>4</sub> and evaporated under high vacuum.  
5  
6  
7 The corresponding crude is purified using flash chromatography and CH<sub>2</sub>Cl<sub>2</sub>:MeOH 40:1  
8  
9 as eluent.  
10

11  
12 *3-((9H-purine-6-yl)amino)phenol (1)*. Yield 29%. M.p. 339-340 °C. <sup>1</sup>H-NMR (500 MHz,  
13 DMSO-*d*<sub>6</sub>): δ (ppm) 13.16 (s, 1H), 9.61 (s, 1H), 9.31 (s, 1H), 8.36 (s, 1H), 8.26 (s, 1H),  
14 7.55 (s, 1H), 7.32 (m, 1H), 7.08 (m, 1H), 6.42 (m, 1H). <sup>13</sup>C-NMR (125 MHz, DMSO-*d*<sub>6</sub>):  
15 δ (ppm) 158.2, 152.8, 150.9, 141.1, 140.0, 128.1, 124.1, 120.0, 112.8, 110.0, 108.3. ESI  
16 calcd for C<sub>11</sub>H<sub>9</sub>N<sub>5</sub>O [M + H]<sup>+</sup> 228.0880. Found: 228.0877  
17  
18

19  
20  
21  
22 *(N-(4-phenoxy)-9H-purin-6-amine) (2)*. Yield 20%. M.p. 336-338 °C. <sup>1</sup>H-NMR (300 MHz,  
23 DMSO-*d*<sub>6</sub>): δ (ppm) 13.06 (s, 1H), 9.47 (s, 1H), 9.14 (s, 1H), 8.26 (s, 1H), 8.20 (s, 1H),  
24 7.64 (d, *J* = 8.7 Hz, 2H), 6.72 (d, *J* = 8.8 Hz, 2H). <sup>13</sup>C-NMR (75 MHz, DMSO-*d*<sub>6</sub>): δ (ppm)  
25 153.1, 152.1, 151.9, 150.1, 139.3, 131.2, 122.8, 121.1, 119.1, 114.8. ESI calcd for  
26 C<sub>11</sub>H<sub>9</sub>N<sub>5</sub>O [M + H]<sup>+</sup> 228.0880. Found: 228.0879  
27  
28

29  
30  
31  
32 *(N-(4-morpholinophenyl)-9H-purin-6-amine) (3)* Yield 70%. M.p. 269-270 °C. <sup>1</sup>H-NMR  
33 (300 MHz, DMSO-*d*<sub>6</sub>): δ (ppm) 13.05 (s, 1H), 9.58 (s, 1H), 8.31 (s, 1H), 8.24 (s, 1H), 7.75  
34 (d, *J* = 9.0 Hz, 2H), 6.92 (d, *J* = 9.1 Hz, 2H), 3.74 (t, *J* = 4.2 Hz, 4H), 3.05 (t, *J* = 4.7 Hz,  
35 4H). <sup>13</sup>C-NMR (75 MHz, DMSO-*d*<sub>6</sub>): δ (ppm) 151.9, 151.6, 150.9, 146.9, 139.9, 132.0,  
36 121.9, 118.4, 115.4, 66.2, 49.1. ESI calcd for C<sub>15</sub>H<sub>16</sub>N<sub>6</sub>O [M + H]<sup>+</sup> 297.1458. Found:  
37 297.1457  
38  
39

40  
41  
42  
43  
44  
45 *(N-(4-chlorophenyl)-9H-purin-6-amine) (4)* Yield 75%. M.p. 329-330 °C. <sup>1</sup>H-NMR (500  
46 MHz, DMSO-*d*<sub>6</sub>): δ (ppm) 13.21 (s, 1H), 9.95 (s, 1H), 8.40 (s, 1H), 8.30 (s, 1H), 8.03 (d,  
47 *J* = 8.9 Hz, 2H), 7.37 (d, *J* = 8.9 Hz, 2H). <sup>13</sup>C-NMR (126 MHz, DMSO-*d*<sub>6</sub>): δ (ppm) 151.7,  
48 151.6, 150.6, 140.2, 138.9, 128.2, 125.8, 121.8, 119.5. ESI calcd for C<sub>11</sub>H<sub>8</sub>ClN<sub>5</sub> [M + H]<sup>+</sup>  
49 246.0541. Found: 246.0542  
50  
51

52  
53  
54  
55  
56  
57 *N-4-chlorophenylthieno[2,3-*d*]pyrimidin-4-amine (5)* Yield 50%. M.p. 179-180 °C. <sup>1</sup>H-  
58 NMR (300 MHz, DMSO-*d*<sub>6</sub>): δ (ppm) 9.75 (s, 1H), 8.52 (s, 1H), 7.95-7.84 (m, 3H), 7.75  
59  
60

(d,  $J = 6.0$  Hz, 1H), 7.43 (d,  $J = 8.9$  Hz, 2H).  $^{13}\text{C-NMR}$  (75 MHz,  $\text{DMSO-}d_6$ ):  $\delta$  (ppm) 166.6, 154.6, 153.0, 138.3, 128.5, 126.8, 124.2, 122.8, 119.4, 117.0. Anal. calcd for  $\text{C}_{12}\text{H}_8\text{ClN}_3\text{S}$ : C, 49.92; H, 3.84; N, 14.55; S 11.10. Found C, 50.22; H, 3.13; N, 14.09; S 10.76.

*N*-phenylthieno[2,3-*d*]pyrimidin-4-amine (**6**) Yield 70%. M.p. 175-176 °C.  $^1\text{H-NMR}$  (300 MHz,  $\text{DMSO-}d_6$ ):  $\delta$  (ppm) 9.65 (s, 1H), 8.49 (s, 1H), 7.89 (d,  $J = 6.0$  Hz, 1H), 7.86-7.81 (m, 2H), 7.73 (d,  $J = 5.9$  Hz, 1H), 7.46-7.31 (m, 2H), 7.16-7.04 (m, 1H).  $^{13}\text{C-NMR}$  (75 MHz,  $\text{DMSO-}d_6$ ):  $\delta$  (ppm) 166.5, 154.8, 153.2, 139.2, 128.5, 123.8, 123.3, 121.5, 119.5, 116.9. Anal. calcd for  $\text{C}_{12}\text{H}_9\text{N}_3\text{S}$ : C, 63.41; H, 3.99; N, 18.49; S 14.11. Found: C, 63.36; H, 4.16; N, 18.46; S 14.07.

*N*-(3-phenol)-7*H*-pyrrolo[2,3-*d*]pyrimidin-4-amine (**7**). Yield 87%. M.p. 253-255 °C.  $^1\text{H-NMR}$  (300 MHz,  $\text{DMSO-}d_6$ ):  $\delta$  (ppm) 11.75 (s, 1H), 9.34 (s, 1H), 9.17 (s, 1H), 8.28 (s, 1H), 7.50 (s, 1H), 7.26 (dd,  $J = 2.0, 7.9$  Hz, 1H), 7.22 (dd,  $J = 3.5, 1.7$  Hz, 1H), 7.10 (t,  $J = 8.0$  Hz, 1H), 6.80 (d,  $J = 3.5$  Hz, 1H), 6.43 (dd,  $J = 8.0, 2.3$  Hz, 1H).  $^{13}\text{C-NMR}$  (75 MHz,  $\text{DMSO-}d_6$ ):  $\delta$  (ppm) 157.8, 153.9, 151.2, 151.0, 141.8, 129.4, 122.4, 111.5, 109.6, 107.7, 104.1, 99.2. ESI calcd for  $\text{C}_{12}\text{H}_{10}\text{N}_4\text{O}$  [ $\text{M} + \text{H}$ ] $^+$  227.0927. Found: 227.0929.

*N*-(4-phenol)-7*H*-pyrrolo[2,3-*d*]pyrimidin-4-amine (**8**) Yield 38%. M.p. 274-276 °C.  $^1\text{H-NMR}$  (300 MHz,  $\text{DMSO-}d_6$ ):  $\delta$  (ppm) 11.65 (s, 1H), 9.17 (s, 1H), 9.05 (s, 1H), 8.18 (s, 1H), 7.56 (d,  $J = 8.8$  Hz, 2H), 7.17 (dd,  $J = 3.5, 2.3$  Hz, 1H), 6.77 (d,  $J = 8.8$  Hz, 2H), 6.63 (dd,  $J = 3.5, 2.1$  Hz, 1H).  $^{13}\text{C-NMR}$  (75 MHz,  $\text{DMSO-}d_6$ ):  $\delta$  (ppm) 154.0, 153.0, 150.9, 150.6, 131.6, 123.0, 121.4, 114.9, 103.0, 98.8. ESI calcd for  $\text{C}_{12}\text{H}_{10}\text{N}_4\text{O}$  [ $\text{M} + \text{H}$ ] $^+$  227.0927. Found: 227.0925.

*N*-(4-morpholinophenyl)-7*H*-pyrrolo[2,3-*d*]pyrimidin-4-amine (**9**) Yield 24%. M.p. 254-255 °C.  $^1\text{H-NMR}$  (300 MHz,  $\text{DMSO-}d_6$ ):  $\delta$  (ppm) 11.65 (s, 1H), 9.10 (s, 1H), 8.20 (s, 1H), 7.67 (d,  $J = 7.2$  Hz, 2H), 7.17 (dd,  $J = 3.5, 2.3$  Hz, 1H), 6.94 (d,  $J = 6.9$  Hz, 2H), 6.67 (dd,  $J = 3.5, 1.8$  Hz, 1H), 3.74 (t,  $J = 9.4, 4.9$  Hz, 4H), 3.06 (t,  $J = 9.2, 4.7$  Hz, 4H).  $^{13}\text{C-NMR}$  (75 MHz,  $\text{DMSO-}d_6$ ):  $\delta$  (ppm) 153.8, 150.9, 150.7, 146.7, 132.5, 122.0, 121.6, 115.4, 103.2, 98.8, 66.1, 49.1. ESI calcd for  $\text{C}_{16}\text{H}_{17}\text{N}_5\text{O}$  [ $\text{M} + \text{H}$ ] $^+$  296.1506. Found: 296.1496.

1  
2  
3 *N*-(4-chlorophenyl)-7*H*-pyrrolo[2,3-*d*]pyrimidin-4-amine (**10**). Yield 92%. M.p. 259-260  
4  
5 °C. <sup>1</sup>H-NMR (300 MHz, DMSO-*d*<sub>6</sub>): δ (ppm) 11.82 (s, 1H), 9.43 (s, 1H), 8.30 (s, 1H), 7.97  
6  
7 (dt, *J* = 8.9, 2.0 Hz, 2H), 7.38 (dt, 2H), 7.26 (dd, *J* = 3.5, 2.3 Hz, 1H), 6.80 (dd, *J* = 3.5,  
8  
9 1.9 Hz, 1H). <sup>13</sup>C-NMR (75 MHz, DMSO-*d*<sub>6</sub>): δ (ppm) 153.2, 150.9, 150.6, 139.5, 128.3,  
10  
11 125.3, 122.4, 121.4, 103.8, 98.7. Anal. calcd for C<sub>12</sub>H<sub>9</sub>ClN<sub>4</sub>: C, 58.91; H, 3.71; N, 22.90.  
12  
13 Found: C, 58.66; H, 3.78; N, 22.83.

14  
15  
16 *N*-(4-chlorobenzyl)-7*H*-pyrrolo[2,3-*d*]pyrimidin-4-amine (**11**). Yield 55%. M.p. 208-209  
17  
18 °C. <sup>1</sup>H-NMR (300 MHz, DMSO-*d*<sub>6</sub>): δ (ppm) 11.53 (s, 1H), 8.08 (s, 1H), 7.97 (t, *J* = 6.1  
19  
20 Hz, 1H), 7.36 (s, 4H), 7.08 (dd, *J* = 3.4, 2.3 Hz, 1H), 6.56 (dd, *J* = 3.4, 1.9 Hz, 1H), 4.69  
21  
22 (d, *J* = 6.1 Hz, 2H). <sup>13</sup>C-NMR (75 MHz, DMSO-*d*<sub>6</sub>): δ (ppm) 156.2, 151.7, 150.5, 139.9,  
23  
24 131.4, 129.4, 129.4, 128.5, 121.4, 102.9, 98.9, 42.8. Anal. calcd for C<sub>13</sub>H<sub>11</sub>ClN<sub>4</sub>: C, 60.35;  
25  
26 H, 4.29; N, 21.66. Found: C, 60.35; H, 4.24; N, 21.47.

27  
28  
29 *N*-(4-chloroethylphenyl)-7*H*-pyrrolo[2,3-*d*]pyrimidin-4-amine (**12**). Yield 25%. M.p. 207-  
30  
31 208 °C. <sup>1</sup>H-NMR (300 MHz, DMSO-*d*<sub>6</sub>): δ (ppm) 11.48 (s, 1H), 8.12 (s, 1H), 7.47 (t, *J* =  
32  
33 5.7 Hz, 1H), 7.43-7.18 (m, 4H), 7.05 (dd, *J* = 3.4, 2.2 Hz, 1H), 6.51 (dd, *J* = 3.4, 1.7 Hz,  
34  
35 1H), 3.67 (q, *J* = 7.2, 5.8 Hz, 2H), 2.91 (t, *J* = 7.3 Hz, 2H). <sup>13</sup>C-NMR (75 MHz, DMSO-  
36  
37 *d*<sub>6</sub>): δ (ppm) 156.0, 151.5, 150.1, 138.9, 130.7, 130.6, 128.2, 120.8, 102.6, 98.5, 41.4,  
38  
39 34.6. ESI calcd for C<sub>14</sub>H<sub>14</sub>ClN<sub>4</sub> [M + H]<sup>+</sup> 273.0902. Found: 273.0895.

40  
41  
42 4-(((7*H*-pyrrolo[2,3-*d*]pyrimidin-4-yl)amino)methyl)phenol (**13**). Yield 14%. M.p. 206-207  
43  
44 °C. <sup>1</sup>H-NMR (300 MHz, DMSO-*d*<sub>6</sub>): δ (ppm) 11.49 (s, 1H), 9.27 (s, 1H), 8.10 (s, 1H), 7.81  
45  
46 (t, 1H), 7.15 (d, *J* = 8.3 Hz, 2H), 7.05 (t, *J* = 2.7 Hz, 1H), 6.69 (d, *J* = 8.5 Hz, 2H), 6.57  
47  
48 (dd, *J* = 3.5, 1.7 Hz, 1H), 4.58 (d, *J* = 5.8 Hz, 2H). <sup>13</sup>C-NMR (75 MHz, DMSO-*d*<sub>6</sub>): δ (ppm)  
49  
50 156.2, 156.0, 151.5, 150.2, 130.5, 128.7, 120.8, 115.0, 102.5, 98.7, 42.7. ESI calcd for  
51  
52 C<sub>13</sub>H<sub>12</sub>N<sub>4</sub>O [M + H]<sup>+</sup> 241.1084. Found: 241.1079

53  
54  
55 4-(2-((7*H*-pyrrolo[2,3-*d*]pyrimidin-4-yl)amino)ethyl)phenol (**14**). Yield 23%. M.p. 246-247  
56  
57 °C. <sup>1</sup>H-NMR (300 MHz, DMSO-*d*<sub>6</sub>): δ (ppm) 11.47 (s, 1H), 9.18 (s, 1H), 8.11 (s, 1H), 7.45  
58  
59 (t, *J* = 5.7 Hz, 1H), 7.09-7.01 (m, 3H), 6.68 (d, *J* = 8.4 Hz, 2H), 6.52 (dd, *J* = 3.4, 1.7 Hz,  
60

1  
2  
3 1H), 3.68-3.48 (m, 2H), 2.79 (t,  $J = 7.6$  Hz, 2H).  $^{13}\text{C}$ -NMR (75 MHz,  $\text{DMSO-}d_6$ ):  $\delta$  (ppm)  
4  
5 156.0, 155.6, 151.5, 150.1, 129.8, 129.5, 120.7, 115.1, 102.5, 98.6, 42.1, 34.6. ESI calcd  
6  
7 for  $\text{C}_{14}\text{H}_{14}\text{N}_4\text{O}$   $[\text{M} + \text{H}]^+$  255.1240. Found: 255.1239  
8  
9

10  
11 *N*-(3-chlorophenyl)-7H-pyrrolo[2,3-d]pyrimidin-4-amine (**15**). Yield 49%. M.p. 234-235 °C.  
12  
13 (lit<sup>40</sup> 227-228 °C).  $^1\text{H}$ -NMR (500 MHz,  $\text{DMSO-}d_6$ ):  $\delta$  (ppm) 12.81 (s, 1H), 11.42 (s, 1H),  
14  
15 8.45 (s, 1H), 7.90 (s, 1H), 7.66 (m, 1H), 7.50 (m, 1H), 7.45 (m, 1H), 7.34 (m, 1H), 7.26  
16  
17 (m, 1H).  $^{13}\text{C}$ -NMR (125 MHz,  $\text{DMSO-}d_6$ ):  $\delta$  (ppm) 151.4, 146.1, 144.7, 138.7, 133.7,  
18  
19 131.2, 125.9, 125.0, 123.7, 122.6, 102.37, 102.3. ESI calcd for  $\text{C}_{12}\text{H}_9\text{ClN}_4$   $[\text{M} + \text{H}]^+$   
20  
21 245.0589. Found: 245.0587  
22

23  
24 *N*-(2-chlorophenyl)-7H-pyrrolo[2,3-d]pyrimidin-4-amine (**16**). Yield 69%. M.p. 220-221  
25  
26 °C.  $^1\text{H}$ -NMR (300 MHz,  $\text{DMSO-}d_6$ ):  $\delta$  (ppm) 11.73 (s, 1H), 9.07 (s, 1H), 8.13 (s, 1H), 7.69  
27  
28 (dd,  $J = 8.0, 1.6$  Hz, 1H), 7.54 (dd,  $J = 8.0, 1.6$  Hz, 1H), 7.37 (dt,  $J = 7.7, 1.6$  Hz, 1H),  
29  
30 7.24 (dt,  $J = 7.6, 1.7$  Hz, 1H), 7.14 (dd,  $J = 3.5, 2.3$  Hz, 1H), 6.51 (dd,  $J = 3.5, 1.8$  Hz,  
31  
32 1H).  $^{13}\text{C}$ -NMR (75 MHz,  $\text{DMSO-}d_6$ ):  $\delta$  (ppm) 154.3, 151.1, 150.9, 136.4, 129.5, 129.4,  
33  
34 128.5, 127.3, 126.4, 122.2, 103.1, 98.7. Anal. calcd for  $\text{C}_{12}\text{H}_9\text{ClN}_4$ : C, 58.91; H, 3.71; N,  
35  
36 22.90. Found: C, 58.77; H, 3.79; N, 22.90.  
37

38  
39 *N*-(2-phenyloxy)-7H-pyrrolo[2,3-d]pyrimidin-4-amine (**17**). Yield 20%. M.p. 233-235 °C.  
40  
41  $^1\text{H}$ -NMR (300 MHz,  $\text{DMSO-}d_6$ ):  $\delta$  (ppm) 11.82 (s, 1H), 10.61 (s, 1H), 8.91 (s, 1H), 8.22  
42  
43 (s, 1H), 7.56 (dd,  $J = 7.9, 1.6$  Hz, 1H), 7.22 (dd,  $J = 3.5, 2.3$  Hz, 1H), 7.02 (ddd,  $J = 8.0,$   
44  
45 7.1, 1.6 Hz, 1H), 6.92 (dd,  $J = 8.0, 1.6$  Hz, 1H), 6.84 (ddd,  $J = 7.9, 7.2, 1.6$  Hz, 1H), 6.70  
46  
47 (dd,  $J = 3.5, 1.8$  Hz, 1H).  $^{13}\text{C}$ -NMR (75 MHz,  $\text{DMSO-}d_6$ ):  $\delta$  (ppm) 153.8, 150.6, 150.2,  
48  
49 149.6, 127.8, 125.0, 124.3, 122.2, 119.1, 117.4, 103.2, 99.1. ESI calcd for  $\text{C}_{12}\text{H}_{10}\text{N}_4\text{O}$   $[\text{M}$   
50  
51  $+ \text{H}]^+$  227.0927. Found: 227.0926  
52

53  
54 *N*-(5,6,7,8-tetrahydronaphthalen-1-yl)-7H-pyrrolo[2,3-d]pyrimidin-4-amine (**18**). Yield  
55  
56 23%. M.p. 239-240 °C.  $^1\text{H}$ -NMR (300 MHz,  $\text{DMSO-}d_6$ ):  $\delta$  (ppm) 11.58 (s, 1H), 8.74 (s,  
57  
58 1H), 8.06 (s, 1H), 7.20- 7.05 (m, 3H), 6.99 (dd,  $J = 7.3, 1.7$  Hz, 1H), 6.22 (dd,  $J = 3.2,$   
59  
60 1.5 Hz, 1H), 2.78 (t,  $J = 5.3$  Hz, 2H), 2.61 (t,  $J = 5.3$  Hz, 2H), 1.68 (t,  $J = 3.4$  Hz, 4H).  $^{13}\text{C}$ -

1  
2  
3 NMR (75 MHz, DMSO-*d*<sub>6</sub>): δ (ppm) 155.7, 151.6, 151.5, 138.0, 137.9, 134.0, 127.0,  
4 125.6, 125.2, 121.9, 103.0, 99.4, 29.7, 25.0, 22.9 (C-18-19). Anal. calcd for C<sub>16</sub>H<sub>16</sub>N<sub>4</sub>: C,  
5 72.70; H, 6.10; N, 21.70. Found: C, 72.50; H, 6.05; N, 21.22.

6  
7  
8  
9 *N*-(benzo[*d*][1,3]dioxol-5-yl)-7*H*-pyrrolo[2,3-*d*]pyrimidin-4-amine (**19**). Yield 15%. M.p.  
10 282-283 °C. <sup>1</sup>H-NMR (300 MHz, DMSO-*d*<sub>6</sub>): δ (ppm) 11.69 (s, 1H), 9.17 (s, 1H), 8.22 (s,  
11 1H), 7.58 (d, *J* = 2.1 Hz, 1H), 7.23-7.15 (m, 2H), 6.89 (d, *J* = 8.4 Hz, 1H), 6.70 (dd, *J* =  
12 3.5, 1.9 Hz, 1H), 6.00 (s, 2H). <sup>13</sup>C-NMR (75 MHz, DMSO-*d*<sub>6</sub>): δ (ppm) 153.6, 150.77,  
13 150.72, 146.9, 142.3, 134.7, 121.9, 113.3, 107.8, 103.3, 103.0, 100.8, 98.7. ESI calcd  
14 for C<sub>13</sub>H<sub>10</sub>N<sub>4</sub>O<sub>2</sub> [M + H]<sup>+</sup> 255.0877. Found: 255.0877.

15  
16  
17  
18  
19  
20  
21  
22 1-(4-((7*H*-pyrrolo[2,3-*d*]pyrimidin-4-yl)amino)phenyl)ethan-1-one (**20**). Yield 25%. M.p.  
23 279-280 °C. <sup>1</sup>H-NMR (300 MHz, DMSO-*d*<sub>6</sub>): δ (ppm) 11.87 (s, 1H), 9.67 (s, 1H), 8.38 (s,  
24 1H), 8.11 (d, *J* = 8.8 Hz, 2H), 7.96 (d, *J* = 8.8 Hz, 2H), 7.31 (dd, *J* = 3.5, 2.3 Hz, 1H), 6.87  
25 (dd, *J* = 3.5, 1.9 Hz, 1H). <sup>13</sup>C-NMR (75 MHz, DMSO-*d*<sub>6</sub>): δ (ppm) 196.6, 153.2, 151.5,  
26 150.9, 145.5, 130.5, 129.7, 123.3, 119.0, 104.7, 99.1, 26.7. Anal. calcd for C<sub>14</sub>H<sub>12</sub>N<sub>4</sub>O:  
27 C, 65.07; H, 5.80; N, 23.71. Found: C, 64.88; H, 5.68; N, 23.20

28  
29  
30  
31  
32  
33  
34  
35 *N*-(3-morpholinophenyl)-7*H*-pyrrolo[2,3-*d*]pyrimidin-4-amine (**21**). Yield 58%. M.p. 258-  
36 259 °C. <sup>1</sup>H-NMR (300 MHz, DMSO-*d*<sub>6</sub>): δ (ppm) 11.65 (s, 1H), 9.10 (s, 1H), 8.20 (s, 1H),  
37 7.67 (dd, *J* = 7.2, 2.2 Hz, 2H), 7.17 (dd, *J* = 3.5, 2.3 Hz, 1H), 6.94 (dd, *J* = 6.9, 2.1 Hz,  
38 2H), 6.67 (dd, *J* = 3.5, 1.8 Hz, 1H), 3.74 (t, *J* = 9.4, 4.9 Hz, 4H), 3.06 (t, *J* = 9.2, 4.7 Hz,  
39 4H). <sup>13</sup>C-NMR (75 MHz, DMSO-*d*<sub>6</sub>): δ (ppm) 153.6, 151.4, 150.8, 150.8, 141.1, 128.8,  
40 122.0, 111.7, 109.4, 107.2, 103.6, 98.7, 66.1, 48.7. Anal. calcd for C<sub>16</sub>H<sub>17</sub>N<sub>5</sub>O C, 65.07;  
41 H, 5.80; N, 23.71. Found: C, 64.88; H, 5.68; N, 23.20.

42  
43  
44  
45  
46  
47  
48  
49  
50  
51 *N*-phenyl-7*H*-pyrrolo[2,3-*d*]pyrimidin-4-amine (**22**). Yield 64%. M.p. 239-240 °C. <sup>1</sup>H-NMR  
52 (300 MHz, DMSO-*d*<sub>6</sub>): δ (ppm) 11.75 (s, 1H), 9.29 (s, 1H), 8.28 (s, 1H), 7.89 (dd, *J* = 7.5,  
53 1.0 Hz, 2H), 7.33 (td, *J* = 8.7, 2.1 Hz, 2H), 7.23 (dd, *J* = 3.5, 2.3 Hz, 1H), 7.01 (tt, *J* = 7.2,  
54 2.4, 1.1 Hz, 1H), 6.79 (dd, *J* = 3.5, 1.8 Hz, 1H). <sup>13</sup>C-NMR (75 MHz, DMSO-*d*<sub>6</sub>): δ (ppm)  
55  
56  
57  
58  
59  
60

1  
2  
3 153.5, 150.8, 150.7, 140.4, 128.4, 122.1, 122.0, 120.2, 103.6, 98.8. ESI calcd for  
4  $C_{12}H_{10}N_4$  [M + H]<sup>+</sup> 211.0978 hallado 211.0979.  
5

6  
7 *N*-(4-methoxyphenyl)-7*H*-pyrrolo[2,3-*d*]pyrimidin-4-amine (**23**). Yield 74%, M.p. 229-230  
8 °C. <sup>1</sup>H-NMR (300 MHz, DMSO-*d*<sub>6</sub>): δ (ppm) 11.66 (s, 1H), 9.14 (s, 1H), 8.20 (s, 1H), 7.71  
9 (d, *J* = 9.0 Hz, 2H), 7.18 (dd, *J* = 3.5, 2.3 Hz, 1H), 6.92 (d, *J* = 9.0 Hz, 2H), 6.67 (dd, *J* =  
10 3.5, 1.9 Hz, 1H), 3.75 (s, 3H). <sup>13</sup>C-NMR (75 MHz, DMSO-*d*<sub>6</sub>): δ (ppm) 156.2, 156.0,  
11 151.5, 150.2, 130.5, 128.7, 120.8, 115.0, 102.5, 98.7, 42.7. Anal. calcd for C<sub>13</sub>H<sub>12</sub>N<sub>4</sub>O:  
12 C, 64.99; H, 5.03; N, 23.32. Found: C, 64.59; H, 5.03; N, 23.03.  
13  
14  
15  
16  
17  
18  
19

20 *N*-(4-(trifluoromethoxy)phenyl)-7*H*-pyrrolo[2,3-*d*]pyrimidine-4-amine (**24**). Yield 92%,  
21 M.p. 202-203 °C. <sup>1</sup>H-NMR (300 MHz, DMSO-*d*<sub>6</sub>): δ (ppm) 11.81 (s, 1H), 9.47 (s, 1H),  
22 8.29 (s, 1H), 8.02 (d, *J* = 9.1 Hz, 2H), 7.34 (dd, *J* = 9.2, 1.0 Hz, 2H), 7.26 (dd, *J* = 3.5,  
23 2.3 Hz, 1H), 6.80 (dd, *J* = 3.5, 1.9 Hz, 1H). <sup>13</sup>C-NMR (75 MHz, DMSO-*d*<sub>6</sub>): δ (ppm) 153.2,  
24 151.0, 150.6, 142.6 (d, *J* = 1.9 Hz), 139.7, 122.5, 121.4, 121.2, 120.2 (d, *J* = 255.3 Hz),  
25 103.8, 98.7. Anal. calcd for C<sub>13</sub>H<sub>9</sub>F<sub>3</sub>N<sub>4</sub>O: C, 53.07; H, 3.08; N, 19.04. Found: C, 52.81;  
26 H, 3.16; N, 18.99.  
27  
28  
29  
30  
31  
32  
33  
34

35 *N*-(4-isopropoxyphenyl)-7*H*-pyrrolo[2,3-*d*]pyrimidin-4-amine (**25**). Yield 66%. M.p. 218-  
36 219 °C. <sup>1</sup>H-NMR (300 MHz, DMSO-*d*<sub>6</sub>): δ (ppm) 11.66 (s, 1H), 9.13 (s, 1H), 8.20 (s, 1H),  
37 7.69 (d, *J* = 9.0 Hz, 2H), 7.17 (dd, *J* = 3.5, 2.3 Hz, 1H), 6.89 (d, *J* = 9.0 Hz, 2H), 6.68 (dd,  
38 *J* = 3.5, 1.8 Hz, 1H), 4.54 (hept, *J* = 6.0, 1H), 1.26 (d, *J* = 6.0, 6H). <sup>13</sup>C-NMR (75 MHz,  
39 DMSO-*d*<sub>6</sub>): δ (ppm) 153.8, 150.9, 150.7, 133.2, 122.4, 121.7, 115.7, 103.2, 98.8, 69.4,  
40 21.9 ESI calcd for C<sub>15</sub>H<sub>16</sub>N<sub>4</sub>O [M + H]<sup>+</sup> 269.1397. Found: 269.1393.  
41  
42  
43  
44  
45  
46  
47

48 *N*-(4-etoxyphenyl)-7*H*-pyrrolo[2,3-*d*]pyrimidin-4-amine (**26**). Yield 20%. M.p. 241-242 °C.  
49 <sup>1</sup>H-NMR (300 MHz, DMSO-*d*<sub>6</sub>): δ (ppm) 11.66 (s, 1H), 9.13 (s, 1H), 8.20 (s, 1H), 7.70 (d,  
50 *J* = 9.1 Hz, 2H), 7.17 (dd, *J* = 3.4, 2.3 Hz, 1H), 6.91 (d, *J* = 9.1 Hz, 2H), 6.67 (dd, *J* = 3.5,  
51 1.9 Hz, 1H), 4.00 (q, *J* = 7.0, 2H), 1.33 (d, *J* = 7.0, 3H). <sup>13</sup>C-NMR (75 MHz, DMSO-*d*<sub>6</sub>): δ  
52 (ppm) 154.0, 153.8, 150.9, 150.7, 133.2, 122.4, 121.7, 114.2, 103.2, 98.8, 63.1, 14.8.  
53  
54  
55  
56  
57  
58  
59 ESI calcd for C<sub>14</sub>H<sub>14</sub>N<sub>4</sub>O [M + H]<sup>+</sup> 255.1240. Found: 255.1236.  
60

1  
2  
3 *N*-(4-phenoxyphenyl)-7*H*-pyrrolo[2,3-*d*]pyrimidin-4-amine (**27**). Yield 53%. M.p. 250-251  
4 °C. <sup>1</sup>H-NMR (300 MHz, DMSO-*d*<sub>6</sub>): δ (ppm) 11.75 (s, 1H), 9.34 (s, 1H), 8.26 (s, 1H), 7.89  
5 (d, *J* = 9.0 Hz, 2H), 7.37 (dd, *J* = 8.6, 7.3 Hz, 2H), 7.23 (dd, *J* = 3.5, 2.3 Hz, 1H), 7.13-  
6 6.96 (m, 5H), 6.77 (dd, *J* = 3.5, 1.9 Hz, 1H). <sup>13</sup>C-NMR (75 MHz, DMSO-*d*<sub>6</sub>): δ (ppm)  
7 157.6, 153.5, 150.8, 150.75, 150.7, 136.3, 129.9, 122.7, 122.1, 122.0, 119.4, 117.6,  
8 103.5, 98.7. Anal. calcd for C<sub>18</sub>H<sub>14</sub>N<sub>4</sub>O: C, 71.51; H, 7.67; N, 18.53. Found: C, 71.04; H,  
9 4.70; N, 18.38.

10  
11  
12  
13  
14  
15  
16  
17  
18  
19 *N*-cyclohexyl-7*H*-pyrrolo[2,3-*d*]pyrimidin-4-amine (**28**). Yield 26%. M.p. 146-147 °C. <sup>1</sup>H-  
20 NMR (300 MHz, DMSO-*d*<sub>6</sub>): δ (ppm) 11.41 (s, 1H), 8.06 (s, 1H), 7.09 (d, *J* = 7.9 Hz, 1H),  
21 7.03 (dd, *J* = 3.4, 2.2 Hz, 1H), 6.57 (dd, *J* = 3.4, 1.8 Hz, 1H), 4.12-3.95 (m, 1H), 2.00-  
22 1.87 (m, 2H), 1.82-1.74 (m, 2H), 1.74-1.56 (m, 2H), 1.44-1.22 (m, 4H). <sup>13</sup>C-NMR (75  
23 MHz, DMSO-*d*<sub>6</sub>): δ (ppm) 155.3, 151.4, 150.2, 120.4, 102.3, 98.7, 48.5, 32.8, 25.5, 25.0.  
24 ESI calcd for C<sub>12</sub>H<sub>16</sub>N<sub>4</sub> [M + H]<sup>+</sup> 217.1448. Found: 217.1439.

25  
26  
27  
28  
29  
30  
31  
32  
33 *N*-(4-(4-chlorophenoxy)phenyl)-7*H*-pyrrolo[2,3-*d*]pyrimidin-4-amine (**29**). Yield 62%.  
34 M.p. 250-251 °C. <sup>1</sup>H-NMR (300 MHz, DMSO-*d*<sub>6</sub>): δ (ppm) 11.77 (s, 1H), 9.36 (s, 1H),  
35 8.26 (s, 1H), 7.92 (d, *J* = 9.0 Hz, 2H), 7.41 (d, *J* = 9.0 Hz, 2H), 7.24 (dd, *J* = 3.4, 2.3 Hz,  
36 1H), 7.06 (d, *J* = 9.0 Hz, 2H), 7.00 (d, *J* = 9.0 Hz, 2H), 6.77 (dd, *J* = 3.5, 1.9 Hz, 1H). <sup>13</sup>C-  
37 NMR (75 MHz, DMSO-*d*<sub>6</sub>): δ (ppm) 156.7, 153.4, 150.8, 150.7, 150.2, 136.8, 129.7,  
38 126.4, 122.1, 121.9, 119.7, 119.2, 103.5, 98.7. Anal. calcd for C<sub>18</sub>H<sub>13</sub>ClN<sub>4</sub>O: C, 64.20; H,  
39 3.89; N, 16.64. Found: C, 65.15; H, 3.96; N, 16.69.

40  
41  
42  
43  
44  
45  
46  
47  
48 *N*-(4-(4-fluorophenoxy)phenyl)-7*H*-pyrrolo[2,3-*d*]pyrimidin-4-amine (**30**). Yield 40%. M.p.  
49 227-228 °C. <sup>1</sup>H-NMR (300 MHz, DMSO-*d*<sub>6</sub>): δ (ppm) 11.75 (s, 1H), 9.33 (s, 1H), 8.25 (s,  
50 1H), 7.88 (d, *J* = 9.0 Hz, 2H), 7.26-7.15 (m, 3H), 7.08-6.95 (m, 4H), 6.76 (dd, *J* = 3.5, 1.9  
51 Hz, 1H). <sup>13</sup>C-NMR (75 MHz, DMSO-*d*<sub>6</sub>): δ (ppm) 159.4 (d, *J* = 238.1 Hz), 153.6 (d, *J* =  
52 2.3 Hz), 153.5, 151.3, 150.8, 136.3, 122.1, 122.0, 119.6 (d, *J* = 8.4 Hz), 119.0, 116.4 (d,  
53 *J* = 23.3 Hz), 103.5, 98.7. Anal. calcd for C<sub>18</sub>H<sub>13</sub>FN<sub>4</sub>O: C, 67.49; H, 4.09; N, 17.49. Found:  
54 C, 67.09; H, 4.09; N, 17.38.



1  
2  
3 *N*-(4-(4-cyanophenoxy)phenyl)-7*H*-pyrrolo[2,3-*d*]pyrimidin-4-amine (**31**). Yield 6%. M.p.  
4 259-260 °C. <sup>1</sup>H-NMR (300 MHz, DMSO-*d*<sub>6</sub>): δ (ppm) 11.77 (s, 1H), 9.41 (s, 1H), 8.28 (s,  
5 1H), 7.99 (d, *J* = 9.0 Hz, 2H), 7.83 (d, *J* = 8.9 Hz, 2H), 7.25 (dd, *J* = 3.5, 2.3 Hz, 1H), 7.15  
6 1H), 7.99 (d, *J* = 9.0 Hz, 2H), 7.09 (d, *J* = 8.9 Hz, 2H), 6.79 (dd, *J* = 3.5, 1.8 Hz Hz, 1H). <sup>13</sup>C-NMR  
7 (75 MHz, DMSO-*d*<sub>6</sub>): δ (ppm) 161.9, 153.3, 150.8, 150.7, 148.4, 137.8, 134.6, 122.2,  
8 121.8, 120.7, 118.8, 117.3, 104.5, 103.6, 98.7. Anal. calcd for C<sub>19</sub>H<sub>13</sub>N<sub>5</sub>O: C, 69.71; H,  
9 4.00; N, 21.39. Found: C, 69.33; H, 4.15; N, 21.01.

10  
11  
12  
13  
14  
15  
16  
17  
18 *N*-(4-(4-methoxyphenoxy)phenyl)-7*H*-pyrrolo[2,3-*d*]pyrimidin-4-amine (**32**). Yield 63%.  
19 M.p. 202-203 °C. <sup>1</sup>H-NMR (300 MHz, DMSO-*d*<sub>6</sub>): δ (ppm) 11.74 (s, 1H), 9.30 (s, 1H),  
20 8.25 (s, 1H), 7.84 (d, *J* = 9.0 Hz, 2H), 7.23 (dd, *J* = 3.5, 2.3 Hz, 1H), 7.04-6.94 (m, 6H),  
21 6.76 (dd, *J* = 3.1, 1.9 Hz, 1H), 3.76 (s, 3H). <sup>13</sup>C-NMR (75 MHz, DMSO-*d*<sub>6</sub>): δ (ppm) 155.2,  
22 153.5, 152.4, 150.8, 150.7, 150.4, 135.5, 122.0, 121.9, 119.8, 118.0, 115.0, 103.4, 98.7,  
23 55.4. Anal. calcd for C<sub>19</sub>H<sub>16</sub>N<sub>4</sub>O<sub>2</sub>: C, 68.66; H, 4.85; N, 16.86. Found: C, 67.97; H, 4.91;  
24 N, 16.64.

25  
26  
27  
28  
29  
30  
31  
32  
33 *N*-(4-(4-trifluoromethylphenoxy)phenyl)-7*H*-pyrrolo[2,3-*d*]pyrimidin-4-amine (**33**). Yield  
34 74%. M.p. 233-234 °C. <sup>1</sup>H-NMR (300 MHz, DMSO-*d*<sub>6</sub>): δ (ppm) 11.77 (s, 1H), 9.40 (s,  
35 1H), 8.28 (s, 1H), 7.98 (d, *J* = 9.0 Hz, 2H), 7.72 (d, *J* = 8.7 Hz, 2H), 7.24 (dd, *J* = 3.5, 2.3  
36 Hz, 1H), 7.14 (t, *J* = 9.1 Hz, 4H), 6.79 (dd, *J* = 3.5, 1.9 Hz, 1H). <sup>13</sup>C-NMR (75 MHz,  
37 DMSO-*d*<sub>6</sub>): δ (ppm) 162.1, 154.3, 151.7, 151.6, 149.9, 138.4, 128.3 (q, *J* = 3.6 Hz, C-20-  
38 22), 125.2 (q, *J* = 271.7 Hz), 123.6 (q, *J* = 32.1 Hz, 123.1, 122.7, 121.4, 118.0, 104.5,  
39 99.6. Anal. calcd for C<sub>19</sub>H<sub>13</sub>F<sub>3</sub>N<sub>4</sub>O: C, 61.62; H, 3.54; N, 15.13. Found: C, 61.55; H, 3.51;  
40 N, 15.04.

41  
42  
43  
44  
45  
46  
47  
48  
49 *N*-(4-(4-bromophenoxy)phenyl)-7*H*-pyrrolo[2,3-*d*]pyrimidin-4-amine (**34**). Yield 83%.  
50 M.p. 257-258 °C. <sup>1</sup>H-NMR (300 MHz, DMSO-*d*<sub>6</sub>): δ (ppm) 11.75 (s, 1H), 9.35 (s, 1H),  
51 8.27 (s, 1H), 7.93 (d, *J* = 9.0 Hz, 2H), 7.54 (d, *J* = 9.0 Hz, 2H), 7.24 (dd, *J* = 3.5, 2.3 Hz,  
52 1H), 7.08 (d, *J* = 9.0 Hz, 2H), 6.96 (d, *J* = 8.9 Hz, 2H), 6.78 (dd, *J* = 3.5, 1.9 Hz, 1H). <sup>13</sup>C-  
53 NMR (75 MHz, DMSO-*d*<sub>6</sub>): δ (ppm) 157.7, 153.9, 151.3, 151.2, 150.6, 137.3, 133.1,  
54  
55  
56  
57  
58  
59  
60

1  
2  
3 122.6, 122.4, 120.2, 120.1, 114.7, 104.0, 99.2. Anal. calcd for C<sub>18</sub>H<sub>13</sub>BrN<sub>4</sub>O: C, 56.71; H,  
4 3.44; N, 14.70. Found: C, 56.21; H, 3.51; N, 14.43.

5  
6  
7 *N*-(4-((4-nitrophenoxy)phenyl)-7*H*-pyrrolo[2,3-*d*]pyrimidin-4-amine (**35**). Yield 83%. M.p.  
8 270-271 °C. <sup>1</sup>H-NMR (300 MHz, DMSO-*d*<sub>6</sub>): δ (ppm) 11.86 (s, 1H), 9.63 (s, 1H), 8.35-  
9 8.16 (m, 3H), 8.00 (d, *J* = 9.0 Hz, 2H), 7.29-7.24 (m, 1H), 7.20 (d, *J* = 9.0 Hz, 2H), 7.14  
10 (d, *J* = 9.3 Hz, 2H), 6.84 (dd, *J* = 3.5, 1.9 Hz, 1H). <sup>13</sup>C-NMR (75 MHz, DMSO-*d*<sub>6</sub>): δ (ppm)  
11 163.6, 153.1, 150.5, 150.1, 148.7, 142.0, 137.7, 126.2, 122.5, 122.3, 120.9, 116.9, 103.6,  
12 99.1. ESI calcd for C<sub>18</sub>H<sub>13</sub>N<sub>5</sub>O<sub>3</sub> [M + H]<sup>+</sup> 348.1091. Found: 348.1088

13  
14  
15  
16  
17  
18  
19  
20 *N*-(4-((4-aminophenoxy)phenyl)-7*H*-pyrrolo[2,3-*d*]pyrimidin-4-amine (**36**). Reduction of  
21 derivative **35** (1 eq) using SnCl<sub>2</sub> (5.5 eq) in EtOH (12 mL) at 100 °C for 20 min under  
22 microwave irradiation. Yield 9%. M.p. 242-243 °C. <sup>1</sup>H-NMR (300 MHz, DMSO-*d*<sub>6</sub>): δ  
23 (ppm) 11.68 (s, 1H), 9.21 (s, 1H), 8.21 (s, 1H), 7.75 (d, *J* = 9.0 Hz, 2H), 7.19 (dd, *J* = 3.5,  
24 2.3 Hz, 1H), 6.87 (d, *J* = 9.0 Hz, 2H), 6.76 (d, *J* = 8.8 Hz, 2H), 6.71 (dd, *J* = 3.5, 1.9 Hz,  
25 1H), 6.58 (d, *J* = 8.8 Hz, 2H), 4.92 (s, 2H). <sup>13</sup>C-NMR (75 MHz, DMSO-*d*<sub>6</sub>): δ (ppm) 153.74,  
26 153.64, 150.8, 150.7, 146.5, 145.1, 134.7, 122.1, 121.9, 120.3, 117.0, 114.8, 103.3, 98.7.  
27  
28  
29  
30  
31  
32  
33  
34  
35 ESI calcd for C<sub>18</sub>H<sub>15</sub>N<sub>5</sub>O [M + H]<sup>+</sup> 318.1349. Found: 318.1348

36  
37 *N*-(4-(*p*-tolylloxy)phenyl)-7*H*-pyrrolo[2,3-*d*]pyrimidin-4-amine (**37**). Yield 57%. M.p. 229  
38 °C. <sup>1</sup>H-NMR (300 MHz, DMSO-*d*<sub>6</sub>): δ (ppm) 11.72 (s, 1H), 9.29 (s, 1H), 8.24 (s, 1H), 7.85  
39 (d, *J* = 9.0 Hz, 2H), 7.22 (dd, *J* = 3.5, 2.4 Hz, 1H), 7.17 (dd, *J* = 8.8, 0.7 Hz, 2H), 6.99 (d,  
40 *J* = 9 Hz, 2H), 6.89 (d, *J* = 8.5 Hz, 2H), 6.75 (dd, *J* = 3.5, 1.9 Hz, 1H), 2.28 (s, 3H). <sup>13</sup>C-  
41 NMR (75 MHz, DMSO-*d*<sub>6</sub>): δ (ppm) 155.2, 153.5, 151.5, 150.8, 136.0, 131.9, 130.3,  
42 122.03, 121.98, 118.9, 117.9, 103.5, 98.7, 20.2. Anal. calcd for C<sub>19</sub>H<sub>16</sub>N<sub>4</sub>O: C, 72.13; H,  
43 5.10; N, 17.71. Found: C, 71.84; H, 5.15; N, 17.96.

44  
45  
46  
47  
48  
49  
50  
51  
52  
53  
54  
55  
56  
57  
58  
59  
60  
*(4*-(*m*-tolylloxy)phenyl)-7*H*-pyrrolo[2,3-*d*]pyrimidine-2,4-diamine (**38**). Yield 80%. M.p.  
212-213 °C. <sup>1</sup>H-NMR (300 MHz, DMSO-*d*<sub>6</sub>): δ (ppm) 11.73 (s, 1H), 9.31 (s, 1H), 8.25 (s,  
1H), 7.88 (d, *J* = 9.0 Hz, 2H), 7.28-7.20 (m, 2H), 7.02 (d, *J* = 9.0 Hz, 2H), 6.91 (ddt, *J* =  
7.5, 1.7, 0.8 Hz, 1H), 6.82-6.78 (m, 3H), 2.28 (s, 3H). <sup>13</sup>C-NMR (75 MHz, DMSO-*d*<sub>6</sub>): δ  
(ppm) 157.7, 153.5, 150.9, 150.79, 150.76, 139.6, 136.3, 129.6, 123.5, 122.1, 121.9,

1  
2  
3 119.4, 118.1, 114.7, 103.5, 98.7, 21.0. ESI calcd for C<sub>19</sub>H<sub>16</sub>N<sub>4</sub>O [M + H]<sup>+</sup> 317.1397.  
4  
5 Found: 317.1393

6  
7 *N*-(4-(3-chlorophenoxy)phenyl)-7*H*-pyrrolo[2,3-*d*]pyrimidin-4-amine (**39**). Yield 62%.  
8  
9 M.p. 224-225 °C. <sup>1</sup>H-NMR (300 MHz, DMSO-*d*<sub>6</sub>): δ (ppm) 11.79 (s, 1H), 9.39 (s, 1H),  
10  
11 8.29 (s, 1H), 7.96 (d, *J* = 9.0 Hz, 2H), 7.41 (t, *J* = 8.1 Hz, 1H), 7.26 (dd, *J* = 3.5, 2.2 Hz,  
12  
13 1H), 7.17 (ddd, *J* = 8.0, 2.0, 0.9 Hz, 1H), 7.12 (d, *J* = 9.0 Hz, 2H), 7.03 (t, *J* = 2.2 Hz, 1H),  
14  
15 6.97 (ddd, *J* = 8.3, 2.3, 0.8 Hz, 1H), 6.80 (dd, *J* = 3.5, 1.8 Hz, 1H). <sup>13</sup>C-NMR (75 MHz,  
16  
17 DMSO-*d*<sub>6</sub>): δ (ppm) 158.9, 153.4, 150.8, 150.8, 149.7, 137.1, 133.9, 131.4, 122.5, 122.2,  
18  
19 121.9, 120.0, 117.2, 116.0, 103.5, 98.7. Anal. calcd for C<sub>18</sub>H<sub>13</sub>ClN<sub>4</sub>O: C, 64.20; H, 3.89;  
20  
21 N, 16.64. Found: C, 64.06; H, 3.91; N, 16.75.

22  
23  
24 *N*-(4-(3-trifluoromethylphenoxy)phenyl)-7*H*-pyrrolo[2,3-*d*]pyrimidin-4-amine (**40**). Yield  
25  
26 78%. M.p. 176-177 °C. <sup>1</sup>H-NMR (300 MHz, DMSO-*d*<sub>6</sub>): δ (ppm) 11.75 (s, 1H), 9.37 (s,  
27  
28 1H), 8.27 (s, 1H), 7.96 (d, *J* = 9.0 Hz, 2H), 7.61 (t, *J* = 7.8 Hz, 1H), 7.44 (d, *J* = 7.9 Hz,  
29  
30 1H), 7.32 - 7.19 (m, 3H), 7.13 (d, *J* = 8.9 Hz, 2H), 6.78 (dd, *J* = 3.5, 1.9 Hz, 1H). <sup>13</sup>C-  
31  
32 NMR (75 MHz, DMSO-*d*<sub>6</sub>): δ (ppm) 158.8, 153.8, 151.2, 151.1, 149.9, 137.6, 131.6,  
33  
34 130.95 (q, *J* = 32 Hz), 127.7 (d, *J* = 272.5 Hz), 122.5, 122.3, 121.5, 120.5, 119.5 (d, *J* =  
35  
36 3.9 Hz), 113.9 (d, *J* = 4.0 Hz), 103.9, 99.1. Anal. calcd for C<sub>19</sub>H<sub>13</sub>F<sub>3</sub>N<sub>4</sub>O: C, 61.62; H,  
37  
38 3.54; N, 15.13. Found: C, 61.06; H, 3.47; N, 15.22.

39  
40  
41 *N*-(4-(3-methoxyphenoxy)phenyl)-7*H*-pyrrolo[2,3-*d*]pyrimidin-4-amine (**41**). Yield 33%.  
42  
43 M.p. 206-207 °C. <sup>1</sup>H-NMR (300 MHz, DMSO-*d*<sub>6</sub>): δ (ppm) 11.73 (s, 1H), 9.32 (s, 1H),  
44  
45 8.25 (s, 1H), 7.89 (d, *J* = 9.0 Hz, 2H), 7.31-7.20 (m, 2H), 7.05 (d, *J* = 9.0 Hz, 2H), 6.76  
46  
47 (dd, *J* = 3.5, 1.8 Hz, 1H), 6.67 (ddd, *J* = 8.3, 2.4, 0.9 Hz, 1H), 6.59-6.48 (m, 2H), 3.73 (s,  
48  
49 3H). <sup>13</sup>C-NMR (75 MHz, DMSO-*d*<sub>6</sub>): δ (ppm) 160.6, 158.9, 153.5, 150.80, 150.75, 150.5,  
50  
51 136.5, 130.4, 122.1, 121.9, 119.6, 109.5, 108.4, 103.7, 103.5, 98.7, 55.2. ESI calcd for  
52  
53 C<sub>19</sub>H<sub>16</sub>N<sub>4</sub>O<sub>2</sub> [M + H]<sup>+</sup> 333.1346. Found: 333.1342.

54  
55  
56 *N*-(4-(2-chlorophenoxy)phenyl)-7*H*-pyrrolo[2,3-*d*]pyrimidin-4-amine (**42**). Yield 79%.  
57  
58 M.p. 214-215 °C. <sup>1</sup>H-NMR (300 MHz, DMSO-*d*<sub>6</sub>): δ (ppm) 11.73 (s, 1H), 9.33 (s, 1H),  
59  
60 8.25 (s, 1H), 7.89 (d, *J* = 9.0 Hz, 2H), 7.58 (dd, *J* = 8.0, 1.6 Hz, 1H), 7.34 (ddd, *J* = 8.2,

1  
2  
3 7.4, 1.6 Hz, 1H), 7.22 (dd,  $J = 3.5, 2.4$  Hz, 1H), 7.17 (ddd,  $J = 8.0, 7.4, 1.5$  Hz, 1H), 7.05-  
4 6.95 (m, 3H), 6.76 (dd,  $J = 3.5, 1.9$  Hz, 1H).  $^{13}\text{C-NMR}$  (75 MHz,  $\text{DMSO-}d_6$ ):  $\delta$  (ppm)  
5 153.5, 152.6, 150.80, 150.74, 150.71, 136.5, 130.6, 128.7, 124.6, 123.8, 122.1, 122.0,  
6 119.8, 118.4, 103.5, 98.7. Anal. calcd for  $\text{C}_{18}\text{H}_{13}\text{ClN}_4\text{O}$ : C, 64.20; H, 3.89; N, 16.64.  
7 Found: C, 64.11; H, 3.96; N, 16.63.  
8  
9

10  
11  
12  
13 *N*-(4-(2-methoxyphenoxy)phenyl)-7H-pyrrolo[2,3-d]pyrimidin-4-amine (**43**). Yield 64%.  
14 M.p. 214-215 °C.  $^1\text{H-NMR}$  (300 MHz,  $\text{DMSO-}d_6$ ):  $\delta$  (ppm) 11.69 (s, 1H), 9.23 (s, 1H),  
15 8.21 (s, 1H), 7.76 (d,  $J = 9.0$  Hz, 2H), 7.20 (dd,  $J = 3.5, 2.3$  Hz, 1H), 7.18-7.14 (m, 2H),  
16 7.02-6.92 (m, 2H), 6.86 (d,  $J = 9.1$  Hz, 2H), 6.71 (dd,  $J = 3.5, 1.9$  Hz, 1H), 3.77 (s, 3H).  
17  $^{13}\text{C-NMR}$  (75 MHz,  $\text{DMSO-}d_6$ ):  $\delta$  (ppm) 153.6, 152.6, 151.1, 150.8, 150.7, 144.6, 135.0,  
18 124.9, 122.1, 121.9, 121.0, 120.7, 116.7, 113.3, 103.3, 98.7, 55.6. Anal. calcd for  
19  $\text{C}_{19}\text{H}_{16}\text{N}_4\text{O}_2$ : C, 68.66; H, 4.85; N, 16.96. Found: C, 68.60; H, 4.82; N, 16.97.  
20  
21  
22

23  
24 *N*-(4-(2,4-chlorophenoxy)phenyl)-7H-pyrrolo[2,3-d]pyrimidin-4-amine (**44**). Yield 63%.  
25 M.p. 252-253 °C.  $^1\text{H-NMR}$  (300 MHz,  $\text{DMSO-}d_6$ ):  $\delta$  (ppm) 11.72 (s, 1H), 9.37 (s, 1H),  
26 8.24 (s, 1H), 7.89 (d,  $J = 9.1$  Hz, 2H), 7.72 (d,  $J = 2.5$  Hz, 1H), 7.39 (dd,  $J = 8.8, 2.6$  Hz,  
27 1H), 7.22 (dd,  $J = 3.5, 2.3$  Hz, 1H), 7.02 (dd,  $J = 8.9, 2.1$  Hz, 3H), 6.75 (dd,  $J = 3.5, 1.9$   
28 Hz, 1H).  $^{13}\text{C-NMR}$  (75 MHz,  $\text{DMSO-}d_6$ ):  $\delta$  (ppm) 153.6, 152.0, 150.9, 150.5, 136.9, 130.1,  
29 128.8, 127.7, 124.9, 122.4, 122.2, 120.9, 118.8, 103.7, 98.9. Anal. calcd for  
30  $\text{C}_{18}\text{H}_{12}\text{Cl}_2\text{N}_4\text{O}$ : C, 58.24; H, 3.26; N, 15.09. Found: C, 58.13; H, 3.33; N, 15.17.  
31  
32  
33

34  
35 *N*4-(4-(4-chlorophenoxy)phenyl)-7H-pyrrolo[2,3-d]pyrimidine-2,4-diamine (**45**). Yield  
36 70%. M.p. 232-233 °C.  $^1\text{H-NMR}$  (300 MHz,  $\text{DMSO-}d_6$ ):  $\delta$  (ppm) 10.83 (s, 1H), 8.94 (s,  
37 1H), 7.98 (d,  $J = 9.1$  Hz, 2H), 7.41 (d,  $J = 9.0$  Hz, 2H), 6.99 (m, 4H), 6.76 (dd,  $J = 3.5,$   
38 2.1 Hz, 1H), 6.53 (dd,  $J = 3.5, 1.9$  Hz, 1H), 5.70 (s, 2H).  $^{13}\text{C-NMR}$  (75 MHz,  $\text{DMSO-}d_6$ ):  
39  $\delta$  (ppm) 159.4, 156.8, 154.0, 153.5, 149.7, 137.5, 129.7, 126.3, 121.3, 119.5, 119.1,  
40 117.8, 98.8, 96.9. ESI calcd for  $\text{C}_{18}\text{H}_{14}\text{ClN}_5\text{O}$   $[\text{M} + \text{H}]^+$  352.0960. Found: 352.0956.  
41  
42

43  
44 *N*4-(4-(4-(trifluoromethyl)phenoxy)phenyl)-7H-pyrrolo[2,3-d]pyrimidine-2,4-diamine (**46**).  
45 Yield 77%. M.p. 201-202 °C.  $^1\text{H-NMR}$  (300 MHz,  $\text{DMSO-}d_6$ ):  $\delta$  (ppm) 10.85 (s, 1H), 8.99  
46 (s, 1H), 8.03 (d,  $J = 9.0$  Hz, 2H), 7.72 (d,  $J = 9.0$  Hz, 2H), 7.11 (dd,  $J = 9.0, 0.8$  Hz, 2H),  
47  
48  
49  
50  
51  
52  
53  
54  
55  
56  
57  
58  
59  
60

1  
2  
3 7.07 (d,  $J = 9.0$  Hz, 2H), 6.77 (dd,  $J = 3.5, 2.2$  Hz, 1H), 6.55 (dd,  $J = 3.5, 1.9$  Hz, 1H),  
4  
5 5.72 (s, 2H).  $^{13}\text{C-NMR}$  (75 MHz,  $\text{DMSO-}d_6$ ):  $\delta$  (ppm) 161.3, 159.4, 153.9, 153.5, 148.5,  
6  
7 138.2, 127.4 (q,  $J = 3.7$  Hz), 124.4 (d,  $J = 271.1$  Hz), 122.7 (d,  $J = 32$  Hz), 121.2, 120.4,  
8  
9 117.9, 117.1, 108.5, 98.8, 96.9. ESI calcd for  $\text{C}_{19}\text{H}_{14}\text{F}_3\text{N}_5\text{O}$   $[\text{M} + \text{H}]^+$  386.1223. Found:  
10 386.1220.

11  
12  
13 *N4-(4-(3-chlorophenoxy)phenyl)-7H-pyrrolo[2,3-d]pyrimidine-2,4-diamine (47)*. Yield  
14 16%. M.p. 177-178 °C.  $^1\text{H-NMR}$  (300 MHz,  $\text{DMSO-}d_6$ ):  $\delta$  (ppm) 10.84 (s, 1H), 8.97 (s,  
15 1H), 8.00 (d,  $J = 9.0$  Hz, 2H), 7.39 (t,  $J = 8.1$  Hz, 1H), 7.14 (ddd,  $J = 8.0, 2.0, 0.9$  Hz, 1H)  
16 7.03 (d,  $J = 9.0$  Hz, 2H) 6.99 (t,  $J = 2.2$  Hz, 1H), 6.94 (ddd,  $J = 8.3, 2.4, 0.9$  Hz, 1H), 6.76  
17 (dd,  $J = 3.5, 2.2$  Hz, 1H), 6.54 (dd,  $J = 3.5, 1.9$  Hz, 1H), 5.71 (s, 2H).  $^{13}\text{C-NMR}$  (75 MHz,  
18  $\text{DMSO-}d_6$ ):  $\delta$  (ppm) 159.4, 159.1, 153.9, 153.5, 149.1, 137.8, 133.9, 131.3, 122.5, 121.3,  
19 119.9, 117.8, 117.1, 116.0, 98.8, 96.9. ESI calcd for  $\text{C}_{18}\text{H}_{14}\text{ClN}_5\text{O}$   $[\text{M} + \text{H}]^+$  352.0960.  
20 Found: 352.0955

21  
22  
23 *N4-(4-(3-(trifluoromethyl)phenoxy)phenyl)-7H-pyrrolo[2,3-d]pyrimidine-2,4-diamine (48)*.  
24 Yield 45%. M.p. 179-180 °C.  $^1\text{H-NMR}$  (300 MHz,  $\text{DMSO-}d_6$ ):  $\delta$  (ppm) 10.84 (s, 1H), 8.98  
25 (s, 1H), 8.02 (d,  $J = 9.1$  Hz, 2H), 7.60 (t,  $J = 7.9$  Hz, 1H), 7.44 (ddt,  $J = 7.7, 1.7, 0.9$  Hz,  
26 1H), 7.32-7.20 (m, 2H), 7.06 (d,  $J = 9.0$  Hz, 2H), 6.76 (dd,  $J = 3.5, 2.2$  Hz, 1H), 6.54 (dd,  
27  $J = 3.5, 2.0$  Hz, 1H), 5.72 (s, 2H).  $^{13}\text{C-NMR}$  (75 MHz,  $\text{DMSO-}d_6$ ):  $\delta$  (ppm) 159.4, 158.6,  
28 153.9, 153.5, 148.9, 138.0, 131.3, 130.6 (d,  $J = 31.9$  Hz), 123.8 (d,  $J = 272.5$  Hz), 121.3,  
29 121.1, 120.0, 119.0 (d,  $J = 4.1$  Hz), 117.9, 113.4 (d,  $J = 4.0$  Hz), 98.8, 96.9. ESI calcd for  
30  $\text{C}_{19}\text{H}_{14}\text{F}_3\text{N}_5\text{O}$   $[\text{M} + \text{H}]^+$  386.1223. Found: 386.1219

31  
32  
33 *N-(4-((4-nitrophenyl)thio)phenyl)-7H-pyrrolo[2,3-d]pyrimidin-4-amine (49)*. Yield 42%.  
34 M.p. 265-266 °C.  $^1\text{H-NMR}$  (300 MHz,  $\text{DMSO-}d_6$ ):  $\delta$  (ppm) 12.46 (s, 1H), 10.72 (s, 1H),  
35 8.43 (s, 1H), 8.17 (d,  $J = 8.6$  Hz, 2H), 8.00 (d,  $J = 8.1$  Hz, 2H), 7.67 (d,  $J = 8.2$  Hz, 2H),  
36 7.44 (t,  $J = 2.6$  Hz, 1H), 7.33 (d,  $J = 8.6$  Hz, 2H), 7.03 (t,  $J = 2.4$  Hz, 1H).  $^{13}\text{C-NMR}$  (75  
37 MHz,  $\text{DMSO-}d_6$ ):  $\delta$  (ppm) 151.7, 148.3, 147.6, 146.6, 144.9, 139.9, 135.7, 126.4, 124.3,  
38 124.1, 123.7, 123.5, 103.7, 100.7. Anal. calcd for  $\text{C}_{18}\text{H}_{13}\text{N}_5\text{O}_2\text{S}$ : C, 59.49; H, 3.61; N,  
39 19.27; S, 8.82. Found: C, 59.42; H, 3.78; N, 19.14; S, 8.74.

1  
2  
3 *N*-(4-((4-aminophenyl)thio)phenyl)-7*H*-pyrrolo[2,3-*d*]pyrimidin-4-amine (**50**). Reduction  
4 of derivative **49** (1 eq) using SnCl<sub>2</sub> (5.5 eq) in EtOH (12 mL) at 100 °C for 20 min under  
5 microwave irradiation. Yield 69%. M.p. 200-201 °C. <sup>1</sup>H-NMR (300 MHz, DMSO-*d*<sub>6</sub>): δ  
6 (ppm) 11.73 (s, 1H), 9.30 (s, 1H), 8.24 (s, 1H), 7.80 (d, *J* = 8.8 Hz, 2H), 7.23 (dd, *J* = 3.5,  
7 2.3 Hz, 1H), 7.22 (dd, *J* = 3.5, 2.3 Hz, 1H), 7.14 (dd, *J* = 16.7, 8.6 Hz, 4H), 6.84 (dd, *J* =  
8 3.5, 1.9 Hz, 1H), 6.61 (d, *J* = 8.5 Hz, 2H), 5.48 (s, 1H). <sup>13</sup>C-NMR (75 MHz, DMSO-*d*<sub>6</sub>): δ  
9 (ppm) 153.3, 150.8, 150.6, 149.3, 138.5, 135.0, 131.3, 128.2, 122.1, 120.9, 117.1, 114.7,  
10 103.6, 98.7. Anal. calcd for C<sub>18</sub>H<sub>15</sub>N<sub>5</sub>S: C, 59.49; H, 3.61; N, 19.27; S, 8.82. Found: C,  
11 59.26; H, 3.70; N, 19.37; S, 8.95.

12  
13  
14  
15  
16  
17  
18  
19  
20  
21  
22 *N*-(4-(benzyloxy)phenyl)-7*H*-pyrrolo[2,3-*d*]pyrimidin-4-amine (**51**). Yield 28%. M.p. 238-  
23 239 °C. <sup>1</sup>H-NMR (300 MHz, DMSO-*d*<sub>6</sub>): δ (ppm) 11.66 (s, 1H), 9.15 (s, 1H), 8.20 (s, 1H),  
24 7.71 (d, *J* = 9.1 Hz, 2H), 7.50-7.29 (m, 5H), 7.18 (dd, *J* = 3.5, 2.4 Hz, 1H), 7.00 (d, *J* =  
25 9.1 Hz, 2H), 6.67 (dd, *J* = 3.5, 1.9 Hz, 1H), 5.09 (s, 2H). <sup>13</sup>C-NMR (75 MHz, DMSO-*d*<sub>6</sub>):  
26 δ (ppm) 153.80, 153.76, 150.9, 150.7, 137.3, 133.5, 128.4, 127.74, 127.66, 122.3, 122.0,  
27 114.7, 103.2, 98.7, 69.4. ESI calcd for C<sub>19</sub>H<sub>16</sub>N<sub>4</sub>O [M + H]<sup>+</sup> 317.1397. Found: 317.1395.

28  
29  
30  
31  
32  
33  
34  
35 4-((7*H*-pyrrolo[2,3-*d*]pyrimidin-4-yl)amino)phenyl)(phenyl)methanone (**52**). Yield 97%.  
36 M.p. 247-248 °C. <sup>1</sup>H-NMR (300 MHz, DMSO-*d*<sub>6</sub>): δ (ppm) 11.91 (s, 1H), 9.76 (s, 1H),  
37 8.38 (s, 1H), 8.16 (d, *J* = 8.9 Hz, 2H), 7.79 (d, *J* = 8.8 Hz, 2H), 7.77-7.53 (m, 5H), 7.32  
38 (dd, *J* = 3.5, 2.3 Hz, 1H), 6.89 (dd, *J* = 3.5, 1.9 Hz, 1H). <sup>13</sup>C-NMR (75 MHz, DMSO-*d*<sub>6</sub>):  
39 δ (ppm) 194.4, 152.8, 151.2, 150.5, 145.1, 137.9, 132.0, 131.1, 129.6, 129.3, 128.4,  
40 123.0, 118.6, 104.4, 98.7. ESI calcd for C<sub>19</sub>H<sub>14</sub>N<sub>4</sub>O [M + H]<sup>+</sup> 315.1240. Found: 315.1238.

41  
42  
43  
44  
45  
46  
47 4-((7*H*-pyrrolo[2,3-*d*]pyrimidin-4-yl)amino)phenyl)(4-fluorophenyl)methanone (**53**).  
48 Yield 19%. M.p. 275-276 °C. <sup>1</sup>H-NMR (300 MHz, DMSO-*d*<sub>6</sub>): δ (ppm) 11.89 (s, 1H), 9.75  
49 (s, 1H), 8.38 (s, 1H), 8.16 (d, *J* = 8.9 Hz, 2H), 7.93-7.72 (m, 4H), 7.39 (t, *J* = 8.9 Hz, 2H),  
50 7.32 (dd, *J* = 3.5, 2.3 Hz, 1H), 6.88 (dd, *J* = 3.5, 2.3, 1H). <sup>13</sup>C-NMR (75 MHz, DMSO-*d*<sub>6</sub>):  
51 δ (ppm) 193.1, 164.3 (d, *J* = 250.3 Hz, 152.9, 151.2, 150.5, 145.2, 134.5 (d, *J* = 3.2 Hz),  
52 132.2 (d, *J* = 9.2 Hz), 131.1, 129.5, 123.0, 118.7, 115.5 (d, *J* = 22.0 Hz), 104.4, 98.8.  
53  
54  
55  
56  
57  
58  
59  
60

1  
2  
3 Anal. calcd for C<sub>19</sub>H<sub>13</sub>FN<sub>4</sub>O: C, 68.67; H, 3.94; N, 16.86. Found: C, 68.32; H, 3.90; N,  
4  
5 16.72.

6  
7 *(4-((7H-pyrrolo[2,3-d]pyrimidin-4-yl)amino)phenyl)(3,4-dichlorophenyl)methanone (54).*

8  
9 Yield 35%. M.p. 274-275 °C. <sup>1</sup>H-NMR (300 MHz, DMSO-*d*<sub>6</sub>): δ (ppm) 11.91 (s, 1H), 9.78  
10  
11 (s, 1H), 8.39 (s, 1H), 8.18 (d, *J* = 8.9 Hz, 2H), 7.91 (d, *J* = 1.9 Hz, 1H), 7.82 (dd, *J* = 8.5,  
12  
13 6.3 Hz, 3H), 7.68 (dd, *J* = 8.3, 2.0 Hz, 1H), 7.33 (dd, *J* = 3.5, 2.3 Hz, 1H), 6.88 (dd, *J* =  
14  
15 3.5, 1.9 Hz, 1H). <sup>13</sup>C-NMR (75 MHz, DMSO-*d*<sub>6</sub>): δ (ppm) 192.0, 152.8, 151.2, 150.5,  
16  
17 145.6, 138.4, 134.6, 131.5, 131.3, 130.9, 130.8, 129.3, 128.7, 123.1, 118.7, 104.5, 98.7.  
18  
19 ESI calcd for C<sub>19</sub>H<sub>12</sub>Cl<sub>2</sub>N<sub>4</sub>O [M + H]<sup>+</sup> 383.0461. Found: 383.0457

20  
21  
22 *N-(4-(pyridin-3-yloxy)phenyl)-7H-pyrrolo[2,3-d]pyrimidin-4-amine (55).* Yield 35%. M.p.

23  
24 203-204 °C. <sup>1</sup>H-NMR (300 MHz, DMSO-*d*<sub>6</sub>): δ (ppm) 11.75 (s, 1H), 9.36 (s, 1H), 8.40-  
25  
26 8.36 (m, 1H), 8.35-8.31 (m, 1H), 8.26 (s, 1H), 7.93 (d, *J* = 9.0 Hz, 2H), 7.45-7.36 (m, 2H),  
27  
28 7.23 (dd, *J* = 3.5, 2.3 Hz, 1H), 7.10 (d, *J* = 9.0 Hz, 2H), 6.77 (dd, *J* = 3.5, 1.9 Hz, 1H).  
29  
30 <sup>13</sup>C-NMR (75 MHz, DMSO-*d*<sub>6</sub>): δ (ppm) 154.2, 153.5, 150.82, 150.74, 150.1, 143.9,  
31  
32 140.2, 137.0, 124.60, 124.55, 122.2, 121.9, 119.5, 103.6, 98.7. ESI calcd for C<sub>17</sub>H<sub>13</sub>N<sub>5</sub>O  
33  
34 [M + H]<sup>+</sup> 304.11193. Found: 304.1191.

35  
36  
37 *Procedure for the synthesis of azides derivatives 56-60:* 1 eq. of 1-(bromomethyl) or 1-  
38  
39 (bromoethyl)benzene and 1.5 eq. of sodium azide were dissolved in 2 mL of DMF. The  
40  
41 reaction mixture was stirred overnight. The organic phase (AcOEt, 10 mL) was washed  
42  
43 with 10x3 mL of iced H<sub>2</sub>O. The organic phase was dried over Na<sub>2</sub>SO<sub>4</sub> and the crude was  
44  
45 used in the following reaction without further purification.

46  
47 *1-(azidomethyl)-4-chlorobenzene (56).* Yield 74%. <sup>1</sup>H-NMR (300 MHz, DMSO-*d*<sub>6</sub>): δ  
48  
49 (ppm) 7.47 (d, *J* = 8.6 Hz, 2H), 7.42 (d, *J* = 8.7 Hz, 2H), 4.47 (s, 2H). <sup>13</sup>C-NMR (75 MHz,  
50  
51 DMSO-*d*<sub>6</sub>): δ (ppm) 135.2, 133.2, 130.8, 129.2, 53.2.

52  
53 *1-(azidomethyl)-2-chlorobenzene (57).* Yield 65%. <sup>1</sup>H-NMR (300 MHz, DMSO-*d*<sub>6</sub>): δ  
54  
55 (ppm) 7.46-7.35 (m, 2H), 7.33-7.24 (m, 2H), 4.50 (s, 2H). <sup>13</sup>C-NMR (75 MHz, DMSO-*d*<sub>6</sub>):  
56  
57 δ (ppm) 133.8, 133.3, 130.0, 129.8, 129.6, 127.2, 52.3.  
58  
59  
60

1  
2  
3 *1-(azydomethyl)-3-chlorobenzene (58)*. Yield 84%. <sup>1</sup>H-NMR (300 MHz, DMSO-*d*<sub>6</sub>): δ  
4 (ppm) 7.32 (dd, *J* = 3.8, 0.8 Hz, 3H), 7.25-7.12 (m, 1H), 4.33 (s, 2H). <sup>13</sup>C-NMR (75 MHz,  
5 DMSO-*d*<sub>6</sub>): δ (ppm) 137.5, 134.9, 130.3, 128.6, 128.3, 126.3, 54.3.  
6  
7

8  
9 *2-azydoethylbenzene (59)*. Yield 53%. <sup>1</sup>H-NMR (300 MHz, DMSO-*d*<sub>6</sub>): δ (ppm) 7.35-7.18  
10 (m, 5H), 3.56 (t, *J* = 7.1 Hz, 2H), 2.85 (t, *J* = 7.1 Hz, 2H). <sup>13</sup>C-NMR (75 MHz, DMSO-*d*<sub>6</sub>):  
11 δ (ppm) 138.8, 129.3, 128.9, 126.9, 52.0, 34.9.  
12  
13

14  
15 *1-(azidomethyl)-4-methylbenzene (60)*. Yield 56%. <sup>1</sup>H-NMR (300 MHz, DMSO-*d*<sub>6</sub>): δ  
16 (ppm) 7.34-7.15 (m, 4H), 4.38 (s, 2H), 2.31 (s, 3H). <sup>13</sup>C-NMR (75 MHz, DMSO-*d*<sub>6</sub>): δ  
17 (ppm) 137.2, 133.0, 129.8, 128.0, 52.2, 21.6.  
18  
19

20  
21 *N-(4-(prop-2-yn-1-yloxy)phenyl)-7H-pyrrolo[2,3-*d*]pyrimidin-4-amine (61)*. [Synthesized  
22 following procedure (a)] Yield 69%. M.p. 217-218 °C. <sup>1</sup>H-NMR (300 MHz, DMSO-*d*<sub>6</sub>): δ  
23 (ppm) 11.70 (s, 1H), 9.19 (s, 1H), 8.21 (s, 1H), 7.74 (dt, *J* = 9.5, 3.4 Hz, 2H) 7.19 (dd, *J*  
24 = 3.5, 2.3 Hz, 1H), 6.98 (dd, *J* = 9.0, 3.4 Hz, 2H), 6.70 (dd, *J* = 3.5, 1.9 Hz, 1H), 4.77 (d,  
25 *J* = 2.4 Hz, 2H), 3.57 (t, *J* = 2.3 Hz, 1H). <sup>13</sup>C-NMR (75 MHz, DMSO-*d*<sub>6</sub>): δ (ppm) 153.7,  
26 152.6, 150.8, 150.7, 134.0, 122.1, 121.8, 114.8, 103.2, 98.7, 79.5, 78.1, 55.6. Anal. calcd  
27 for C<sub>15</sub>H<sub>12</sub>N<sub>4</sub>O: C, 68.17; H, 4.58; N, 21.20. Found: C, 67.86; H, 4.63; N, 21.23.  
28  
29  
30  
31  
32  
33  
34

35  
36 *Procedure for the synthesis of triazol derivatives 62-67*: A mixture of compound **61** (1  
37 eq.) and the corresponding azide (1 eq.) in DMF was reacted overnight at r.t. in presence  
38 of copper sulfate (CuSO<sub>4</sub>·5H<sub>2</sub>O) (0.1 eq.), tris(benzyltriazolylmethyl)amine (TBTA) (0.1  
39 eq.) and sodium ascorbate (0.2 eq.). The reaction mixture was poured onto water,  
40 extracted with CH<sub>2</sub>Cl<sub>2</sub>:MeOH (9:1), washed with saturated sodium chloride solution, dried  
41 over magnesium sulfate (MgSO<sub>4</sub>), concentrated and purified using flash chromatography  
42 on silica gel (CH<sub>2</sub>Cl<sub>2</sub>:MeOH mixture).  
43  
44  
45  
46  
47  
48  
49

50  
51 *N-(4-((1-phenyl-1*H*-1,2,3-triazol-4-yl)methoxy)phenyl)-7H-pyrrolo[2,3-*d*]pyrimidin-4-  
52 amine (62)*. Yield 34%. M.p. 267-268 °C. <sup>1</sup>H-NMR (500 MHz, DMSO-*d*<sub>6</sub>): δ (ppm) 11.68  
53 (s, 1H), 9.18 (s, 1H), 8.97 (s, 1H), 8.22 (s, 1H), 7.92 (dd, *J* = 7.0, 1.5 Hz, 2H), 7.76 (d, *J*  
54 = 9.0 Hz, 2H), 7.61 (t, *J* = 7.9 Hz, 2H), 7.50 (t, *J* = 7.5, 1.0 Hz, 1H), 7.19 (dd, *J* = 3.5, 2.2  
55 Hz, 1H), 7.08 (d, *J* = 9.1, 2H), 6.70 (dd, *J* = 3.5, 1.8 Hz, 1H), 5.23 (s, 2H). <sup>13</sup>C-NMR (125  
56  
57  
58  
59  
60



MHz, DMSO-*d*<sub>6</sub>):  $\delta$  (ppm) 153.7, 153.4, 150.9, 150.7, 144.1, 136.6, 133.8, 129.9, 122.8, 122.2, 121.8, 120.1, 114.7, 103.3, 98.8, 61.3. ESI calcd for C<sub>21</sub>H<sub>17</sub>N<sub>7</sub>O [M + H]<sup>+</sup> 384.1567. Found: 384.1564.

*N*-(4-((1-(4-chlorobenzyl)-1*H*-1,2,3-triazol-4-yl)methoxy)phenyl)-7*H*-pyrrolo[2,3-*d*]pyrimidin-4-amine (**63**). Yield 64%. M.p. 207-208 °C. <sup>1</sup>H-NMR (300 MHz, DMSO-*d*<sub>6</sub>):  $\delta$  (ppm) 11.67 (s, 1H), 9.16 (s, 1H), 8.29 (s, 1H), 8.20 (s, 1H), 7.73 (d, *J* = 9.1 Hz, 2H), 7.45 (d, *J* = 8.5 Hz, 2H), 7.35 (d, *J* = 8.5 Hz, 2H), 7.18 (dd, *J* = 3.5, 2.3 Hz, 1H), 7.01 (d, *J* = 9.1 Hz, 2H), 6.68 (dd, *J* = 3.5, 1.8 Hz, 1H), 5.62 (s, 2H), 5.12 (s, 2H). <sup>13</sup>C-NMR (75 MHz, DMSO-*d*<sub>6</sub>):  $\delta$  (ppm) 153.7, 153.4, 150.9, 150.7, 143.3, 135.0, 133.7, 132.9, 129.9, 128.8, 124.7, 122.2, 121.8, 114.7, 112.2, 98.8, 61.3, 52.0. ESI calcd for C<sub>22</sub>H<sub>18</sub>N<sub>7</sub>O [M + H]<sup>+</sup> 432.1334. Found: 432.1320.

*N*-(4-((1-(2-chlorobenzyl)-1*H*-1,2,3-triazol-4-yl)methoxy)phenyl)-7*H*-pyrrolo[2,3-*d*]pyrimidin-4-amine (**64**). Yield 31%. M.p. 173-174 °C. <sup>1</sup>H-NMR (500 MHz, DMSO-*d*<sub>6</sub>):  $\delta$  (ppm) 11.67 (s, 1H), 9.16 (s, 1H), 8.27 (s, 1H), 8.21 (s, 1H), 7.73 (d, *J* = 9.0 Hz, 2H), 7.53 (dd, *J* = 7.5, 1.7 Hz, 1H), 7.39 (dd, *J* = 7.4, 1.7 Hz, 2H), 7.22 (dd, *J* = 7.3, 2.1 Hz, 1H), 7.18 (dd, *J* = 3.4, 2.3 Hz, 1H), 7.02 (d, *J* = 9.0 Hz, 2H), 6.68 (dd, *J* = 3.4, 1.9 Hz, 1H), 5.73 (s, 2H), 5.13 (s, 2H). <sup>13</sup>C-NMR (125 MHz, DMSO-*d*<sub>6</sub>):  $\delta$  (ppm) 153.7, 153.4, 150.9, 150.7, 143.0, 133.7, 133.3, 132.6, 130.5, 130.2, 129.6, 127.7, 125.0, 122.2, 121.8, 114.7, 103.2, 98.7, 61.3, 50.6. ESI calcd for C<sub>22</sub>H<sub>18</sub>N<sub>7</sub>O [M + H]<sup>+</sup> 432.1334. Found: 432.1337.

*N*-(4-((1-(3-chlorobenzyl)-1*H*-1,2,3-triazol-4-yl)methoxy)phenyl)-7*H*-pyrrolo[2,3-*d*]pyrimidin-4-amine (**65**). Yield 33%. mp 177-178 °C. <sup>1</sup>H-NMR (500 MHz, DMSO-*d*<sub>6</sub>):  $\delta$  (ppm) 11.67 (s, 1H), 9.15 (s, 1H), 8.33 (s, 1H), 8.20 (s, 1H), 7.73 (d, *J* = 9.1 Hz, 2H), 7.41 (d, *J* = 3.1 Hz, 3H), 7.32-7.25 (m, 1H), 7.18 (dd, *J* = 3.4, 2.3 Hz, 1H), 7.02 (d, *J* = 9.0 Hz, 2H), 6.68 (dd, *J* = 3.5, 1.9 Hz, 1H), 5.64 (s, 2H), 5.33 (s, 2H). <sup>13</sup>C-NMR (125 MHz, DMSO-*d*<sub>6</sub>):  $\delta$  (ppm) 153.7, 53.4, 150.9, 150.7, 143.3, 138.4, 133.7, 133.3, 130.7, 128.1, 127.9, 126.7, 124.8, 122.2, 121.8, 114.7, 103.2, 98.7. ESI calcd for C<sub>22</sub>H<sub>18</sub>N<sub>7</sub>O [M + H]<sup>+</sup> 432.1334. Found: 432.1328.

1  
2  
3 *N*-(4-((1-phenethyl-1*H*-1,2,3-triazol-4-yl)methoxy)phenyl)-7*H*-pyrrolo[2,3-*d*]pyrimidin-4-  
4 *amine* (**66**). Yield 64%. M.p. 206-207 °C. <sup>1</sup>H-NMR (500 MHz, DMSO-*d*<sub>6</sub>): δ (ppm) 11.67  
5 (s, 1H), 9.16 (s, 1H), 8.21 (s, 1H), 8.16 (s, 1H), 7.73 (d, *J* = 9.1 Hz, 2H), 7.30-7.16 (m,  
6 6H), 7.00 (d, *J* = 9.1 Hz, 2H), 6.69 (dd, *J* = 3.5, 2.1 Hz, 1H), 5.10 (s, 2H), 4.62 (t, *J* = 7.4  
7 Hz, 2H), 3.17 (t, *J* = 7.4 Hz, 2H). <sup>13</sup>C-NMR (125 MHz, DMSO-*d*<sub>6</sub>): δ (ppm) 153.7, 153.4,  
8 150.9, 150.7, 142.7, 142.7, 133.7, 128.7, 128.4, 126.6, 124.4, 122.2, 121.8, 114.7, 103.2,  
9 98.7, 62.3, 50.5, 35.7. ESI calcd for C<sub>23</sub>H<sub>21</sub>N<sub>7</sub>O [M + H]<sup>+</sup> 412.1880. Found: 412.1873.

10  
11  
12  
13  
14  
15  
16  
17  
18 *N*-(4-((1-(4-methylbenzyl)-1*H*-1,2,3-triazol-4-yl)methoxy)phenyl)-7*H*-pyrrolo[2,3-  
19 *d*]pyrimidin-4-*amine* (**67**). Yield 73%. M.p. 215-216 °C. <sup>1</sup>H-NMR (500 MHz, DMSO-*d*<sub>6</sub>): δ  
20 (ppm) 11.67 (s, 1H), 9.15 (s, 1H), 8.24 (s, 1H), 8.20 (s, 1H), 7.72 (d, *J* = 9.0 Hz, 2H),  
21 7.22 (d, *J* = 8.0 Hz, 2H), 7.20-7.15 (m, 3H), 7.00 (d, *J* = 9.0 Hz, 2H), 6.68 (d, *J* = 3.3 Hz,  
22 1H), 5.55 (s, 2H), 5.11 (s, 2H), 2.27 (s, 3H). <sup>13</sup>C-NMR (125 MHz, DMSO-*d*<sub>6</sub>): δ (ppm)  
23 153.7, 153.4, 150.9, 150.7, 143.1, 137.5, 133.7, 133.0, 129.3, 128.0, 124.6, 122.2, 121.8,  
24 114.7, 103.2, 98.7, 61.3, 52.6, 20.7 ESI calcd for C<sub>23</sub>H<sub>21</sub>N<sub>7</sub>O [M + H]<sup>+</sup> 412.1880. Found:  
25 412.1876  
26  
27  
28  
29  
30  
31  
32  
33

### 34 35 36 **X-Ray diffraction studies**

37  
38  
39 **Protein expression and purification.** The protein was expressed following the protocol  
40 by Xue et. al.<sup>24</sup> In brief, the gene of human TTBK1 coding for the catalytic domain,  
41 residues from 14 to 313 (GeneScrip hTTBK\_coli\_pET-28a(+)-TEV) was expressed in *E.*  
42 *coli* (BL21DE3). A pre-culture was grown overnight in LB medium, diluted 1:25 in fresh  
43 LB medium and incubated at 37 °C with shaking until an OD600 0.6 was reached.  
44 Induction was carried out using 1 mM IPTG at 20 °C overnight.  
45  
46  
47  
48  
49

50  
51  
52  
53  
54  
55  
56  
57  
58  
59  
60  
Harvested cells were resuspended in buffer A (20 mM Tris, pH 8.0, 5 mM MgCl<sub>2</sub>, 300  
mM NaCl, 5% (v/v) glycerol, 0.05% (w/v) CHAPS, 1 mM tris(2-carboxyethyl)phosphine  
(TCEP), 10 mM imidazole) with EDTA-free Protease Inhibitor Cocktail (Roche) and lysed  
with a single passage through a cell disruptor (MIXONIX Inc.). Lysate was clarified by  
centrifugation, and the supernatant loaded onto a 1 mL HiTrap Crude column (GE

1  
2  
3 Healthcare). After washing with buffer A with 30 column volumes (CV), the protein was  
4 eluted with increasing concentrations of buffer A supplemented with 250 mM imidazole.  
5  
6 Fractions containing TTBK1 were pooled and diluted 3-fold with buffer C (20 mM HEPES,  
7  
8 pH 7.0, 5% (v/v) glycerol) and loaded onto a pre-equilibrated 10 mL Resource S column  
9  
10 (GE Healthcare). The column was washed with 5 CV of buffer C, and the bound protein  
11  
12 was eluted by a salt gradient with buffer C containing 1 M NaCl. Fractions containing  
13  
14 TTBK1 were then loaded onto a Hiloal 16/60 Superdex 200 pre-equilibrated with buffer  
15  
16 D (20 mM Tris, pH 8.0, 0.5 mM MgCl<sub>2</sub>, 300 mM NaCl, 5% (v/v) glycerol, 0.05% (w/v)  
17  
18 CHAPS, 2 mM TCEP). Finally, fractions containing TTBK1 were concentrated in Amicon  
19  
20 Ultra centrifugal units (10 K MWCO) and snap frozen in liquid nitrogen. This protein was  
21  
22 used for the 29-complexed crystallization.  
23  
24  
25

26 For the other crystal structures, TTBK1 (aa 13-320) and TTBK2 (aa 1-299) were  
27  
28 recombinantly co-expressed with lambda phosphatase in E. coli Rosetta as a His-Sumo-  
29  
30 and His-tagged proteins, respectively. Both proteins were initially purified by Ni<sup>2+</sup>-affinity  
31  
32 chromatography, and the tags were cleaved either by SENP1 protease (TTBK1) or TEV  
33  
34 (TTBK2). The cleaved proteins were further purified by size exclusion chromatography,  
35  
36 and the pure proteins were stored in buffer 25 mM HEPES pH 7.5, 250 mM NaCl, 0.5  
37  
38 mM TCEP and 10% glycerol.  
39  
40  
41

42 **Crystallization.** For derivative **29**, crystallization experiments were performed in pre-  
43  
44 greased 24-well plates (Crystalgen Inc, NY, USA) and reagents were purchased from  
45  
46 commercial sources. TEV-TTBK1(14-313) protein was used in crystallization. All TTBK1  
47  
48 crystals were obtained using hanging drop technique at 20 °C mixing 0.5 μL of protein  
49  
50 (9.5 mg mL<sup>-1</sup>) with 0.5 μL of reservoir solution and equilibrated against 1 mL of reservoir  
51  
52 solution. **29**-TTBK1 co-crystals were obtained preincubating the protein with the  
53  
54 compound in 3 fold-excess molar in 27% (w/v) PEG 4000, 200mM NH<sub>4</sub>SO<sub>4</sub>, 100 mM  
55  
56 Na Citrate pH5.6 and 10 mM TCEP solution. Needle-like crystals appear after one week  
57  
58  
59  
60

1  
2  
3 and grow until 50  $\mu\text{m}$  in size. Crystals were transferred to a cryo solution consisting in  
4 well solution plus 20% (v/v) ethylenglycol.  
5  
6

7 For other structures, crystallization was performed using sitting drop vapor diffusion at  
8 20  $^{\circ}\text{C}$  and the kinases at  $\sim 10$  mg/mL that were pre-incubated with 1 mM inhibitors. For  
9 TTBK2, crystallization condition was 1.6 M Na/K phosphate pH 7.0, 5% glycerol and 0.1  
10 M Tris pH 7.5-8.5, while for TTBK1 the condition was 26% PEG 3350, 0.2 M sodium  
11 acetate pH 7.0 and 0.1 M Tris, pH 7.5-8.5. The complexed crystals were cryo-protected  
12 with mother liquor supplemented with glycerol or ethylene glycol for TTBK2 and TTBK1,  
13 respectively.  
14  
15  
16  
17  
18  
19  
20  
21  
22  
23

24 **Structure determination.** Diffraction data for TTBK1-29 were collected in the XALOC  
25 beamline at the ALBA synchrotron (Barcelona, Spain). For the other crystal structures,  
26 diffraction data were collected at Swiss Light Source. The collected datasets were  
27 processed with XDS<sup>41</sup> and AIMLESS.<sup>42</sup> Structure determination was performed by  
28 molecular replacement method with PHASER<sup>43</sup> using the previously TTBK1 KD structure  
29 (PDB code 4BTM). Structure refinement was done by several cycles of computational  
30 refinement with REFMAC5<sup>44</sup> and manual rebuilding using Coot.<sup>45</sup> Crystallographic data  
31 collection and refinement statistic are summarized in Table S1.  
32  
33  
34  
35  
36  
37  
38  
39  
40  
41  
42

### 43 **Computational studies.**

44  
45 The protein-ligand docking was performed using Glide and related Schrödinger  
46 packages.<sup>46-47</sup> The binding site was defined by the crystallographic structures obtained  
47 for TTBK1 and TTBK2 in complex with the inhibitors reported in this work (PDB codes:  
48 7Q8V, 7Q8W, 7Q8Z, 7Q90, 7Q8Y). Before docking calculations, the protein was  
49 prepared using Maestro Protein Preparation Wizard,<sup>48</sup> removing ligands, metals and  
50 water molecules, adding hydrogens, ionizing residues at pH 7.5 and filling in missing  
51 side chains using Prime. Minimization of the protein structure was done with OPLS3  
52 force field. TTBKs inhibitors were also prepared using OPLS force field to minimize  
53  
54  
55  
56  
57  
58  
59  
60

1  
2  
3 energy. The grid box was defined using the ligands co-crystallized in TTBK1 and TTBK2  
4 as center of the boxes. The docking was performed with Glide standard precision (SP)  
5 function,<sup>49</sup> and the top-10 poses per docked ligand were selected and subjected to re-  
6 scoring with the Molecular mechanics generalized Born surface area (MM-GBSA) with  
7 Prime. This computational method combines molecular mechanics energy and implicit  
8 solvation models that enables to re-score the docking results and correlate the  
9 experimental activities ( $IC_{50}$ ) with the predicted binding energies ( $\Delta G_{bind}$ ]. The binding  
10 free energies between the ligands and the receptor were calculated as previously  
11 reported.<sup>15</sup>

12  
13 The crystal structures of complexes **29**-TTBK1, **42**-TTBK1 and **42**-TTBK2 as well as the  
14 best docking solutions between compound **38** and TTBK1 and TTBK2, which presents  
15 the best predicted binding free energy (MM-GBSA), were subjected to 525 ns of  
16 molecular dynamics simulations (MDs) using Desmond software<sup>50</sup> and the OPLS3e force  
17 field.<sup>51</sup> To prepare the systems, the complexes were solvated with pre-equilibrated SPC  
18 water molecules in a periodic boundary condition box. Then the systems were  
19 neutralized by adding  $Na^+$  or  $Cl^-$  counter ions to balance the net charge of the systems  
20 and NaCl at a concentration of 0.15 M was added to simulate physiological conditions.  
21 Each system was relaxed using the default Desmond relaxation protocol and then  
22 equilibrated with a spring constant force of  $5.0 \text{ kcal} \times \text{mol}^{-1} \times \text{\AA}^{-2}$  applied to the TTBKs  
23 backbone atoms and the ligands for 25 ns using the NPT ensemble at constant pressure  
24 (1 atm), temperature (300 K), and number of atoms using the isothermal-isobaric  
25 ensemble and the Nosé–Hoover method with a relaxation time of 1 ps applying the MTK  
26 algorithm,<sup>52</sup> with a timestep of 2 fs. Then the last frame was taken and a second non-  
27 restricted 500 ns MDs was performed using the same conditions previously described.  
28 Systems were analyzed using the *in house*, PyMol, VMD, and a modification of the  
29 KNIME workflow to profile interactions between ligands and targets along MD  
30 trajectories.  
31  
32  
33  
34  
35  
36  
37  
38  
39  
40  
41  
42  
43  
44  
45  
46  
47  
48  
49  
50  
51  
52  
53  
54  
55  
56  
57  
58  
59  
60

## Biology

***In vitro* inhibition of TTBK1 and TTBK2 human recombinant kinases.** The inhibition experiments were performed in the MRC Phosphorylation Unit (University of Dundee). TTBK1 or TTBK2 (human recombinant enzyme) (5–20 mU diluted in 50 mM Tris pH 7.5, 0.1 mM EGTA, 0.1%  $\beta$ -mercaptoethanol, 1mg/mL BSA, 10mM DTT) is assayed against RRKDLHDDEEDEAMSITA in a final volume of 25.5  $\mu$ L containing 50 mM Tris pH 7.5, 0.1 mM EGTA, 0.3 mM RRKDLHDDEEDEAMSITA, 10 mM magnesium acetate and 0.005 mM [ $^{33}$ P- $\gamma$ -ATP] (50-1000 cpm/pmol) and incubated for 30 min at room temperature. Assays are stopped by addition of 5  $\mu$ L of 0.5 M (3%) orthophosphoric acid and then harvested onto P81 Unifilter plates with a wash buffer of 50 mM orthophosphoric acid.

**Kinase profiling.** The kinase profiling studies were carried out by MRC Phosphorylation Unit (University of Dundee). using the appropriate protocol in any case.<sup>53</sup>

**Parallel Artificial Membrane Permeability Assay (PAMPA) Blood-Brain Barrier (BBB).** Prediction of the blood brain barrier penetration was performed with the Parallel Artificial Membrane Permeability Assay (PAMPA).<sup>54</sup> Ten commercial drugs of known BBB permeability, were used as controls in each experiment to validate the analysis set; Caffeine, Enoxacin, Hydrocortisone, Desipramine, Ofloxacin, Piroxicam, Testosterone, Promazine, Verapamil and Atenolol. Controls and TTBK1 inhibitors were dissolved in 5 mL of experimental buffer (phosphate buffer saline solution at pH 7.4 (PBS): EtOH (70:30 respectively)). The donor 96-well plate (Millipore, catalog no. MAIPS4510) was filled with 180  $\mu$ L of each filtered compound solution after being coated with 4  $\mu$ L of porcine brain lipid in dodecane (20 mg mL<sup>-1</sup>) (Avanti Polar Lipids, catalog no. 141101). The acceptor 96-well plate (Millipore, catalog no. 141101) was filled with 180  $\mu$ L of experimental buffer. Then the donor plate was carefully put on the acceptor plate to form a “sandwich” for 2h and 30 min at room temperature. During incubation time

1  
2  
3 compounds diffused from the donor plate through the brain lipid membrane into the  
4 acceptor plate. After incubation, the donor plate was removed and compounds  
5 concentration was determined in the acceptor and the donor plates by UV  
6 (Thermoscientific, Multiskan spectrum). Every sample was analyzed at three to five  
7 wavelengths, in 3 wells and in two independent runs. Results are given as the mean  $\pm$   
8 standard deviation (SD) of the two runs. Commercial drugs, PBS, Ethanol and dodecane  
9 were purchased from Sigma, Acros organics, Merck, Aldrich and Fluka.  
10  
11  
12  
13  
14  
15  
16  
17

18 **Cell lines.** All components for cell culture were obtained from Invitrogen (Barcelona,  
19 Spain). Antibodies used in this study are listed in Table S5.  
20  
21  
22

23 **Neuronal cell culture.** Human neuroblastoma (SH-SY5Y) cells were purchased from  
24 the European Collection of Cell Cultures (Health Protection Agency, Salisbury, UK), and  
25 were propagated in Dulbecco's Modified Eagle Medium containing L-glutamine (2 mM),  
26 1% non-essential amino acids, 10% fetal bovine serum and 1% penicillin/streptomycin,  
27 under humidified 5% CO<sub>2</sub> conditions at 37 °C. On attaining semiconfluency, cells were  
28 pre-treated with TTBK1 inhibitors (5  $\mu$ M) or the commercial GSK3 $\beta$  inhibitor (Tideglusib,  
29 5  $\mu$ M) and exposed 1 hour later to ethacrynic acid (40  $\mu$ M) for 24 hours. After the  
30 incubation time, cultures were processed for cell viability assay or Western blotting  
31 analysis. Cell viability was determined by the MTT assay, as previously described.<sup>55</sup> Cell  
32 survival was normalized to untreated controls and is presented as a percentage.  
33  
34  
35  
36  
37  
38  
39  
40  
41  
42  
43  
44

45 **Lymphoblasts from ALS and Control individuals.** Lymphocytes were obtained from  
46 blood samples of patients or healthy individuals (Table 5) after written informed consent.  
47 Patients were diagnosed as sporadic ALS according to El Escorial criteria<sup>56</sup> in the Doce  
48 de Octubre Hospital (Madrid, Spain).  
49  
50  
51  
52  
53

54 All study protocols were approved by the Spanish Council of Higher Research  
55 Institutional Review Board and the Doce de Octubre Hospital and are in accordance with  
56 National and European Union Guidelines. Establishment of lymphoblastoid cell lines was  
57  
58  
59  
60

1  
2  
3 performed in our laboratory as previously described by infecting peripheral blood  
4 lymphocytes with the Epstein-Barr virus.<sup>57</sup> Cells were grown in suspension in T flasks, in  
5 RPMI-1640 medium (Gibco, BRL) that contained 2 mM L-glutamine, 10% (v/v) fetal  
6 bovine serum (FBS) and 100 µg/mL penicillin/streptomycin and maintained in a  
7 humidified 5% CO<sub>2</sub> incubator at 37 °C Lymphoblasts were seeded at an initial density of  
8 1 x 10<sup>6</sup> x mL<sup>-1</sup> in presence or absence of TTBK1 inhibitors (5, 10 µM) for 24 hours. Then,  
9 cells were harvested and processed for Western blotting analysis.  
10  
11  
12  
13  
14  
15  
16  
17  
18

19 **Primary rat microglia culture.** Wistar Rats were house hold with free access to food  
20 and water and kept in a light-dark 12/12 h cycle. Experimental designs and procedures  
21 were in accordance to European Community and Italian laws and approved by the  
22 Ethical Committee for Animal Experimentation of the University of Bologna (Protocol No.  
23 17-72-1212).  
24  
25  
26  
27  
28  
29

30 Flasks used for cell cultured were previously covered with poly-L-lysine (10 µg/mL)  
31 (Sigma Aldrich, St. Louis, MO, USA). Mixed cultures of glial cells were obtained from  
32 cerebral cortices of newborn rats as previously described.<sup>58</sup> Briefly, cerebral cortices  
33 were trypsinized and mechanically dissected after cleared from meninges. The cell  
34 suspension was washed and resuspended in Basal Medium Eagle (BME, Life  
35 Technologies Ltd, Paisley, UK) supplemented with 10% fetal bovine serum (FBS, Life  
36 Technologies), 50 mg/mL gentamicin and 2 mM L-glutamine (Sigma-Aldrich). After 6/7  
37 days in culture, pure microglial cells were obtained through mechanical detachment,  
38 resuspended in serum-free BME and plated on 35-mm diameter dishes at a density of  
39 1.5 x 10<sup>6</sup> cells/1.5 mL medium/well. The medium was change 30 min later in order to  
40 remove non-adhering cells. Cultures were maintained in standard conditions (5% CO<sub>2</sub>  
41 at 37 °C) and treated the day after plated. Microglia cells were exposed to LPS (100  
42 ng/mL) (Sigma-Aldrich) for 24 hours. Compound **29** was added to the culture 1 hour  
43 before the treatment with LPS at increasing concentrations (5 and 25 µM). Cells were  
44 collected for immunoblotting analysis.  
45  
46  
47  
48  
49  
50  
51  
52  
53  
54  
55  
56  
57  
58  
59  
60



1  
2  
3 **Immunoblotting analysis.** Total protein extracts were obtained by lysing the cells,  
4 collected by centrifugation, as previously described.<sup>59</sup> Cytosolic and nuclear fractions  
5 were obtained using the Subcellular Protein Fractionation Kit, (Cat#78840, Thermo  
6 Fisher Scientific, Madrid, Spain) following the manufacturer's instructions.  $\alpha$ -Tubulin and  
7 Lamin B1 were used as markers for cytosolic and nuclear fractions respectively. Protein  
8 quantification was carried out using the Pierce BCA Protein Assay kit (ThermoFisher,  
9 Madrid Spain). Equal amounts of proteins were resolved by SDS–polyacrylamide gel  
10 electrophoresis. Proteins were then transferred to polyvinylidene fluoride (PVDF)  
11 membranes and immunodetected, as previously described. The primary antibodies used  
12 are listed in **Table 5**. Signals from the primary antibodies were amplified using species-  
13 specific antisera antibodies conjugated with horseradish peroxidase and detected with a  
14 chemiluminescent substrate detection system ECL (Bio-Rad, Alcobendas, Madrid,  
15 Spain). Relative band intensities were quantified using a ChemiDoc station with Quantity  
16 One 1D analysis software (Bio-Rad Laboratories, Madrid, Spain) and normalized by  
17 those of GAPDH,  $\alpha$ -tubulin or Lamin B1.

18  
19  
20  
21  
22  
23  
24  
25  
26  
27  
28  
29  
30  
31  
32  
33  
34  
35 **Immunofluorescence.** Cells were permeabilized for 10 min at RT with 0.25% Triton X-  
36 100 (Sigma Aldrich), rinsed with PBS and blocked with 2% BSA (Sigma Aldrich) and  
37 0.1% casein (Sigma Aldrich) for 30 min at RT. After being fixed, cells were incubated  
38 with TDP-43 monoclonal antibody (**Table 5**) in 6% BSA for 1 h at 37 °C, rinsed with PBS  
39 and incubated with Alexa Fluor 488 anti-rabbit antibody (1:600, Jackson Immuno  
40 Research). HCS NuclearMask Deep Red (1:250, Thermo Fisher) was used to stained  
41 cell nuclei. Finally, preparations were washed with 1% BSA and 0.1% casein and  
42 mounted onto Fluoromount Mounting Medium (Sigma Aldrich). Images were acquired  
43 for ~ 60 cells per group in n = 3 independent experiments using a confocal laser scanning  
44 microscope (CLMS) Leica TCS SP5 with 63x oil immersion objective. Quantification of  
45 TDP-43 was performed using Image J software.

1  
2  
3 **Pharmacokinetic Studies.** The study was conducted according to the guidelines of the  
4 Institutional Animal Ethics Committee (IAEC), and approved by Sai Life Sciences  
5 (Hinjewadi, Pune, India) (no. SAIDMPK/PK-21-03-262, March 2021). Healthy male  
6 BALB/c mice (8-12 weeks old) weighing between 17 to 30 g were used in the study.  
7 Total forty-eight male mice were divided into two groups as Group 1 (n=24) and Group  
8 2 (n=24) with 3 mice/time points design. In both cases, the formulation was based in 90%  
9 of phosphate buffer saline (PBS, pH 7.4) with a 5% of solutol HS-15 and 5% of N-methyl-  
10 2-pyrrolidone at a dose of 5 mg/kg or 10 mg/Kg for i.p. and p.o administration,  
11 respectively. Blood samples ( $\approx 60 \mu\text{L}$ ) were collected from a set of three mice at each  
12 time point (0.08 (for i.p. only), 0.25, 0.5, 1, 2, 4, 6 (only for p.o), 8 and 24 h). In addition,  
13 along with terminal blood samples, brain samples were collected at 0.08 (for i.p only),  
14 0.25, 0.5, 1, 2, 4, 6 (only for p.o.), 8 and 24 h post dosing from 3 mice per time point.  
15 Immediately after collection of blood, brain samples were collected from set of three  
16 animals for bioanalysis. Concentrations of compound in mouse plasma and brain  
17 samples were determined by fit-for-purpose LC-MS/MS method. Non-Compartmental-  
18 Analysis tool of Phoenix WinNonlin® (Version 8.0) was used to assess the  
19 pharmacokinetic parameters.  
20  
21  
22  
23  
24  
25  
26  
27  
28  
29  
30  
31  
32  
33  
34  
35  
36  
37  
38  
39

40 **Animal procedures, treatment and sampling.** Protocol authorized by the ethical  
41 committees of the regulatory institution and the UCM (ref. PROEX 059/16) in agreement  
42 with regulations (2010/63/EU) from European Commission was in place for all the  
43 experiments done. Wild-type and Prp-hTDP-43(A315T) transgenic littermate sibling  
44 mice were purchased from Jackson Laboratories (Bar Harbor, ME, USA) and bred in  
45 house. Mice were maintained with food and water ad libitum in a temperature-controlled  
46 atmosphere ( $22 \pm 1^\circ\text{C}$ ) and on a cycle of 12 h light/dark. Genotyping of offspring were  
47 done as previously reported,<sup>38</sup> and four groups of male mice were randomly done (n=8).  
48 Compound **29** was dissolved in 2.9% DMSO and Tween 80-saline buffer (1:16) and  
49 administered i.p. at a dose of 5 mg/Kg daily. Control animals received vehicle injections.  
50  
51  
52  
53  
54  
55  
56  
57  
58  
59  
60

1  
2  
3 Treatment started at the age of 65 days old, until animal sacrifice 30 days later. During  
4 all the treatment, physical appearance and animal weight gain were recorded. Spinal  
5 cords were rapidly collected and flash-frozen in 2-methylbutane cooled in dry ice and  
6 stored at -80 °C.  
7  
8  
9

10  
11  
12 **Tissue slicing.** Fixed spinal cords were sliced with a cryostat at the lumbar level (L4-L6)  
13 to obtain coronal sections (20 µm thick) that were collected on gelatin-coated slides.  
14 Sections were used for procedures of Nissl-staining and immunofluorescence.  
15  
16

17  
18 **Nissl staining.** Slices were used for Nissl staining using cresyl violet, as previously  
19 described, which permitted to determine the effects of each treatment on cell number. A  
20 Leica DMRB microscope (Leica, Wetzlar, Germany) and a DFC300Fx camera (Leica)  
21 were used to study and photograph the tissue, respectively. To count the number of  
22 Nissl-stained motor neurons (> 400 µm<sup>2</sup>) in the ventral horn, high-resolution  
23 photomicrographs were taken with a 10x objective under the same conditions of light,  
24 brightness, and contrast. Counting was carried out with ImageJ software (U.S. National  
25 Institutes of Health, Bethesda, Maryland, USA, <http://imagej.nih.gov/ij/>, 1997-2012). At  
26 least 6 images *per* animal were analyzed to calculate the mean of each group (n≥5).  
27 Analyses were always conducted by experimenters who were blinded to genotype and  
28 treatment conditions. In all analyses, data were transformed to the percentage over the  
29 mean obtained in the wild-type group for each parameter.  
30  
31  
32

33  
34 **Immunofluorescence analysis.** Spinal slices were used for detection and quantification  
35 of Iba-1, GFAP, or ChAT immunofluorescence. After preincubation for 1 hour with Tris-  
36 buffered saline with 0.1% Triton X-100 (pH 7.5), sections were sequentially incubated  
37 overnight at 4 °C with the following polyclonal antibodies: (i) anti-Iba-1 (Wako Chemicals,  
38 Richmond, VI, USA) used at 1:500; (ii) anti-GFAP (Dako Cytomation, Glostrup,  
39 Denmark) used at 1:200 or (iii) ChAT (Merck Millipore, MA, USA) used at 1:100. After  
40 incubation, sections were washed with Tris-buffered saline and secondary antibodies  
41 were incubated for 2 hours at 37 °C For Iba-1 and GFAP staining, anti-rabbit secondary  
42  
43  
44  
45  
46  
47  
48  
49  
50  
51  
52  
53  
54  
55  
56  
57  
58  
59  
60

1  
2  
3 antibody conjugated with Alexa 488 (Invitrogen, Carlsbad, CA, USA) was used at 1:200.  
4  
5 For ChAT staining, anti-goat secondary antibody conjugated with Alexa 546  
6  
7 (Invitrogen™, ThermoFisher Scientific, MA, USA). Sections were then washed and  
8  
9 mounted with Faramount aqueous mounting medium (Dako Cytomation, Glostrup,  
10  
11 Denmark). A DMRB microscope and a DFC300Fx camera (Leica, Wetzlar, Germany)  
12  
13 were used for slide observation and photography. The mean density of immunolabelling  
14  
15 was measured in the selected areas with ImageJ software (NIH, USA). At least 6 images  
16  
17 *per* animal were analyzed to calculate the mean of each group ( $n \geq 5$ ). Again, all data  
18  
19 were transformed to the percentage over the mean obtained in the wild-type group for  
20  
21 each parameter.  
22  
23

24 **Statistical Analysis.** Statistical analyses were performed with Graph Pad Prism 9. All  
25  
26 the statistical data are presented as mean  $\pm$  standard error of the mean (SEM). Normality  
27  
28 was checked with the Shapiro–Wilk test. Parametric tests were therefore used in the  
29  
30 statistical analysis. Significant differences between groups were evaluated by using  
31  
32 Student's t-test or by analysis of variance (ANOVA) followed by the Fisher's LSD test for  
33  
34 multiple comparisons. A value of  $p < 0.05$  was considered significant.  
35  
36  
37  
38  
39

### 40 **Supporting information**

41  
42 The Supporting Information is available free of charge on the ACS Publications website.  
43  
44 Data collection, refinement statistics and crystal structures (table S1 and figure S1); MM-  
45  
46 GBSA parameters for modelled compounds (tables S2, S3 and figure S1, S2);  
47  
48 experimental permeability data in the PAMPA-BBB assay (table S4 and figure S4);  
49  
50 antibodies used in WB and immunohistochemistry (table S5); viability studies for TTBK1  
51  
52 inhibitors (figure S5); neuroprotection of TTBK1 inhibitors in a okadaic acid cell-based  
53  
54 assay (figure S6); images of the immunomodulatory effect of compound **29** in the spinal  
55  
56 cord of the *in vivo* ALS model (figure S7); HPLC-MS chromatogram of lead compounds  
57  
58 (figure S8).  
59  
60

1  
2  
3 Molecular Formula Strings are also included.

4  
5 PDB ID of New Crystal (X-ray) Structures: Authors will release the atomic coordinates  
6  
7 upon article publication.  
8  
9

10 **Corresponding authors information:**

11  
12  
13 \*A.M.: e-mail [ana.martinez@csic.es](mailto:ana.martinez@csic.es)  
14  
15

16  
17 ORCID

18  
19 Ana Martínez: 0000-0002-2707-8110

20  
21 Eva de Lago: 0000-0002-6260-3777

22  
23 Valle Palomo: 0000-0002-1473-4086

24  
25 Ángeles Martín-Requero: 0000-0002-3416-9-440

26  
27 Carmen Gil: 0000-0002-3882-6081

28  
29 David Ramírez: 0000-0003-0002-1189

30  
31 Vanesa Nozal: 0000-0001-5260-5683

32  
33 Loreto Martínez-González: 0000-0003-4593-4889

34  
35 Daniel Lietha: 0000-0002-6133-6486

36  
37 Barbara Monti: 0000-0003-0330-482X

38  
39 Stefan Knapp: 0000-0001-5995-6494

40  
41 Apirat Chaikwad: 0000-0003-1120-2209  
42  
43  
44  
45  
46

47 **Notes:** The authors declare no competing financial interest  
48  
49

50 **Acknowledgements**

51  
52  
53 This work was supported by Comunidad de Madrid (grant B2017/BMD-3813), and  
54  
55 European Social Fund + (ESF+), MINECO (grant SAF2016-76693-R to A.M., RTI2018-  
56  
57 0988885-B-I00 to E.dL. and CTQ2015-66313-R to A.M.R.), AIE (RTI2018-099318-B-I00  
58  
59 to D.L., co-funded by the European Regional Development Fund (FEDER), ISCiii  
60

1  
2  
3 CIBERNED (CB18/05/00040 to A.M., C.G. and A.M.R, and CB06/05/0089 to E.dL.),  
4  
5 MECD (FPU16/04466 to V.N.), Cost Action CA15135 “MuTaLig” (COST-STSM-  
6  
7 CA15135-37514 to LMG), FONDECYT (grant no. 11180604 to D.R.). V.P. has received  
8  
9 financial support through the Postdoctoral Junior Leader Fellowship Program  
10  
11 (LCF/BQ/PR18/11640007) from “la Caixa” Banking Foundation. This work has been  
12  
13 awarded by the SEQT (Spanish Society of Medicinal Chemistry) for young researchers  
14  
15 in their XX edition. We thank the staff at the ALBA synchrotron facilities for their  
16  
17 assistance during the X-ray diffraction data collection and Pilar López Navajas for help  
18  
19 during TTBK1 protein purification.  
20  
21  
22  
23  
24  
25

#### 26 **Abbreviations used**

27  
28  
29 AD, Alzheimer’s disease; ALS, amyotrophic lateral sclerosis; BBB, Blood brain barrier;  
30  
31 CNS, central nervous system; EA, ethacrynic acid; FTD-TDP, frontotemporal dementia  
32  
33 with TDP-43 aggregates; LATE, limbic-predominant age-related TDP-43 encephalopathy;  
34  
35 LPS, lipopolysaccharide; MM-GBSA, molecular mechanics generalized Born surface  
36  
37 area; iNOS, inducible nitric oxide synthase; OA, okadaic acid; PAMPA, parallel artificial  
38  
39 membranes permeability assay; RMSD, root-mean-square deviation; TDP-43,  
40  
41 transactive response DNA binding protein of 43 kDa; TREM2, triggering receptor  
42  
43 expressed on myeloid cells 2; TTBK1, tau-tubulin kinase 1; TTBK2, tau-tubulin kinase 2.  
44  
45  
46  
47  
48  
49  
50  
51  
52  
53  
54  
55  
56  
57  
58  
59  
60

## References

- (1) Scotter, E. L.; Chen, H. J.; Shaw, C. E. TDP-43 proteinopathy and ALS: Insights into disease mechanisms and therapeutic targets. *Neurotherapeutics* **2015**, *12*, 352-363.
- (2) Weskamp, K.; Barmada, S. J. TDP43 and RNA instability in amyotrophic lateral sclerosis. *Brain Res* **2018**, *1693*, 67-74.
- (3) de Boer, E. M. J.; Orié, V. K.; Williams, T.; Baker, M. R.; De Oliveira, H. M.; Polvikoski, T.; Silsby, M.; Menon, P.; van den Bos, M.; Halliday, G. M.; van den Berg, L. H.; Van Den Bosch, L.; van Damme, P.; Kiernan, M. C.; van Es, M. A.; Vucic, S. TDP-43 proteinopathies: a new wave of neurodegenerative diseases. *J Neurol Neurosurg Psychiatry* **2020**, *92*, 86-95.
- (4) Suk, T. R.; Rousseaux, M. W. C. The role of TDP-43 mislocalization in amyotrophic lateral sclerosis. *Mol Neurodegener* **2020**, *15*, 45-61.
- (5) Prasad, A.; Bharathi, V.; Sivalingam, V.; Girdhar, A.; Patel, B. K. Molecular mechanisms of TDP-43 misfolding and pathology in amyotrophic lateral sclerosis. *Front Mol Neurosci* **2019**, *12*, 25.
- (6) Palomo, V.; Tosat-Bitrian, C.; Nozal, V.; Nagaraj, S.; Martin-Requero, A.; Martinez, A. TDP-43: A key therapeutic target beyond amyotrophic lateral sclerosis. *ACS Chem Neurosci* **2019**, *10*, 1183-1196.
- (7) Moujalled, D.; James, J. L.; Parker, S. J.; Lidgerwood, G. E.; Duncan, C.; Meyerowitz, J.; Nonaka, T.; Hasegawa, M.; Kanninen, K. M.; Grubman, A.; Liddell, J. R.; Crouch, P. J.; White, A. R. Kinase inhibitor screening identifies cyclin-dependent kinases and glycogen synthase kinase 3 as potential modulators of TDP-43 cytosolic accumulation during cell stress. *PLoS One* **2013**, *8*, e67433.
- (8) Kametani, F.; Nonaka, T.; Suzuki, T.; Arai, T.; Dohmae, N.; Akiyama, H.; Hasegawa, M. Identification of casein kinase-1 phosphorylation sites on TDP-43. *Biochem Biophys Res Commun* **2009**, *382*, 405-409.
- (9) Liachko, N. F.; McMillan, P. J.; Guthrie, C. R.; Bird, T. D.; Leverenz, J. B.; Kraemer, B. C. CDC7 inhibition blocks pathological TDP-43 phosphorylation and neurodegeneration. *Ann Neurol* **2013**, *74*, 39-52.
- (10) Li, W.; Reeb, A. N.; Lin, B.; Subramanian, P.; Fey, E. E.; Knoverek, C. R.; French, R. L.; Bigio, E. H.; Ayala, Y. M. Heat shock-induced phosphorylation of TAR DNA-binding protein 43 (TDP-43) by MAPK/ERK kinase regulates TDP-43 function. *J Biol Chem* **2017**, *292*, 5089-5100.
- (11) Liachko, N. F.; McMillan, P. J.; Strovas, T. J.; Loomis, E.; Greenup, L.; Murrell, J. R.; Ghetti, B.; Raskind, M. A.; Montine, T. J.; Bird, T. D.; Leverenz, J. B.; Kraemer, B. C.

1  
2  
3 The tau tubulin kinases TTBK1/2 promote accumulation of pathological TDP-43. *PLoS*  
4 *Genet* **2014**, *10*, e1004803.

6 (12) Palomo, V.; Nozal, V.; Rojas-Prats, E.; Gil, C.; Martinez, A. Protein kinase  
7 inhibitors for amyotrophic lateral sclerosis therapy. *Br J Pharmacol* **2021**, *178*, 1316-  
8 1335.

11 (13) Martinez-Gonzalez, L.; Gonzalo-Consuegra, C.; Gomez-Almeria, M.; Porras, G.;  
12 de Lago, E.; Martin-Requero, A.; Martinez, A. Tideglusib, a non-ATP competitive inhibitor  
13 of GSK-3beta as a drug candidate for the treatment of amyotrophic lateral sclerosis. *Int*  
14 *J Mol Sci* **2021**, *22*, 8975-8989.

17 (14) Martinez-Gonzalez, L.; Rodriguez-Cueto, C.; Cabezudo, D.; Bartolome, F.;  
18 Andres-Benito, P.; Ferrer, I.; Gil, C.; Martin-Requero, A.; Fernandez-Ruiz, J.; Martinez,  
19 A.; de Lago, E. Motor neuron preservation and decrease of in vivo TDP-43  
20 phosphorylation by protein CK-1delta kinase inhibitor treatment. *Sci Rep* **2020**, *10*, 4449.

23 (15) Rojas-Prats, E.; Martinez-Gonzalez, L.; Gonzalo-Consuegra, C.; Liachko, N. F.;  
24 Perez, C.; Ramirez, D.; Kraemer, B. C.; Martin-Requero, A.; Perez, D. I.; Gil, C.; de Lago,  
25 E.; Martinez, A. Targeting nuclear protein TDP-43 by cell division cycle kinase 7  
26 inhibitors: A new therapeutic approach for amyotrophic lateral sclerosis. *Eur J Med Chem*  
27 **2021**, *210*, 112968.

31 (16) Halkina, T.; Henderson, J. L.; Lin, E. Y.; Himmelbauer, M. K.; Jones, J. H.;  
32 Nevalainen, M.; Feng, J.; King, K.; Rooney, M.; Johnson, J. L.; Marcotte, D. J.;  
33 Chodaparambil, J. V.; Kumar, P. R.; Patterson, T. A.; Murugan, P.; Schuman, E.; Wong,  
34 L.; Hesson, T.; Lamore, S.; Bao, C.; Calhoun, M.; Certo, H.; Amaral, B.; Dillon, G. M.;  
35 Gilfillan, R.; de Turiso, F. G. Discovery of potent and brain-penetrant tau tubulin kinase  
36 1 (TTBK1) inhibitors that lower tau phosphorylation in vivo. *J Med Chem* **2021**, *64*, 6358-  
37 6380.

40 (17) Jackson, P. K. TTBK2 kinase: Linking primary cilia and cerebellar ataxias. *Cell*  
41 **2012**, *151*, 697-699.

44 (18) Cajanek, L.; Nigg, E. A. Cep164 triggers ciliogenesis by recruiting tau tubulin  
45 kinase 2 to the mother centriole. *Proc Natl Acad Sci U S A* **2014**, *111*, E2841-2850.

48 (19) Taylor, L. M.; McMillan, P. J.; Kraemer, B. C.; Liachko, N. F. Tau tubulin kinases  
49 in proteinopathy. *FEBS J* **2019**, *286*, 2434-2446.

52 (20) Sato, S.; Cerny, R. L.; Buescher, J. L.; Ikezu, T. Tau-tubulin kinase 1 (TTBK1), a  
53 neuron-specific tau kinase candidate, is involved in tau phosphorylation and aggregation.  
54 *J Neurochem* **2006**, *98*, 1573-1584.

56 (21) Lund, H.; Cowburn, R. F.; Gustafsson, E.; Stromberg, K.; Svensson, A.; Dahllund,  
57 L.; Malinowsky, D.; Sunnemark, D. Tau-tubulin kinase 1 expression, phosphorylation and  
58  
59  
60



1  
2  
3 co-localization with phospho-Ser422 tau in the Alzheimer's disease brain. *Brain Pathol*  
4 **2013**, *23*, 378-389.

5  
6 (22) Bao, C.; Bajrami, B.; Marcotte, D. J.; Chodaparambil, J. V.; Kerns, H. M.;  
7 Henderson, J.; Wei, R.; Gao, B.; Dillon, G. M. Mechanisms of regulation and diverse  
8 activities of tau-tubulin kinase (TTBK) isoforms. *Cell Mol Neurobiol* **2021**, *41*, 669-685.

9  
10 (23) Nozal, V.; Martinez, A. Tau tubulin kinase 1 (TTBK1), a new player in the fight  
11 against neurodegenerative diseases. *Eur J Med Chem* **2019**, *161*, 39.

12  
13 (24) Xue, Y.; Wan, P. T.; Hillertz, P.; Schweikart, F.; Zhao, Y.; Wissler, L.; Dekker, N.  
14 X-ray structural analysis of tau-tubulin kinase 1 and its interactions with small molecular  
15 inhibitors. *ChemMedChem* **2013**, *8*, 1846-1854.

16  
17 (25) Kiefer, S. E.; Chang, C. J.; Kimura, S. R.; Gao, M.; Xie, D.; Zhang, Y.; Zhang, G.;  
18 Gill, M. B.; Mastalerz, H.; Thompson, L. A.; Cacace, A. M.; Sheriff, S. The structure of  
19 human tau-tubulin kinase 1 both in the apo form and in complex with an inhibitor. *Acta*  
20 *Crystallogr F Struct Biol Commun* **2014**, *70*, 173-181.

21  
22 (26) Dillon, G. M.; Henderson, J. L.; Bao, C.; Joyce, J. A.; Calhoun, M.; Amaral, B.;  
23 King, K. W.; Bajrami, B.; Rabah, D. Acute inhibition of the CNS-specific kinase TTBK1  
24 significantly lowers tau phosphorylation at several disease relevant sites. *PLoS One*  
25 **2020**, *15*, e0228771.

26  
27 (27) Marcotte, D. J.; Spilker, K. A.; Wen, D.; Hesson, T.; Patterson, T. A.; Kumar, P.  
28 R.; Chodaparambil, J. V. The crystal structure of the catalytic domain of tau tubulin  
29 kinase 2 in complex with a small-molecule inhibitor. *Acta Crystallogr F Struct Biol*  
30 *Commun* **2020**, *76*, 103-108.

31  
32 (28) Attwood, M. M.; Fabbro, D.; Sokolov, A. V.; Knapp, S.; Schioth, H. B. Trends in  
33 kinase drug discovery: Targets, indications and inhibitor design. *Nat Rev Drug Discov*  
34 **2021**, *20*, 839-861.

35  
36 (29) Staderini, M.; Bolognesi, M. L.; Menéndez, J. C. Lewis acid-catalyzed generation  
37 of C-C and C-N bonds on  $\pi$ -deficient heterocyclic substrates. *Adv Synth Catal* **2015**,  
38 *357*, 185-195.

39  
40 (30) Kolb, H. C.; Finn, M. G.; Sharpless, K. B. Click chemistry: Diverse chemical  
41 function from a few good reactions. *Angew Chem Int Ed Engl* **2001**, *40*, 2004-2021.

42  
43 (31) Young, M. A.; Shah, N. P.; Chao, L. H.; Seeliger, M.; Milanov, Z. V.; Biggs, W.  
44 H., 3rd; Treiber, D. K.; Patel, H. K.; Zarrinkar, P. P.; Lockhart, D. J.; Sawyers, C. L.;  
45 Kuriyan, J. Structure of the kinase domain of an imatinib-resistant Abl mutant in complex  
46 with the Aurora kinase inhibitor VX-680. *Cancer Res* **2006**, *66*, 1007-1014.

47  
48 (32) Schroder, M.; Bullock, A. N.; Fedorov, O.; Bracher, F.; Chaikuad, A.; Knapp, S.  
49 DFG-1 residue controls inhibitor binding mode and affinity, providing a basis for rational  
50 design of kinase inhibitor selectivity. *J Med Chem* **2020**, *63*, 10224-10234.  
51  
52  
53  
54  
55  
56  
57  
58  
59  
60

- 1  
2  
3 (33) Cheng, A. C.; Eksterowicz, J.; Geuns-Meyer, S.; Sun, Y. Analysis of kinase  
4 inhibitor selectivity using a thermodynamics-based partition index. *J Med Chem* **2010**,  
5 *53*, 4502-4510.  
6  
7 (34) Iguchi, Y.; Katsuno, M.; Takagi, S.; Ishigaki, S.; Niwa, J.; Hasegawa, M.; Tanaka,  
8 F.; Sobue, G. Oxidative stress induced by glutathione depletion reproduces pathological  
9 modifications of TDP-43 linked to TDP-43 proteinopathies. *Neurobiol Dis* **2012**, *45*, 862-  
10 870.  
11  
12 (35) Boban, M.; Babic Leko, M.; Miskic, T.; Hof, P. R.; Simic, G. Human  
13 neuroblastoma SH-SY5Y cells treated with okadaic acid express phosphorylated high  
14 molecular weight tau-immunoreactive protein species. *J Neurosci Methods* **2019**, *319*,  
15 60-68.  
16  
17 (36) Haukedal, H.; Freude, K. Implications of microglia in amyotrophic lateral sclerosis  
18 and frontotemporal dementia. *J Mol Biol* **2019**, *431*, 1818-1829.  
19  
20 (37) Tang, Y.; Le, W. Differential roles of M1 and M2 microglia in neurodegenerative  
21 diseases. *Mol Neurobiol* **2016**, *53*, 1181-1194.  
22  
23 (38) Wegorzewska, I.; Bell, S.; Cairns, N. J.; Miller, T. M.; Baloh, R. H. TDP-43 mutant  
24 transgenic mice develop features of ALS and frontotemporal lobar degeneration. *Proc*  
25 *Natl Acad Sci U S A* **2009**, *106*, 18809-18814.  
26  
27 (39) Posa, D.; Martinez-Gonzalez, L.; Bartolome, F.; Nagaraj, S.; Porras, G.; Martinez,  
28 A.; Martin-Requero, A. Recapitulation of pathological TDP-43 features in immortalized  
29 lymphocytes from sporadic ALS patients. *Mol Neurobiol* **2019**, *56*, 2424-2432.  
30  
31 (40) Arnold, L. A.; Moyer, M. P.; Sobolov-Jaynes, S. B. Heterocyclic ring-fused  
32 pyrimidine derivatives. US 6395733 B1. **1995**.  
33  
34 (41) Kabsch, W. Integration, scaling, space-group assignment and post-refinement.  
35 *Acta Crystallogr D Biol Crystallogr* **2010**, *66*, 133-144.  
36  
37 (42) Evans, P. R.; Murshudov, G. N. How good are my data and what is the resolution?  
38 *Acta Crystallogr D Biol Crystallogr* **2013**, *69*, 1204-1214.  
39  
40 (43) McCoy, A. J.; Grosse-Kunstleve, R. W.; Adams, P. D.; Winn, M. D.; Storoni, L.  
41 C.; Read, R. J. Phaser crystallographic software. *J Appl Crystallogr* **2007**, *40*, 658-674.  
42  
43 (44) Murshudov, G. N.; Vagin, A. A.; Dodson, E. J. Refinement of macromolecular  
44 structures by the maximum-likelihood method. *Acta Crystallogr D Biol Crystallogr* **1997**,  
45 *53*, 240-255.  
46  
47 (45) Emsley, P.; Cowtan, K. Coot: Model-building tools for molecular graphics. *Acta*  
48 *Crystallogr D Biol Crystallogr* **2004**, *60*, 2126-2132.  
49  
50 (46) Halgren, T. A.; Murphy, R. B.; Friesner, R. A.; Beard, H. S.; Frye, L. L.; Pollard,  
51 W. T.; Banks, J. L. Glide: A new approach for rapid, accurate docking and scoring. 2.  
52 Enrichment factors in database screening. *J Med Chem* **2004**, *47*, 1750-1759.  
53  
54  
55  
56  
57  
58  
59  
60

- 1  
2  
3 (47) Friesner, R. A.; Banks, J. L.; Murphy, R. B.; Halgren, T. A.; Klicic, J. J.; Mainz, D.  
4 T.; Repasky, M. P.; Knoll, E. H.; Shelley, M.; Perry, J. K.; Shaw, D. E.; Francis, P.;  
5 Shenkin, P. S. Glide: A new approach for rapid, accurate docking and scoring. 1. Method  
6 and assessment of docking accuracy. *J Med Chem* **2004**, *47*, 1739-1749.
- 7  
8 (48) Sastry, G. M.; Adzhigirey, M.; Day, T.; Annabhimoju, R.; Sherman, W. Protein  
9 and ligand preparation: Parameters, protocols, and influence on virtual screening  
10 enrichments. *J Comput Aided Mol Des* **2013**, *27*, 221-234.
- 11  
12 (49) Friesner, R. A.; Murphy, R. B.; Repasky, M. P.; Frye, L. L.; Greenwood, J. R.;  
13 Halgren, T. A.; Sanschagrin, P. C.; Mainz, D. T. Extra precision glide: docking and  
14 scoring incorporating a model of hydrophobic enclosure for protein-ligand complexes. *J*  
15 *Med Chem* **2006**, *49*, 6177-6196.
- 16  
17 (50) Bowers, K. J.; Chow, E.; Xu, H.; Dror, R. O.; Eastwood, M. P.; Gregersen, B. A.;  
18 Klepeis, J. L.; Kolossvary, I.; Moraes, M. A.; Sacerdoti, F. D.; Salmon, J. K.; Shan, Y.;  
19 Shaw, D. E. Scalable algorithms for molecular dynamics simulations on commodity  
20 clusters. *SC '06: Proceedings of the 2006 ACM/IEEE Conference on Supercomputing*  
21 **2006**, Tampa, Florida.
- 22  
23 (51) Roos, K.; Wu, C.; Damm, W.; Reboul, M.; Stevenson, J. M.; Lu, C.; Dahlgren, M.  
24 K.; Mondal, S.; Chen, W.; Wang, L.; Abel, R.; Friesner, R. A.; Harder, E. D. OPLS3e:  
25 Extending force field coverage for drug-like small molecules. *J Chem Theory Comput*  
26 **2019**, *15*, 1863-1874.
- 27  
28 (52) Martyna, G. J.; Tobias, D. J.; Klein, M. L. Constant pressure molecular dynamics  
29 algorithms. *J Chem Phys* **1994**, *101*, 4177-4189.
- 30  
31 (53) Bain, J.; Plater, L.; Elliott, M.; Shpiro, N.; Hastie, C. J.; McLauchlan, H.; Klevernic,  
32 I.; Arthur, J. S.; Alessi, D. R.; Cohen, P. The selectivity of protein kinase inhibitors: a  
33 further update. *Biochem J* **2007**, *408*, 297-315.
- 34  
35 (54) Di, L.; Kerns, E. H.; Fan, K.; McConnell, O. J.; Carter, G. T. High throughput  
36 artificial membrane permeability assay for blood-brain barrier. *Eur J Med Chem* **2003**,  
37 *38*, 223-232.
- 38  
39 (55) Morgan, D. M. Tetrazolium (MTT) assay for cellular viability and activity. *Methods*  
40 *Mol Biol* **1998**, *79*, 179-183.
- 41  
42 (56) Agosta, F.; Al-Chalabi, A.; Filippi, M.; Hardiman, O.; Kaji, R.; Meininger, V.;  
43 Nakano, I.; Shaw, P.; Shefner, J.; van den Berg, L. H.; Ludolph, A. WFN Research Group  
44 on ALS/MND. The El Escorial criteria: Strengths and weaknesses. *Amyotroph Lateral*  
45 *Scler Frontotemporal Degener* **2015**, *16*.
- 46  
47 (57) Omi, N.; Tokuda, Y.; Ikeda, Y.; Ueno, M.; Mori, K.; Sotozono, C.; Kinoshita, S.;  
48 Nakano, M.; Tashiro, K. Efficient and reliable establishment of lymphoblastoid cell lines  
49  
50  
51  
52  
53  
54  
55  
56  
57  
58  
59  
60

1  
2  
3 by Epstein-Barr virus transformation from a limited amount of peripheral blood. *Sci Rep*  
4 **2017**, *7*, 43833.

5  
6 (58) Polazzi, E.; Gianni, T.; Contestabile, A. Microglial cells protect cerebellar granule  
7 neurons from apoptosis: Evidence for reciprocal signaling. *Glia* **2001**, *36*, 271-280.

8  
9 (59) Alquezar, C.; Salado, I. G.; de la Encarnacion, A.; Perez, D. I.; Moreno, F.; Gil,  
10 C.; de Munain, A. L.; Martinez, A.; Martin-Requero, A. Targeting TDP-43 phosphorylation  
11 by casein kinase-1delta inhibitors: a novel strategy for the treatment of frontotemporal  
12 dementia. *Mol Neurodegener* **2016**, *11*, 36-50.  
13  
14  
15  
16  
17  
18  
19  
20  
21  
22  
23  
24  
25  
26  
27  
28  
29  
30  
31  
32  
33  
34  
35  
36  
37  
38  
39  
40  
41  
42  
43  
44  
45  
46  
47  
48  
49  
50  
51  
52  
53  
54  
55  
56  
57  
58  
59  
60

